Mechanism of Corticocardiac Coupling in Sudden Cardiac Arrest

by

Fangyun Tian

A dissertation submitted in partial fulfillment
of the requirements for the degree of
Doctor of Philosophy
(Molecular and Integrative Physiology)
in the University of Michigan
2018

Doctoral Committee:

Associate Professor Jimo Borjigin, Chair
Associate Professor Anuska V. Andjelkovic-Zochowska
Professor Daniel A. Beard
Professor Richard F. Keep
Research Assistant Professor UnCheol Lee

Fangyun Tian

fangyun@umich.edu

ORCID ID: 0000-0003-2321-3407

ACKNOWLEDGEMENTS

I would like to express my sincere thankfulness to my advisor, Dr. Jimo Borjigin. Thank her for inspiring me to pursue my passion of applying computational techniques to explore neurophysiological questions, and helping me to realize my goal through the study of brain-heart connection using signal processing approach. She is not only an excellent scientist who has many novel and creative research ideas, but also an outstanding mentor. She is always accessible to students, and would like to listen to and respect students' ideas. She taught me how to do research, how to apply for grant, how to write manuscript, and so on. Without her kind guidance and enormous support over the past few years, this thesis could not have been possible. I really feel fortunate to be her student and consider studying in her lab as a very precious life experience. Thanks to our previous lab technician, Dr. Tiecheng Liu, for teaching me animal surgery and his great assistance with data collection. Thanks to Drs. Duan Li and Gang Xu for teaching me and answering many questions about signal processing. My thanks also go to all other Borjigin Lab members, especially to undergraduate students Talha Ghazi, Azeem Sajjad, and Trever Shick who had spent hundreds of hours in helping analyzing the data.

I would also like to thank my thesis committee members, Drs. Anuska Andjelkovic-Zochowska, Daniel Beard, Richard Keep, and UnCheol Lee for taking their time to attend my thesis committee meeting every six months, and for all their insightful and constructive comments to my research project. Thanks to Dr. Anuska Andjelkovic-Zochowska for her expertise on stroke models. Thanks to Dr. Daniel Beard for his expert insights on cardiac

physiology. I am very grateful to Dr. Richard Keep for his timely and thoughtful reply to every one of my questions. Thanks to Dr. UnCheol Lee for his helpful suggestions and professional advice on signal processing. I really benefited a lot from the great discussions with my thesis committee members and greatly appreciate the valuable feedback they provided. In addition, I would like to thank our collaborators, Drs. Michael Wang, Peter Farrehi, Jack Parent, and Temenuzhka (Nusha) Mihaylova. Thanks Dr. Michael Wang for his great support to my American Heart Association predoctoral fellowship application. Thanks to Dr. Peter Farrehi for his kind assistance and helpful discussions about cardiac arrhythmias. Thanks to Drs. Jack Parent and Temenuzhka (Nusha) Mihaylova for generously providing the human data. I am also very indebted to Dr. Victoria Booth for introducing me to the field of computational neuroscience and for her time and great patience in teaching me Matlab programming.

Thanks to Molecular and Integrative Physiology graduate committee chair Drs. Scott Pletcher, Sue Moenter, and Daniel Michele. I thank Drs. Sue Mentor and Daniel Michele for spending their time to discuss with me about my annual progress to ensure the smooth progression of my thesis project and for their helpful advice on my career plan. Thanks to our PhD program coordinator Ms. Michele Boggs, who has been always friendly and helpful with course selection, graduation policies, room scheduling, and so on. Thanks to all other people in the Department of Molecular and Integrative Physiology and the Program in Biomedical Sciences. Thanks to all of you for making my PhD journey more meaningful and more fulfilling.

Last but not least, I would like to thank my beloved parents, who consistently support and encourage me to pursue my dream. Thank you for all your love.

TABLE OF CONTENTS

LIST OF TABLES

LIST OF FIGURES

ABSTRACT

Sudden cardiac arrest is a leading cause of death in the United States. The neurophysiological mechanism underlying sudden cardiac arrest is not well understood. Recent studies from our laboratory demonstrate that asphyxia-induced sudden cardiac arrest leads to a surge of brain-heart coupling, a novel form of neurophysiological activity measured by corticocardiac coherence (CCCoh) and directional connectivity (CCCon), prior to sudden death. In addition, surgical blockade of efferent signaling from the brain to the heart significantly delayed the death of both the heart and the brain during asphyxic cardiac arrest. We hypothesized that the stimulated brain functions to resuscitate the heart via activation of the sympathetic nervous system and that the surge of brain-heart coupling may be a potential biomarker for sudden cardiac arrest. In current thesis project, we tested our hypothesis in 3 different cardiac arrest models.

In the first study, we tested the effectiveness of adrenergic blockers, phentolamine and atenolol, individually or combined, in prolonging functionality of the vital organs in asphyxic cardiac arrest model. Rats received either saline, phentolamine, atenolol, or phentolamine plus atenolol, 30 minutes before the onset of asphyxia. Electrocardiogram (ECG) and electroencephalogram (EEG) signals were simultaneously collected and investigated. We found that adrenergic blockade significantly (1) suppressed the initial decline of cardiac output, (2) prolonged electrical activities of both the brain and heart, and (3) altered CCCoh and CCCon bi-directionally and hemispherically. The protective effects of adrenergic blockers paralleled the suppression of brain and heart electrical connectivity, especially in the right hemisphere

associated with central regulation of sympathetic function. In the second study, we investigated corticocardiac coupling in a patient died from cardiac arrest. Consistent with previous findings from rats, there was a marked increase of CCCoh and CCCon in the dying patient. However, different from rat model, CCCoh and CCCon in human patient showed changes unique to individual cortical channels and limited to particular frequency ranges. We also identified a surge of cardiac event-related potential at near-death in the right prefrontal and left occipital cortical region, which have been shown to play a role in autonomic control of the heart. In studies 1 and 2, we investigated corticocardiac coupling in sudden death induced by asphyxia that affects both the heart and the brain, or cardiac abnormalities. In the third project, we investigated corticocardiac coupling in forebrain ischemic stroke-induced sudden cardiac arrest rat model. EEG and ECG signals were simultaneously collected from 9 spontaneously hypertensive stroke-prone rats (SHRSP) and 8 Wistar-Kyoto (WKY) rats. Forebrain ischemic stroke resulted in 100% mortality in SHRSP rats within 14 hours, whereas no mortality was observed in control WKY rats. The functionality of both the brain and the heart were significantly altered in SHRSP compared to WKY rats after forebrain ischemia. In contrast to WKY rats, SHRSP rats exhibited intermittent surge of CCCoh, which was in parallel with elevated CCCon and reduced heart rate variability before sudden death, suggesting that an elevated brain-heart coupling is consistently associated with the disruption of the autonomic nervous system and the risk of sudden death.

Results from these three studies suggest that strong corticocardiac coupling may be a shared mechanism for sudden cardiac arrest in both rat models and human patients. This study could improve our understanding on the mechanism underlying sudden cardiac arrest, and may provide important information for prevention of sudden death.

Chapter 1 Introduction

1.1 Sudden cardiac arrest

Sudden cardiac death is defined as the unexpected natural death due to cardiac causes, heralded by abrupt loss of consciousness within 1 hour of the onset of acute symptoms or, if unwitnessed, within 24 hours of last being seen alive, in patients with or without preexisting heart diseases [Zipes, et al., 2006; Myerburg and Castellanos, 2015]. Sudden cardiac arrest is a leading cause of death in the United States and other countries. The overall survival rate of sudden cardiac arrest was found to be 4.6% in a North American analysis [Nichol et al., 2008]. In the United States alone, about 300,000 to 400,000 people of all ages experience sudden cardiac death each year, which accounts for approximately 5.6% of all causes of deaths [Stecker et al., 2014]. The incidence of sudden cardiac death is higher in male (76 per 100,000 population) than female (45 per 100,000 population) [Stecker et al., 2014]. In male, the incidence of sudden cardiac death exceeds many other causes of death, which includes lung cancer, prostate cancer, colorectal cancer, accidents, chronic lower respiratory disease, cerebrovascular disease, and diabetes mellitus (Table 1.1) [Stecker et al., 2014]. The incidence of sudden cardiac death in female is similar to lung cancer, cerebrovascular disease, and chronic lower respiratory disease, and is higher than that of many other causes of death, including breast cancer, colorectal cancer, Alzheimer disease, and accidents (Table 1.1) [Stecker et al., 2014]. The high incidence and mortality of sudden cardiac arrest among a variety of common diseases and cancers suggest that it remains a major public health problem.

Table 1.1 Mortality for sudden cardiac death, cancers, and common diseases. [modified from Stecker et al., 2014]

Disease	Male		Female	
	No. of death	Death rate	No. of death	Death rate
Sudden cardiac death	114,948 (99,722-131,505)	76 (66-87)	69,524 (58,152-82,294)	45 (37-53)
Lung cancer	88,527	59	70,040	45
Prostate*/Breast cancer#	28,464	19	40,576	26
Colorectal cancer	26,923	18	25,918	17
Cerebrovascular disease	52,073	35	79,769	49
Chronic lower respiratory disease	65,119	43	72,234	46
Diabetes mellitus*/ Alzheimer disease#	35,054	23	54,916	35
Accidents	75,022	50	42,999	28

*Only applicable to male, #only applicable to female, death rates are expressed per 100,000 national male or female population, parenthesis shows 95% confidence intervals.

Sudden cardiac death has a multitude of potential etiologies. It has been estimated that nearly 50% of people with sudden cardiac arrest has no previously diagnosed heart diseases [Stecker et al., 2014]. In patients aged 50 years and above, coronary artery disease and ischemic cardiomyopathy are the predominant causes of sudden cardiac death [Israel, 2014]. However, study in young patients ($\leq$ 35 years) showed that sudden cardiac death may occur in patients with structurally normal heart (Figure 1.1) [Papadakis et al., 2009]. Central nervous system disorders including epilepsy, ischemic stroke, intracranial bleeding, and traumatic head injury can result in sudden cardiac death [Finsterer and Wahbi, 2014]. Although the detailed physiological mechanism is unknown, it has been speculated that these cerebral abnormalities induce catastrophic cardiac events like severe bradycardia, ventricular tachycardia (VT), and ventricular fibrillation (VF), and eventually lead to sudden cardiac death through the disruption of the autonomic nervous system [Finsterer and Wahbi, 2014]. In addition to neurological disorders, asphyxia induced by drowning, abnormalities of breathing/statues asthmatics, or choking could also lead to sudden cardiac death [Papadakis et al., 2009]. The multifactorial properties of sudden cardiac death make its prediction, prevention, and management a challenging task.

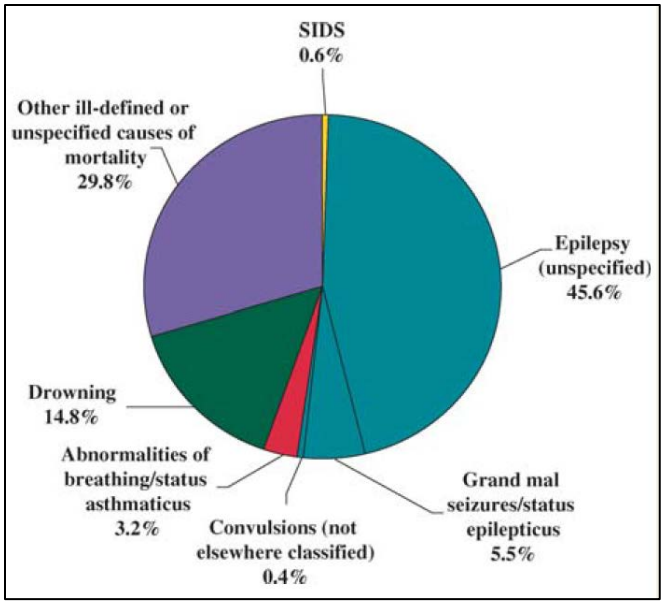

Figure 1.1 Causes of sudden cardiac death expressed as percentage of the total number of possible cardiac death in 433 young people. SIDS: sudden infant death syndrome. [Papadakis et al., 2009]

1.2 Conventional view on the mechanism of sudden cardiac arrest

As cardiac arrhythmias, including VT, VF, pulseless electrical activity (PEA), and asystole, are frequently the last events before death, the mechanisms causing these arrhythmias are often considered as the predominant mechanisms underlying sudden cardiac arrest [Israel, 2014]. Consequently, many current pharmacological treatments which include anti-ischemic interventions and heart failure therapies are targeting on the electrophysiological substrate or mechanisms that cause these detrimental arrhythmias. Although beneficial to patients who had advanced chronic heart diseases [Israel, 2014], these therapies have proven unsuccessful when applied to high or moderate risk patients without prior documented clinical arrhythmias [Fishman et al., 2010]. In addition, there is also no effective strategies for the prevention of sudden cardiac death. The combination of implantable cardioverter-defibrillator (ICD) with heart failure drug therapy is the main approach for sudden cardiac death prevention [Moss et al., 2002; Bardy et al., 2005], but is likely to benefit only the small population who can be identified at high risk for sudden cardiac arrest [de Vreede-Swagemakers et al., 1997; Stecker et al., 2006].

For low-risk individuals without established heart disease, which comprise the largest proportion of sudden cardia death, there is no effective preventive strategies available [Cupples et al., 1992; Albert et al., 2003; Gorgels et al., 2003].

The lack of effective methodologies for the prediction and prevention of sudden cardiac arrest may due to two major gaps with current research on sudden cardiac arrest: 1) The lack of clear understanding on the mechanism of sudden cardiac arrest. As sudden cardiac arrest could be induced by either abnormality with the heart (cardiovascular diseases), the brain (neurological disorders), or both the brain and the heart (asphyxia), it is possible that these detrimental cardiac arrhythmias are the indirect cause of sudden cardiac death. Simply focusing on these terminal arrhythmias may prevent us from identifying the most fundamental causes of sudden cardiac death. 2) The lack of novel research tools to investigate the mechanism underlying sudden cardiac arrest. Most current studies are investigating molecular and cellular events that happen on large time scale, like hours or days. To study sudden death events that occur within minutes or seconds, more advanced tools that could measure electrophysiological processes that happen on short time scale are needed.

1.3 New hypothesis on the mechanism of sudden cardiac arrest

1.3.1 The concept of brain-heart connection

A growing body of evidence from both psychological studies in healthy subjects and studies on neurocardiological diseases suggest that there might be a tight connection between the brain and the heart. The bidirectional brain-heart connection could be conceptualized from two perspectives: 1) The heart's effects on the brain. In normal physiological conditions, heartbeat evoked potential has been consistently detected in the cortical signals of subjects when

performing behavioral tasks [Gray et al., 2007; Baranauskas et al., 2017]. In disease conditions, cardiac arrhythmias could trigger neurological response, such as the sensation of cardiac pain. 2) The brain's effects on the heart. In normal conditions, activities such as yoga and meditation could lead to decrease in heart rate via activation of the vagus nerve [Kubota et al., 2001; Vinay et al., 2016]. In addition, fearful visual images, processed centrally, are well known to impact cardiac functions by elevating heart rate [Hagenaars et al., 2015]. In disease conditions, brain disorders such as stroke could induce cardiac arrhythmias or myocardial injury, and lead to sudden death via autonomic imbalance [Oppenheimer et al., 1991; Soros and Hachinski, 2012; Finsterer and Wahbi, 2014]. Through transneuronal labeling, functional magnetic resonance imaging (fMRI), and cortical stimulation studies, several forebrain regions, including the prefrontal cortex, insular cortex, cingulate cortex, and other subcortical and brainstem nuclei have been showed to send projections to cardioregulatory center and may be involved in moment-to-moment modulation of cardiac functions (Figure 1.2) [Palma and Benarroch, 2014].

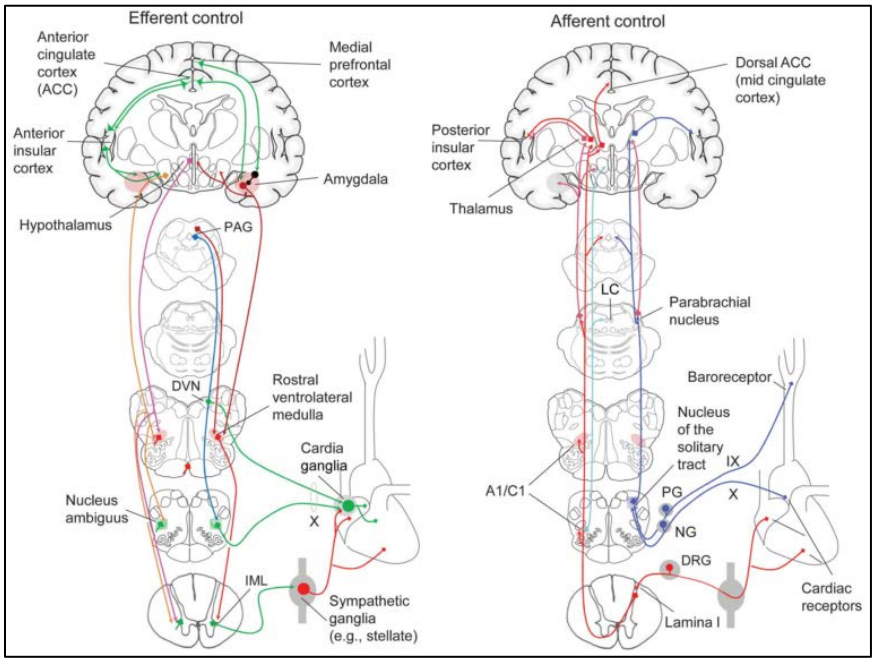

Figure 1.2 Efferent and afferent control of cardiac function. ACC: anterior cingulate cortex, PAG: periaqueductal gray, DVN: dorsal vagal nucleus, IML: intermediolateral, LC: locus ceruleus, PG: petrosal ganglion, NG: nodose ganglion, DRG: dorsal root ganglia. [Palma and Benarroch, 2014]

Though the concept of brain-heart connection has been brought up for years and abnormal brain-heart connection has been associated with many diseases like neurogenic heart diseases, cardiac source embolic stroke, and neurocardiac syndromes [Samuels, 2007], mechanism by which cortical neural circuitry affects cardiac function in normal and disease conditions remains unclear. In sudden cardiac arrest models, brain-heart connection has not been investigated comprehensively. It is generally believed that the brain does not play an active role during sudden cardiac arrest. This is partially due to several early studies in cardiac arrest animal models, which showed that EEG activity disappeared earlier than ECG signals during cardiac arrest (Figure 1.3) [Komura and Fujimura, 1974]. As a measurement of the electrical activity of the brain, the early termination of EEG than ECG was interpreted as the cessation of cortical functional activity before the devastating cardiac events. Thus, the brain was not considered to be involved in the dying process. Similar results have been obtained in several other sudden cardiac arrest animal models [Tisherman et al., 1985; Eshel et al., 1990; Coenen et al., 1995]. These data further strengthen the concept that brain damage occurs more rapidly than cardiac asystole and should not play a role in mediating sudden death.

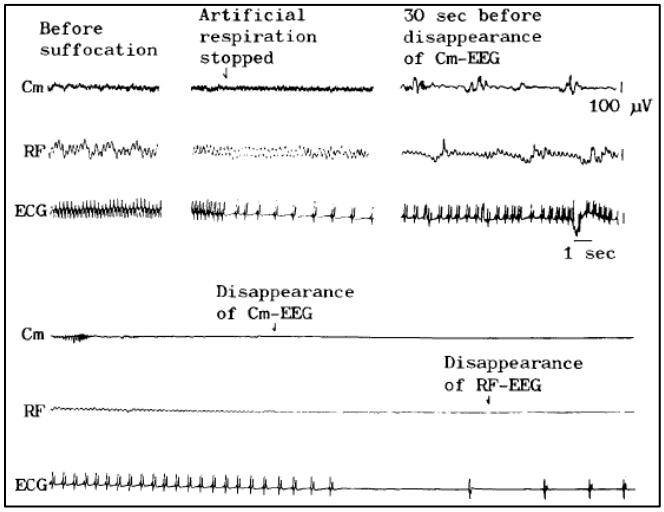

Figure 1.3 EEG and ECG from rabbits suffered from asphyxia by respiratory arrest. Cm: cortex sensitivo-motorius, surface EEG; RF: reticular formation, deep EEG. [Komura and Fujimura, 1974]

1.3.2 A well-organized series of high-frequency activity discovered in the brain after cardiac arrest

To systematically investigate the neurophysiological state of the brain following cardiac arrest, we performed continuous EEG and ECG recording in rats undergoing experimental cardiac arrest induced by intracardiac injection of KCl [Borjigin et al., 2013]. We identified a well-organized series of high-frequency activity in the brain after the heart stops (Figure 1.4). As shown in panel A, all signals seem to be isoelectric immediately after cardiac arrest. However, if we zoom in a 40-second-long epoch before and after cardiac arrest, as shown in panel B, we found that ECG signals stopped right after cardiac arrest, whereas EEG signals maintained normal amplitude for 3 seconds before transitioning to low-amplitude oscillations that lasted for about 30 seconds. According to its features, this cardiac arrest (CA) period was divided into 4 sequential and distinctive stages: CAS1, CAS2, CAS3, and CAS4. Further zoom in of these 4 representative stages after cardiac arrest revealed unique features associated with EEG signals. As shown in panel C, EEG signals showed marked increase in gamma oscillations in all 6 channels in CAS1. CAS2 displayed theta oscillations coupled with high-frequency gamma

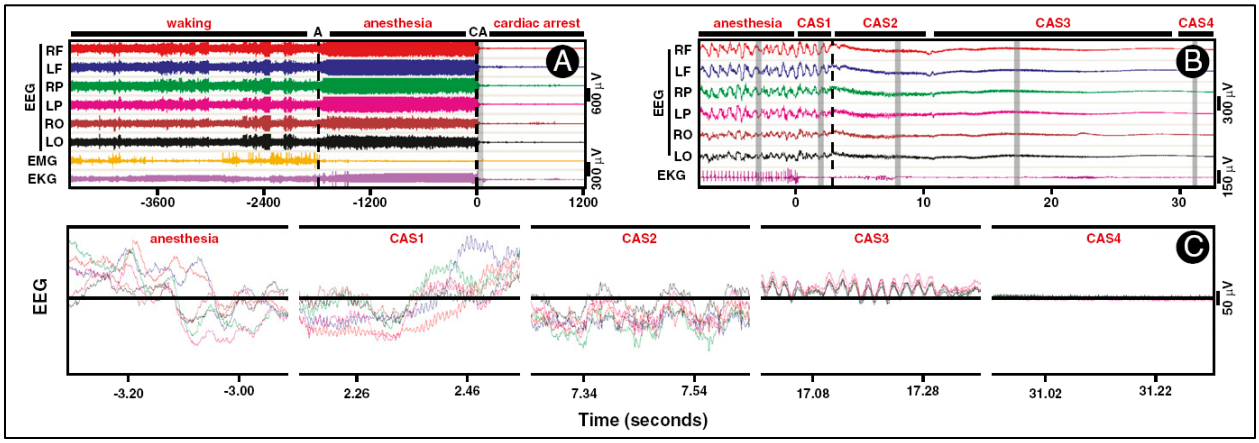

Figure 1.4 EEG displays a well-organized series of high-frequency activity following cardiac arrest. RF: right frontal, LF: left frontal, RP: right parietal, LP: left parietal, RO: right occipital, LO: left occipital, CAS: cardiac arrest stage. [Borjigin et al., 2013]

oscillations across all 6 channels. CAS3 is dominated by low-gamma oscillations that were highly synchronous. In CAS4, EEG signals become isoelectric. It is known that gamma signals are associated with waking consciousness, altered states of consciousness during meditation, and rapid eye movement (REM) sleep [Llinas and Ribary, 1993; Lutz et al., 2004; Fries, 2009; Cahn et al., 2010; Buzsaki and Wang, 2012]. Theta oscillations are important for synaptic plasticity, information coding, and working memory [Benchenane et al., 2010; Molter et al., 2012]. The significant increase in theta and gamma oscillations indicates that there are internally highly activated functional activities in the brain, even after the heart stops beating. Further analysis of EEG signals using advanced signal processing techniques, which include functional connectivity (coherence), effective (directional) connectivity, and cross-frequency coupling, demonstrates that there are high level of interregional coherence and feedback connectivity as well as cross-frequency coupling within the brain at near-death. In contrast to the conventional view that the brain is extremely quiet in the dying process, our data strongly suggest that the brain is highly aroused during cardiac arrest.

This study showed for the first time that the brain is highly activated during cardiac arrest. To future investigate the role of a highly activated brain in the dying process and its potential interaction with the heart, we performed a follow-up study [Li et al., 2015]. In that study, EEG and ECG signals were collected and analyzed in an asphyxic cardiac arrest model induced by CO_2 inhalation, which is the most common method of euthanasia for rats, mice, and many other small rodents. Different from KCl injection-induced cardiac arrest model used in previous study, in which the activity of the brain was measured when the cardiac activity was stopped, asphyxic cardiac arrest model allowed us to study the time-dependent deterioration of the brain and the heart at the same time. By simultaneous recording of EEG and ECG signals in

rats before and after asphyxia, possible interactions between the brain and the heart during cardiac arrest could be investigated.

1.3.3 A surge of corticocardiac coupling during asphyxia-induced sudden cardiac arrest

The electrical signal coupling and communication both within the brain and between the brain and the heart during asphyxic cardiac arrest were studied using coherence and directional connectivity analysis. While coherence is a well-established method to study the synchronization between electrical signals from two different brain loci, directional connectivity is widely used to investigate the causal information flow between two or more signals [Lee et al., 2009; Borjigin et al., 2013; Li et al., 2015]. We found that asphyxia stimulated a marked surge of coherence and directional connectivity both within the brain and between the brain and the heart during asphyxic cardiac arrest (Figure 1.5). As shown in panel A, heart rate changes exhibited four distinct phases A1, A2, A3, and A4 after CO_2 administrated at time 0. Immediately following

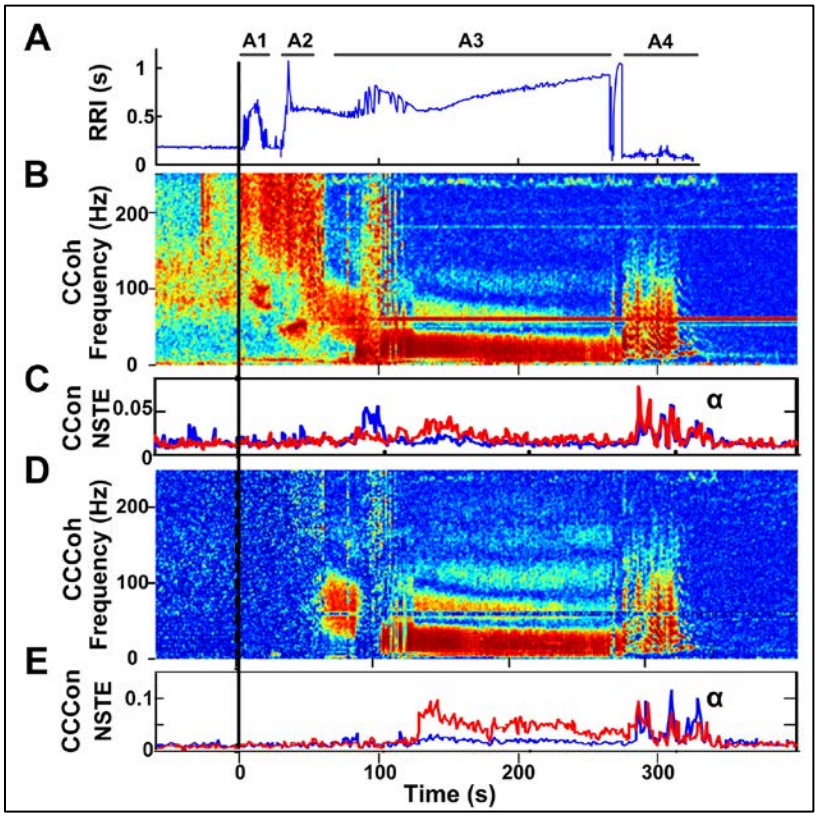

Figure 1.5 A surge of coherence and connectivity both within the brain and between the brain and the heart during asphyxic cardiac arrest. RRI: RR interval **(A)**, CCoh: cortical coherence **(B)**, CCon: cortical directional connectivity **(C)**, CCCoh: corticocardiac coherence **(D)**, CCCon: corticocardiac directional connectivity **(E)**, NSTE: normalized symbolic transfer entropy, red trace in panel C: frontal to parietal/occipital, blue trace in panel C: occipital/parietal to frontal, red trace in panel E: brain to heart, blue trace in panel E: heart to brain, alpha: 10-15Hz. [modified from Li et al., 2015]

asphyxia, there is a rapid increase of RR interval (RRI) followed by a complete recovery in A1 and a second surge of RRI followed by an incomplete recovery in A2. In parallel with the response of the heart to asphyxic challenge, the brain displayed intense coherent patterns (CCoh) in A1 and A2, especially for high frequency gamma rhythms, which are often associated with cognition and conscious perception (Figure 1.5B) [Panagiotaropoulos et al., 2012; Cavinato et al., 2015]. The lack of corticocardiac coherence (CCCoh) and corticocardiac directional connectivity (CCCon) during earlier stages of A1 and A2 suggest that there is no signal communication between the cortex and the heart in these early phases (Figure 1.5D and 1.5E). The immediate surge of high frequency CCoh and the dramatic fluctuations of RRI in A1 and A2 may be regulated by subcortical mechanisms. After this early phase of asphyxia, severe bradycardia with mild fluctuation of RRI is observed in A3 (Figure 1.5A). Interestingly, strong CCCoh, indicator for intense brain and heart electrical signal synchronization, appeared during this stage (Figure 1.5D). In addition, increased CCCon was also identified in A3, with the information flow from the brain to the heart dominants (Figure 1.5E). Based on these results, we postulated the following hypotheses: (1) Immediately after asphyxia onset, the heart may strive to restore its normal function using autonomic feedback loop; (2) When the autonomic feedback is insufficient to restore the normal function of the heart, as shown by the incomplete recovery of RRI in A2, the brain suspends all non-essential functions, and focuses on restoring basic cardiac function that is more fundamental for survival; (3) The ineffective restoration of RRI in A3 subsequently stimulated a more robust activation of the brain and corticocardiac coupling at higher frequency, which then triggered the onset of VT and VF in A4. The sequential changes of RRI, CCon, CCoh, CCCon, and CCCoh demonstrate that asphyxia activates a programmed surge of cortical activity and coupling between the brain and the heart during asphyxic cardiac arrest.

1.3.4 A dramatic release of cortical neurotransmitters during asphyxia-induced sudden cardiac arrest

To investigate the neurochemical basis of the increased cortical activities during cardiac arrest, microdialysis was performed in the frontal and occipital lobes of the rats before and after asphyxia. The results of 6 chemicals are shown in Figure 1.6. As expected, levels of glucose dropped rapidly within 2 minutes of asphyxia. A significant surge of secretion was detected for all 5 neurotransmitters, which includes adenosine, dopamine, norepinephrine, serotonin, and GABA. These neurotransmitters are known to be involved in the regulation of brain functional activities, such as arousal, attention, cognition, and hallucination [Inada et al., 1996; Espana et al., 2016; Carr et al., 2017]. Some of them are also involved in the regulation of cardiac functions. For example, elevated central norepinephrine is thought to act within the brainstem to

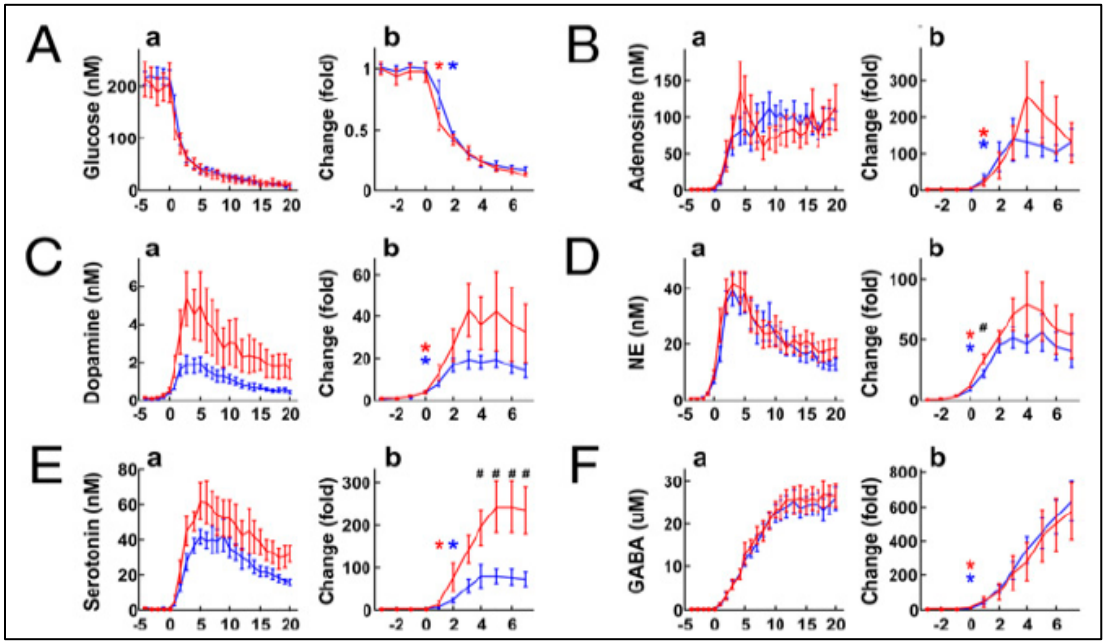

Figure 1.6 Asphyxia stimulated an immediate and marked surge of cortical neurotransmitter. Red tracing: frontal lobe, blue tracing: occipital lobe, star: significant increase over baseline, pound: significant difference between frontal and occipital lobes. [Li et al., 2015]

inhibit parasympathetic cardiac vagal neurons [Boychuk et al., 2011]. Serotonin plays an important role in the regulation of cardiovascular reflexes [Ramage and Villalon, 2008]. It has

been shown that overexpression of serotonin auto-receptor in the raphe complex results in autonomic dysregulation [Audero et al., 2008]. GABA release is known to be associated with the increased sympathetic tone and the inhibition of parasympathetic vagal neurons projecting to the heart [Zhong et al., 2008; Wang et al., 2010; Bowman and Goodchild, 2015]. The dramatically increased release of cortical neurotransmitters that are involved in the regulation of cardiac function suggests that the brain may play an important role in the regulation of the heart during asphyxic cardiac arrest. Although the detailed mechanisms of how the marked increase of neurotransmitter release after asphyxia mediates sudden cardiac arrest are still unknown, these data at least provide the neurochemical evidence to support that the brain actively participates in the regulation of cardiac functions during asphyxic cardiac arrest.

1.3.5 Cutting brain-heart connection prolongs survival after asphyxic cardiac arrest

Based on results from Figure 1.5 and Figure 1.6 that there is increased cortical functional activity and surge of key cortical neurotransmitters during asphyxic cardiac arrest, we hypothesize that the brain may play an important role in the dying process. To test this hypothesis, we studied the survival time for both the heart and the brain after disconnecting the heart from the brain using two approaches: 1) C7 transaction (C7X), which is spinal cord transection at cervical level 7. This surgery terminates all the sympathetic outflows traveling down the spinal cord. 2) Blockade of parasympathetic action using atropine. In this experiment, rats received C7X or sham surgery were treated without or with atropine 30 minutes before the onset of asphyxia. We found significantly longer survival time of both the heart (increased duration of ECG signal) and the brain (increased duration of CCoh) in rats received C7X, but this effect was not significantly affected by the injection of atropine (Figure 1.7) [Li et al., 2015]. These data indicate that asphyxia-stimulated brain-heart signaling during cardiac arrest is mediated mainly by the

sympathetic nervous system and the blockade of sympathetic nerves may be an effective approach to delay the death of both the heart and the brain.

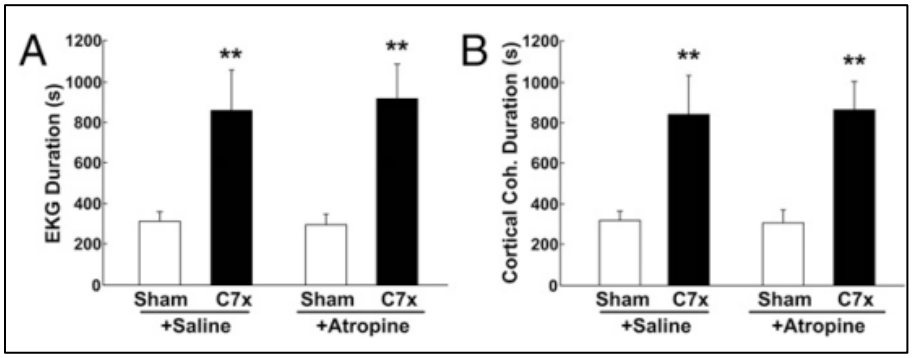

Figure 1.7 C7 transection prolongs the survival of both the heart and the brain during asphyxia cardiac arrest. C7X: C7 transection, $^{**}p < 0.01$. [Li et al., 2015]

In contrast, sympathetic agonist epinephrine is currently the primary drug administered during cardiopulmonary resuscitation to reverse cardiac arrest [Hermreck, 1988; Field et al., 2010]. Epinephrine has been used to resuscitate patients for 120 years and is recommended in American Heart Association (AHA) guidelines for advanced cardiovascular life support [Morrison et al., 2010; Neumar et al., 2010]. The addition of epinephrine into the guideline dramatically increases the number of patients who were given epinephrine. However, despite its long time use and incorporation into guidelines, epinephrine suffers from a lack of evidence regarding its effects on survival. A recent paper, reviewing 6 studies investigating whether epinephrine provides any overall benefits for patients, demonstrates that epinephrine administered during cardiac arrest has no benefit or even harmful effects for improving cardiac outcomes [Callaway, 2013]. There are also studies that showed that the use of epinephrine is significantly associated with decreased chance of survival and negative neurological outcomes [Herlitz et al., 1995; Stiell et al., 2004; Ohshige et al., 2005; Olasveengen et al., 2009; Hagihara et al., 2012]. These studies led us to conclude that stimulating the sympathetic nervous system

does not improve, but harm both the brain and the heart. Blockade of sympathetic nervous system may be the right approach to save the heart and the brain.

1.3.6 New hypothesis: corticocardiac coupling as a mechanism for sudden cardiac arrest

Based on the above discussion, we proposed a new mechanism for sudden cardiac arrest. Different from the conventional view that the brain is hypoactive during sudden cardiac arrest, our data strongly suggest that the brain plays an active role in mediating the dying process. This is supported by the robust and sustained activation of functional and effective connectivity within the brain, immediate and marked surge of a set of cortical neurotransmitters, and delayed activation of functional coupling and electrical signal communication between the brain and the heart at near-death. Instead of playing a passive role, we proposed that the brain plays an active role in mediating the dying process by sending strong electrical signals to resuscitate the heart, which unintentionally causes premature and rapid deterioration of the cardiac function via the over-activated sympathetic nervous system. Blockade of sympathetic signaling significantly delayed the death of both the heart and the brain and may become a promising approach for preventing sudden cardiac arrest and extending survival.

1.4 Overview of thesis project

As a follow-up of two previous studies [Borjigin et al., 2013; Li et al., 2015], the current thesis continued to investigate the mechanism of corticocardiac coupling in different sudden cardiac arrest models using advanced signal processing approaches. In Li et al., 2015, using C7X, we showed for the first time that activated brain sends harmful signals to the heart via the over-activated sympathetic nervous system. Since C7X is an invasive surgery, in **Chapter 2**, we tested if pharmacological blockade of sympathetic nervous system using alpha and beta blockers could

reproduce the results obtained from C7X in the same asphyxic cardiac arrest rat model (Figure 1.8). As sudden cardiac arrest could also be induced by abnormalities in the heart or neurological diseases, in addition to KCl injection-induced cardiac arrest rat model [Borjigin et al., 2013] and asphyxia-induced cardiac arrest rat model [Li et al., 2015], we studied corticocardiac coupling in two other models. In **Chapter 3**, we tested if corticocardiac coupling exist in human patient suffered from cardiac arrest. In **Chapter 4**, we investigated corticocardiac coupling in forebrain ischemic stroke-induced sudden cardiac arrest rat model. The understanding on the mechanism of corticocardiac coupling during sudden cardiac arrest is still in its early stage. Through this thesis project, we hope to establish that elevated corticocardiac coupling may be a basic common mechanism for sudden cardiac arrest induced by different causes and that the blockade of efferent sympathetic signaling is a potential effective strategy to prevent sudden cardiac arrest. This study is expected to have significant clinical impact, because it would build a new framework for understanding sudden cardiac arrest associated with different causes and for the development of effective strategies to prevent sudden cardiac arrest.

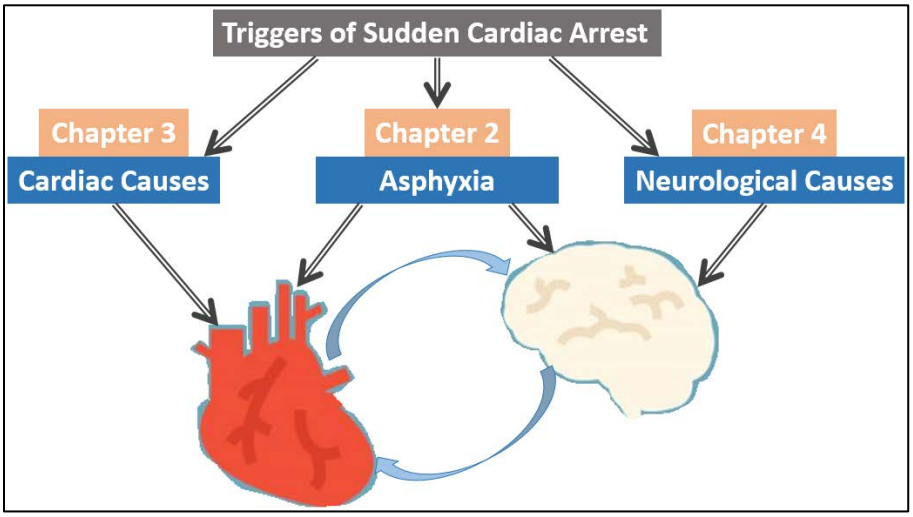

Figure 1.8 Overview of thesis project. Chapter 2: corticocardiac coupling in asphyxia-induced sudden cardiac arrest rat model. Chapter 3: corticocardiac coupling in a human patient died from cardiac arrest. Chapter 4: corticocardiac coupling in forebrain ischemic stroke-induced sudden cardiac arrest rat model.

1.5 References

Albert, C. M., Chae, C. U., Grodstein, F., Rose, L. M., Rexrode, K. M., Ruskin, J. N., . . . Manson, J. E. (2003). Prospective study of sudden cardiac death among women in the United States. Circulation, 107(16), 2096-2101. doi:10.1161/01.CIR.0000065223.21530.11

Audero, E., Coppi, E., Mlinar, B., Rossetti, T., Caprioli, A., Banchaabouchi, M. A., . . . Gross, C. (2008). Sporadic autonomic dysregulation and death associated with excessive serotonin autoinhibition. Science, 321(5885), 130-133. doi:10.1126/science.1157871

Baranauskas, M., Grabauskaite, A., & Griskova-Bulanova, I. (2017). Brain responses and self-reported indices of interoception: Heartbeat evoked potentials are inversely associated with worrying about body sensations. Physiol Behav, 180, 1-7. doi:10.1016/j.physbeh.2017.07.032

Bardy, G. H., Lee, K. L., Mark, D. B., Poole, J. E., Packer, D. L., Boineau, R., . . . Sudden Cardiac Death in Heart Failure Trial, I. (2005). Amiodarone or an implantable cardioverter-defibrillator for congestive heart failure. N Engl J Med, 352(3), 225-237. doi:10.1056/NEJMoa043399

Benchenane, K., Peyrache, A., Khamassi, M., Tierney, P. L., Gioanni, Y., Battaglia, F. P., & Wiener, S. I. (2010). Coherent theta oscillations and reorganization of spike timing in the hippocampal- prefrontal network upon learning. Neuron, 66(6), 921-936. doi:10.1016/j.neuron.2010.05.013

Borjigin, J., Lee, U., Liu, T., Pal, D., Huff, S., Klarr, D., . . . Mashour, G. A. (2013). Surge of neurophysiological coherence and connectivity in the dying brain. Proc Natl Acad Sci U S A, 110(35), 14432-14437. doi:10.1073/pnas.1308285110

Bowman, B. R., & Goodchild, A. K. (2015). GABA and enkephalin tonically alter sympathetic outflows in the rat spinal cord. Auton Neurosci, 193, 84-91. doi:10.1016/j.autneu.2015.08.006

Boychuk, C. R., Bateman, R. J., Philbin, K. E., & Mendelowitz, D. (2011). alpha1-adrenergic receptors facilitate inhibitory neurotransmission to cardiac vagal neurons in the nucleus ambiguus. Neuroscience, 193, 154-161. doi:10.1016/j.neuroscience.2011.07.024

Buzsaki, G., & Wang, X. J. (2012). Mechanisms of gamma oscillations. Annu Rev Neurosci, 35, 203-225. doi:10.1146/annurev-neuro-062111-150444

Cahn, B. R., Delorme, A., & Polich, J. (2010). Occipital gamma activation during Vipassana meditation. Cogn Process, 11(1), 39-56. doi:10.1007/s10339-009-0352-1

Callaway, C. W. (2013). Epinephrine for cardiac arrest. Curr Opin Cardiol, 28(1), 36-42. doi:10.1097/HCO.0b013e32835b0979

Carr, G. V., Maltese, F., Sibley, D. R., Weinberger, D. R., & Papaleo, F. (2017). The Dopamine D5 Receptor Is Involved in Working Memory. Front Pharmacol, 8, 666. doi:10.3389/fphar.2017.00666

Cavinato, M., Genna, C., Manganotti, P., Formaggio, E., Storti, S. F., Campostrini, S., . . . Piccione, F. (2015). Coherence and Consciousness: Study of Fronto-Parietal Gamma

Synchrony in Patients with Disorders of Consciousness. Brain Topogr, 28(4), 570-579. doi:10.1007/s10548-014-0383-5

Coenen, A. M., Drinkenburg, W. H., Hoenderken, R., & van Luijtelaar, E. L. (1995). Carbon dioxide euthanasia in rats: oxygen supplementation minimizes signs of agitation and asphyxia. Lab Anim, 29(3), 262-268. doi:10.1258/002367795781088289

Cupples, L. A., Gagnon, D. R., & Kannel, W. B. (1992). Long- and short-term risk of sudden coronary death. Circulation, 85(1 Suppl), I11-18.

de Vreede-Swagemakers, J. J., Gorgels, A. P., Dubois-Arbouw, W. I., van Ree, J. W., Daemen, M. J., Houben, L. G., & Wellens, H. J. (1997). Out-of-hospital cardiac arrest in the 1990's: a population-based study in the Maastricht area on incidence, characteristics and survival. J Am Coll Cardiol, 30(6), 1500-1505.

Eshel, G., Safar, P., Sassano, J., & Stezoski, W. (1990). Hyperthermia-induced cardiac arrest in dogs and monkeys. Resuscitation, 20(2), 129-143.

Espana, R. A., Schmeichel, B. E., & Berridge, C. W. (2016). Norepinephrine at the nexus of arousal, motivation and relapse. Brain Res, 1641(Pt B), 207-216. doi:10.1016/j.brainres.2016.01.002

Field, J. M., Hazinski, M. F., Sayre, M. R., Chameides, L., Schexnayder, S. M., Hemphill, R., . . . Vanden Hoek, T. L. (2010). Part 1: executive summary: 2010 American Heart Association Guidelines for Cardiopulmonary Resuscitation and Emergency Cardiovascular Care. Circulation, 122(18 Suppl 3), S640-656. doi:10.1161/CIRCULATIONAHA.110.970889

Finsterer, J., & Wahbi, K. (2014). CNS-disease affecting the heart: brain-heart disorders. J Neurol Sci, 345(1-2), 8-14. doi:10.1016/j.jns.2014.07.003

Fishman, G. I., Chugh, S. S., Dimarco, J. P., Albert, C. M., Anderson, M. E., Bonow, R. O., . . . Zheng, Z. J. (2010). Sudden cardiac death prediction and prevention: report from a National Heart, Lung, and Blood Institute and Heart Rhythm Society Workshop. Circulation, 122(22), 2335-2348. doi:10.1161/CIRCULATIONAHA.110.976092

Fries, P. (2009). Neuronal gamma-band synchronization as a fundamental process in cortical computation. Annu Rev Neurosci, 32, 209-224. doi:10.1146/annurev.neuro.051508.135603

Gorgels, A. P., Gijsbers, C., de Vreede-Swagemakers, J., Lousberg, A., & Wellens, H. J. (2003). Out-of-hospital cardiac arrest--the relevance of heart failure. The Maastricht Circulatory Arrest Registry. Eur Heart J, 24(13), 1204-1209.

Gray, M. A., Taggart, P., Sutton, P. M., Groves, D., Holdright, D. R., Bradbury, D., . . . Critchley, H. D. (2007). A cortical potential reflecting cardiac function. Proc Natl Acad Sci U S A, 104(16), 6818-6823. doi:10.1073/pnas.0609509104

Hagenaars, M. A., Mesbah, R., & Cremers, H. (2015). Mental Imagery Affects Subsequent Automatic Defense Responses. Front Psychiatry, 6, 73. doi:10.3389/fpsyt.2015.00073

Hagihara, A., Hasegawa, M., Abe, T., Nagata, T., Wakata, Y., & Miyazaki, S. (2012). Prehospital epinephrine use and survival among patients with out-of-hospital cardiac arrest. JAMA, 307(11), 1161-1168. doi:10.1001/jama.2012.294

Herlitz, J., Ekstrom, L., Wennerblom, B., Axelsson, A., Bang, A., & Holmberg, S. (1995). Adrenaline in out-of-hospital ventricular fibrillation. Does it make any difference? Resuscitation, 29(3), 195-201.

Hermreck, A. S. (1988). The history of cardiopulmonary resuscitation. Am J Surg, 156(6), 430-436.

Inada, T., Sugita, T., Dobashi, I., Inagaki, A., Kitao, Y., Matsuda, G., . . . Asai, M. (1996). Dopamine transporter gene polymorphism and psychiatric symptoms seen in schizophrenic patients at their first episode. Am J Med Genet, 67(4), 406-408. doi:10.1002/(SICI)1096-8628(19960726)67:4<406::AID-AJMG15>3.0.CO;2-N

Israel, C. W. (2014). Mechanisms of sudden cardiac death. Indian Heart J, 66 Suppl 1, S10-17. doi:10.1016/j.ihj.2014.01.005

Komura, S., & Fujimura, K. (1974). Heart rate and fatal course in rabbits asphyxiated by respiratory arrest. Tohoku J Exp Med, 114(3), 273-275.

Kubota, Y., Sato, W., Toichi, M., Murai, T., Okada, T., Hayashi, A., & Sengoku, A. (2001). Frontal midline theta rhythm is correlated with cardiac autonomic activities during the performance of an attention demanding meditation procedure. Brain Res Cogn Brain Res, 11(2), 281-287.

Lee, U., Kim, S., Noh, G. J., Choi, B. M., Hwang, E., & Mashour, G. A. (2009). The directionality and functional organization of frontoparietal connectivity during consciousness and anesthesia in humans. Conscious Cogn, 18(4), 1069-1078. doi:10.1016/j.concog.2009.04.004

Li, D., Mabrouk, O. S., Liu, T., Tian, F., Xu, G., Rengifo, S., . . . Borjigin, J. (2015). Asphyxia-activated corticocardiac signaling accelerates onset of cardiac arrest. Proc Natl Acad Sci U S A, 112(16), E2073-2082. doi:10.1073/pnas.1423936112

Llinas, R., & Ribary, U. (1993). Coherent 40-Hz oscillation characterizes dream state in humans. Proc Natl Acad Sci U S A, 90(5), 2078-2081.

Lutz, A., Greischar, L. L., Rawlings, N. B., Ricard, M., & Davidson, R. J. (2004). Long-term meditators self-induce high-amplitude gamma synchrony during mental practice. Proc Natl Acad Sci U S A, 101(46), 16369-16373. doi:10.1073/pnas.0407401101

Molter, C., O'Neill, J., Yamaguchi, Y., Hirase, H., & Leinekugel, X. (2012). Rhythmic modulation of theta oscillations supports encoding of spatial and behavioral information in the rat hippocampus. Neuron, 75(5), 889-903. doi:10.1016/j.neuron.2012.06.036

Morrison, L. J., Deakin, C. D., Morley, P. T., Callaway, C. W., Kerber, R. E., Kronick, S. L., . . . Advanced Life Support Chapter, C. (2010). Part 8: Advanced life support: 2010 International Consensus on Cardiopulmonary Resuscitation and Emergency Cardiovascular Care Science With Treatment Recommendations. Circulation, 122(16 Suppl 2), S345-421. doi:10.1161/CIRCULATIONAHA.110.971051

Moss, A. J., Zareba, W., Hall, W. J., Klein, H., Wilber, D. J., Cannom, D. S., . . . Multicenter Automatic Defibrillator Implantation Trial, I. I. I. (2002). Prophylactic implantation of a defibrillator in patients with myocardial infarction and reduced ejection fraction. N Engl J Med, 346(12), 877-883. doi:10.1056/NEJMoa013474

Myerburg R.J., Castellanos A (2015). Cardiac arrest and sudden cardiac death, in: Heart Disease: A Textbook of Cardiovascular Medicine, eds E. Braunwald, chap. 39;821-860.

Neumar, R. W., Otto, C. W., Link, M. S., Kronick, S. L., Shuster, M., Callaway, C. W., . . . Morrison, L. J. (2010). Part 8: adult advanced cardiovascular life support: 2010 American Heart Association Guidelines for Cardiopulmonary Resuscitation and Emergency Cardiovascular Care. Circulation, 122(18 Suppl 3), S729-767. doi:10.1161/CIRCULATIONAHA.110.970988

Nichol, G., Thomas, E., Callaway, C. W., Hedges, J., Powell, J. L., Aufderheide, T. P., . . . Resuscitation Outcomes Consortium, I. (2008). Regional variation in out-of-hospital cardiac arrest incidence and outcome. JAMA, 300(12), 1423-1431. doi:10.1001/jama.300.12.1423

Ohshige, K., Shimazaki, S., Hirasawa, H., Nakamura, M., Kin, H., Fujii, C., . . . Tochikubo, O. (2005). Evaluation of out-of-hospital cardiopulmonary resuscitation with resuscitative drugs: a prospective comparative study in Japan. Resuscitation, 66(1), 53-61. doi:10.1016/j.resuscitation.2004.10.019

Olasveengen, T. M., Sunde, K., Brunborg, C., Thowsen, J., Steen, P. A., & Wik, L. (2009). Intravenous drug administration during out-of-hospital cardiac arrest: a randomized trial. JAMA, 302(20), 2222-2229. doi:10.1001/jama.2009.1729

Oppenheimer, S. M., Wilson, J. X., Guiraudon, C., & Cechetto, D. F. (1991). Insular cortex stimulation produces lethal cardiac arrhythmias: a mechanism of sudden death? Brain Res, 550(1), 115-121.

Palma, J. A., & Benarroch, E. E. (2014). Neural control of the heart: recent concepts and clinical correlations. Neurology, 83(3), 261-271. doi:10.1212/WNL.0000000000000605

Panagiotaropoulos, T. I., Deco, G., Kapoor, V., & Logothetis, N. K. (2012). Neuronal discharges and gamma oscillations explicitly reflect visual consciousness in the lateral prefrontal cortex. Neuron, 74(5), 924-935. doi:10.1016/j.neuron.2012.04.013

Papadakis, M., Sharma, S., Cox, S., Sheppard, M. N., Panoulas, V. F., & Behr, E. R. (2009). The magnitude of sudden cardiac death in the young: a death certificate-based review in England and Wales. Europace, 11(10), 1353-1358. doi:10.1093/europace/eup229

Ramage, A. G., & Villalon, C. M. (2008). 5-hydroxytryptamine and cardiovascular regulation. Trends Pharmacol Sci, 29(9), 472-481.

Samuels, M. A. (2007). The brain-heart connection. Circulation, 116(1), 77-84. doi:10.1161/CIRCULATIONAHA.106.678995

Soros, P., & Hachinski, V. (2012). Cardiovascular and neurological causes of sudden death after ischaemic stroke. Lancet Neurol, 11(2), 179-188. doi:10.1016/S1474-4422(11)70291-5

Stecker, E. C., Reinier, K., Marijon, E., Narayanan, K., Teodorescu, C., Uy-Evanado, A., . . . Chugh, S. S. (2014). Public health burden of sudden cardiac death in the United States. Circ Arrhythm Electrophysiol, 7(2), 212-217. doi:10.1161/CIRCEP.113.001034

Stecker, E. C., Vickers, C., Waltz, J., Socoteanu, C., John, B. T., Mariani, R., . . . Chugh, S. S. (2006). Population-based analysis of sudden cardiac death with and without left ventricular systolic dysfunction: two-year findings from the Oregon Sudden Unexpected Death Study. J Am Coll Cardiol, 47(6), 1161-1166. doi:10.1016/j.jacc.2005.11.045

Stiell, I. G., Wells, G. A., Field, B., Spaite, D. W., Nesbitt, L. P., De Maio, V. J., . . . Ontario Prehospital Advanced Life Support Study, G. (2004). Advanced cardiac life support in out-of-hospital cardiac arrest. N Engl J Med, 351(7), 647-656. doi:10.1056/NEJMoa040325

Tisherman, S., Chabal, C., Safar, P., & Stezoski, W. (1985). Resuscitation of dogs from cold-water submersion using cardiopulmonary bypass. Ann Emerg Med, 14(5), 389-396.

Vinay, A. V., Venkatesh, D., & Ambarish, V. (2016). Impact of short-term practice of yoga on heart rate variability. Int J Yoga, 9(1), 62-66. doi:10.4103/0973-6131.171714

Wang, L., Bruce, G., Spary, E., Deuchars, J., & Deuchars, S. A. (2010). GABA(B) Mediated Regulation of Sympathetic Preganglionic Neurons: Pre- and Postsynaptic Sites of Action. Front Neurol, 1, 142. doi:10.3389/fneur.2010.00142

Zhong, M. K., Shi, Z., Zhou, L. M., Gao, J., Liao, Z. H., Wang, W., . . . Zhu, G. Q. (2008). Regulation of cardiac sympathetic afferent reflex by GABA(A) and GABA(B) receptors in paraventricular nucleus in rats. Eur J Neurosci, 27(12), 3226-3232. doi:10.1111/j.1460-9568.2008.06261.x

Zipes, D. P., Camm, A. J., Borggrefe, M., Buxton, A. E., Chaitman, B., Fromer, M., . . . Heart Rhythm, S. (2006). ACC/AHA/ESC 2006 Guidelines for Management of Patients With Ventricular Arrhythmias and the Prevention of Sudden Cardiac Death: a report of the American College of Cardiology/American Heart Association Task Force and the European Society of Cardiology Committee for Practice Guidelines (writing committee to develop Guidelines for Management of Patients With Ventricular Arrhythmias and the Prevention of Sudden Cardiac Death): developed in collaboration with the European Heart Rhythm Association and the Heart Rhythm Society. Circulation, 114(10), e385-484. doi:10.1161/CIRCULATIONAHA.106.178233

Chapter 2 Adrenergic blockade bi-directionally and asymmetrically alters functional brain-heart communication and prolongs electrical activities of the brain and heart during asphyxic cardiac arrest

2.1 Introduction

Fatal cardiac arrest affects more than 400,000 Americans each year [Chugh et al., 2008; Stecker et al., 2014]. Despite decades of intensive research efforts, survival rate from cardiac arrest is only about 5% [Nolan et al., 2012; Stecker et al., 2014]. Sudden death occurs in patients with cardiovascular disease as well as those with no known history of heart disease, including individuals with ischemic stroke, traumatic brain injury, epilepsy, chronic obstructive pulmonary disease, and asphyxia [Samuels, 2007; Sörös and Hachinski, 2012; Israel, 2014; Lahousse et al., 2015]. Unfortunately, current studies of cardiac arrest are largely focused on the cardiovascular pathology and methods of cardiac resuscitation; very little attention has been given to the role of the brain prior to the arrest of the heart.

Recent studies from our laboratory demonstrate that the brain plays a key role in cardiac arrest. Experimental cardiac arrest [Borjigin et al., 2013] and asphyxic cardiac arrest [Li et al., 2015a] both lead to a rapid surge of functional connectivity (coherence) and effective connectivity in the dying brain. The marked surge of cortical coherence (CCoh) and directional cortical connectivity (CCon) paralleled dramatically increased release of a set of core neurotransmitters in the brain [Li et al., 2015a]. Importantly, asphyxia activates a delayed surge of cortex-heart coupling, a novel form of communication measured by corticocardiac coherence

(CCCoh) and directional corticocardiac connectivity (CCCon) [Li et al., 2015a]. We hypothesized that the stimulated brain functions to resuscitate the heart internally by activating the sympathetic nervous system [Li et al., 2015a], the main mechanism thought to lead to sudden cardiac arrest in high risk patients [Samuels, 2007; Dhalla et al., 2010]. Past studies have shown that experimental cardiac arrest stimulates excessive neural release of catecholamines leading to fatal ventricular arrhythmias [Foley et al., 1987; Borovsky et al., 1998; Dhalla et al., 2010]. Consistent with these reports, a marked surge of cardiac sympathetic activity was reported in patients with sustained ventricular arrhythmias [Meredith et al., 1991]. These data demonstrate that increased cardiac sympathetic activity is causally linked with cardiac failures [Samuels, 2007; Taggart et al., 2011; Silvani et al., 2016].

Beta blockers (blockers of beta-adrenergic receptors) are widely used to manage cardiac arrhythmias and to prevent a second myocardial infarction in heart attack patients [Yusuf et al., 1985; Freemantle et al., 1999; Bourque et al., 2007] and are shown to reduce the incidence of ventricular fibrillation (VF) after acute myocardial infarction [Rydén et al., 1983; Norris et al., 1984]. Despite the mounting evidence for the positive effects of beta blockers to protect diseased hearts, the mechanism by which beta-blockers prevent ventricular arrhythmias is not well understood [Yusuf et al., 1985; Bourque et al., 2007].

In our earlier study [Li et al., 2015a], surgical blockade of efferent neuronal outflows travelling down the spinal cord below the cervical level 7 (C7) significantly extends the electrical activities of both the heart and the brain in the dying rats. Since sympathetic signals exit the spinal cord below C7 in rats, the beneficial effects of the C7 transection procedure is likely mediated by the blockade of sympathetic impact on the heart. The present study is designed to test if and how pharmacological blockade of the adrenergic receptors of the heart influences the

cortical oscillations and changes the dynamics of the brain-heart electrical coupling in CO_2-mediated asphyxic cardiac arrest model.

The sympathetic nervous system regulates the cardiovascular function via both alpha- and beta-adrenergic receptors. While alpha- and beta-adrenergic receptor blockers are used together to increase efficacy of hypertension treatment [Ram and Kaplan, 1979; Wong et al., 2015], their combined impact on delaying the onset of cardiac arrest has not been evaluated. In this study, we tested the impact of phentolamine (non-selective alpha adrenergic receptor blocker) and atenolol (selective beta-1 adrenergic receptor blocker), alone or combined, on the duration of cortical and cardiac electrical activity, CCoh, CCCoh, and CCCon in asphyxic rats.

2.2 Materials and methods

2.2.1 Animals

Inbred male Fischer 344 rats from Harlan were acclimatized in our housing facility for at least 1 week before surgical implantation of electrodes. After implantation, rats were allowed to recover for at least 1 week before online recording. All experiments were conducted using adult rats (300-400 g) maintained on a light: dark cycle of 12: 12 hour and provided with ad libitum food and water. This study was carried out in accordance with the recommendations of the University of Michigan Committee on Use and Care of Animals. The protocol was approved by the University of Michigan Committee on Use and Care of Animals.

2.2.2 Electrode implantation and configuration

Rats were implanted with electrodes for ECG and EEG recording under surgical anesthesia [1.8% (vol/vol) isoflurane]. ECG was recorded through flexible and insulated multi-stranded wires (Cooner Wire) inserted into the subcutaneous muscles flanking the heart. EEG was

recorded through screw electrodes implanted bilaterally on the frontal [anteroposterior (AP): + 3.0 mm; mediolateral (ML): ± 2.5 mm, bregma], parietal (AP: -3.0 mm; ML ± 2.5 mm, bregma), and occipital (AP: -8.0 mm; ML: ± 2.5 mm, bregma) cortices. A nose electrode was used as the EEG reference (Borjigin et al., 2013). The ECG and EEG electrodes were interfaced with two six-pin pedestals (Plastics One) and secured on the skull with dental acrylic.

2.2.3 Signal acquisition

Before data collection, rats were acclimatized overnight in the recording chamber. ECG and EEG were recorded using Grass Model 15LT physiodata amplifier system (15A54 Quad amplifiers, Astro-Med, Inc.) interfaced with BIOPAC MP-150 data acquisition unit and AcqKnowledge software (version 4.1.1, BIOPAC Systems, Inc.). Signals were filtered between 0.1 and 300 Hz and sampled at 1,000 Hz. ECG and EEG recordings were initiated consistently at 10:00 am to control for circadian factors. The rats were divided into 4 groups. Baseline signals were recorded for at least 30 minutes for all the rats. Then each group of rats received either saline (n=10), phentolamine (10mg/kg, n=7), atenolol (10mg/kg, n=8), or phentolamine plus atenolol (10mg/kg, 10mg/kg, n=11). Thirty minutes after drug injection, cardiac arrest was induced by inhalation of CO_2 (30%) for 2 minutes. Recording was continued for another 30 minutes after asphyxia.

2.2.4 Analysis of RR interval (RRI) and cardiac arrhythmias

To analyze the RRI (the time intervals between the R-peaks of two adjacent heartbeats), baseline drift correction was first implemented using second-order Butterworth high-pass filtering with a cutoff frequency at 1 Hz (butter.m and filtfilt.m in Matlab Signal Processing Toolbox; MathWorks Inc.). R-peak of ECG signals was then detected using variable threshold method [Kew and Jeong, 2011]. Specifically, an amplitude threshold in each nonoverlapping 1 s epoch

was applied to select the candidates for R peaks, which can be verified only if the RRI value exceeds a predefined threshold. In this study, the interval threshold was selected as half of the median value of the RRI values in the last 1 s epoch. The automatically detected R peaks were manually validated through a custom user interface developed in Matlab (MathWorks Inc.). To analyze the number and types of cardiac arrhythmias, ECG signals were examined and cardiac arrhythmias were manually labeled using a custom user interface developed in Matlab (MathWorks Inc.).

2.2.5 Construction of electrocardiomatrix (ECM)

The ECM is designed to facilitate the visualization of RRI, the amplitude, and the morphology of ECG signals. For construction of ECM [Li et al., 2015b], a window centered on the detected ECG R peaks (for example, from - 0.1 s to 0.3 s, with 0 corresponding to the time of R-peak) was extracted from the ECG signal after baseline drift correction. All ECG windows were sorted according to the order of R-peak time and then plotted as parallel colored lines to form a colored rectangular image. The intensity of ECG signal was denoted on *z*-axis, with warmer color indicates positive peaks with higher voltage, while cooler color indicates negative peaks with lower voltage. The color scheme could be adjusted according to the need.

2.2.6 Analysis of CCoh and CCCoh

The coherence between six EEG channels (CCoh) or between one ECG and each of the six EEG channels (CCCoh) were measured by amplitude squared coherence ($C_{xy}(f)$) (mscohere.m in Matlab Signal Processing Toolbox; MathWorks Inc.), which is a coherence estimate of the input signals x and y using Welch's averaged, modified periodogram method. The magnitude squared

coherence $C_{xy}(f)$ is a function of frequency with values between 0 and 1 that indicates how well signal x corresponds to signal y at each frequency.

$$C_{xy}(f) = \frac{|P_{xy}(f)|^2}{P_{xx}(f)P_{yy}(f)}, 0 \leq C_{xy}(f) \leq 1 \qquad (1)$$

where $P_{xx}(f)$ and $P_{yy}(f)$ are the power spectral density of x and y, and $P_{xy}(f)$ is the cross power spectrum spectral density.

In current study, electrophysiological signals were first segmented into 2 s epochs with 1 s overlap. The magnitude squared coherence was then calculated at each epoch and frequency bin (from 0.5 to 250 Hz). Before coherence analysis, a notch filter was used to remove the 60 Hz artifact and its possible super-harmonics. For each rat, the mean coherence among 15 pairs of six EEG channels (Figure 2.2A), the mean coherence among one ECG and six EEG channels (Figure 2.5A), as well as the coherence between one ECG and each of the six EEG channels (6 pairs; Figure 2.6A) were calculated and plotted for frequencies from 0.5 to 250 Hz. The mean and standard deviation (SD) of coherence between one ECG and six EEG channels (Figure 2.5B) and the coherence between one ECG and each of the six EEG channels (Figure 2.6B) were calculated for frequencies from theta to gamma 1 (theta: 5-10 Hz, alpha: 10-15 Hz, beta: 15-25 Hz, and gamma 1: 25-55 Hz).

2.2.7 Analysis of CCCon

The directional connectivity between the heart and brain (or between one ECG and each of the six EEG channels, CCCon) was measured by a modified [Li et al., 2015a] Normalized Symbolic Transfer Entropy (NSTE) method [Lee et al., 2009], which is a nonlinear and model-free estimation of directional functional connection based on information theory. STE denotes the amount of information provided by the additional knowledge from the past of the source signal

X (X^P) in the model describing the information between the past Y (Y^P) and the future Y (Y^F) of the target signal Y, which is defined as follows:

$$STE_{X\to Y} = I(Y^F; X^P|Y^P) = H(Y^F|Y^P) - H(Y^F|X^P, Y^P) \quad (2)$$

where $H(Y^F|Y^P)$ is the entropy of the process Y^F conditional on its past. Each vector for Y^F, X^P *and* Y^P is a symbolized vector point. The potential bias of STE was removed with a shuffled data, and the unbiased STE is normalized as follows:

$$NSTE_{X\to Y} = \frac{STE_{X\to Y} - STE_{X\to Y}^{Shuffled}}{H(Y^F|Y^P)} \in [0, 1] \quad (3)$$

where $STE_{X\to Y}^{Shuffled} = H(Y^F|Y^P) - H(Y^F|X_{Shuff}^P, Y^P)$. X_{Shuff}^P is a shuffled data created by dividing the data into sections and rearranging them at random. Therefore, NSTE is normalized STE (dimensionless), in which the bias of STE is subtracted from the original STE and then divided by the entropy within the target signal, $H(Y^F|Y^P)$.

For CCCon, the feedback (FB) connectivity ($\overline{NSTE}_{EEG\to EKG}$) was calculated by averaging NSTE over six pairs of EEG channels to ECG channel, which are defined as follows:

$$\overline{NSTE}_{EEG\to EKG} = \frac{1}{n_{EEG}} \sum_{i=1}^{n_{EEG}} NSTE_{i\to EKG} \quad (4)$$

where $n_{EEG} = 6$. The feedforward (FF) connectivity ($\overline{NSTE}_{EKG\to EEG}$) from the ECG to six EEG channels is vice versa.

Specifically, we first filtered EEG and ECG signals into 4 frequency bands (theta, alpha, beta, and gamma 1) and then segmented the filtered signals into 2 s long epochs with 1 s overlapping. The mean CCCon ($\overline{NSTE}_{EEG\to EKG}$ and $\overline{NSTE}_{EKG\to EEG}$) were sequentially calculated for each epoch and each frequency band. Three parameters: embedding dimension (d_E), time delay (τ), and prediction time (δ), were required in the calculation. In this study, we selected the parameter setting that could yield maximum $NSTE_{X\to Y}$ by fixing the embedding dimension (d_E)

at 3, and optimizing prediction time δ (from 1 to 50, corresponding to 1-50 ms with the sampling frequency of 1,000 Hz) and time delay τ (1-300 ms). The same procedure was used to calculate $NSTE_{Y\rightarrow X}$, provided that the information between two signals is transferred through different neuronal pathway. The mean and SD of the averaged CCCon for all 4 frequencies among six EEG channels (Figure 2.8) and that for each of the six EEG channels (6 pairs; Figure 2.9) were calculated and plotted.

2.2.8 Statistical analysis

For all of the statistical analyses, Shapiro-Wilk normality test was first implemented to determine if the data was normally distributed. To test the differences of ECG duration (defined as the duration from the asphyxia onset at time 0 until the onset of isoelectric activity; Figure 2.1B), CCoh duration (Figure 2.2B), mean CCoh during A3 phase (Figure 2.3C), RRI change (Figure 2.5Ab), mean CCCoh (Figure 2.6B) and mean CCCon (Figure 2.8B) among 4 groups of rats, as well as the mean CCCoh (Figure 2.6B) and CCCon (Figure 2.8B) among six EEG channels, one way ANOVA with Bonferroni post hoc comparisons (for normally distributed data) or Kruskal-Wallis Test with Mann-Whitney post hoc comparisons (for non-normally distributed data) were used. To analyze the correlation between ECG duration and CCoh duration (Figure 2.4), between RRI change and ECG duration (Figure 2.5Ba), and between RRI change and CCoh duration (Figure 2.5Bb), Pearson (for normally distributed data) or Spearman (for non-normally distributed data) correlation analysis was performed. For all the comparisons, $p < 0.05$ was considered as statistically significant. Statistical analyses were carried out in consultation with the Center for Statistical Consultation and Research at the University of Michigan. Statistical analyses were performed using the software SPSS (version 19.0; IBM SPSS Statistics).

2.3 Results

2.3.1 Adrenergic blockade prolongs cardiac electrical activity during asphyxia

Cardiac electrical activity was investigated using ECM to facilitate the visualization of dynamic temporal changes of RRI and cardiac arrhythmias before and after asphyxia (Figure 2.1A). Raw ECG traces of representative rats were also included for traditional viewing (Supplement Figure 1 in Appendix). Before asphyxia, all 4 groups of rats had relatively stable RRI of about 0.2 sec with no cardiac arrhythmias. Following the onset of asphyxia, the RRI exhibited dramatic and distinct changes in the four groups of rats. We divided the changes of RRI and cardiac arrhythmias into 5 stages (A1 to A5) according to their cardiac features. Immediately following the asphyxia onset in saline treated rats (Figure 2.1Aa), RRI began to expand rapidly, from 0.2 sec at baseline to 0.6 sec at the peak within 10 sec (A1 stage), indicating a rapid onset of bradycardia. PR interval lengthened, suggestive of first-degree heart block. Furthermore, T-waves increased in peak height, and remained high for the entire bradycardia period in all rats. The A1 stage was followed by a transient recovery of RRI that lasted for about 20 sec (A2 stage). During this period, two cardiac features are worth noting: elevated T-wave peak height and peak duration and gradually lengthened PR interval. Stages A1 and A2 show similar durations among four groups of rats. The rapid increase of RRI at A1 was reproducibly observed in rats injected with saline (Figure 2.1Aa) and phentolamine (Figure 2.1Ab), but was less prominent in rats received atenolol (Figure 2.1Ac) and phentolamine plus atenolol (Figure 2.1Ad). T wave elevation was also noted in all 4 groups of rats during the A2 period, but no statistical significance was found between the groups. During this early phase of asphyxia, a variety of cardiac arrhythmias was identified in all rats, which includes premature atrial

contraction, premature junctional contraction, premature ventricular contraction, junctional rhythm, and sinus arrhythmias.

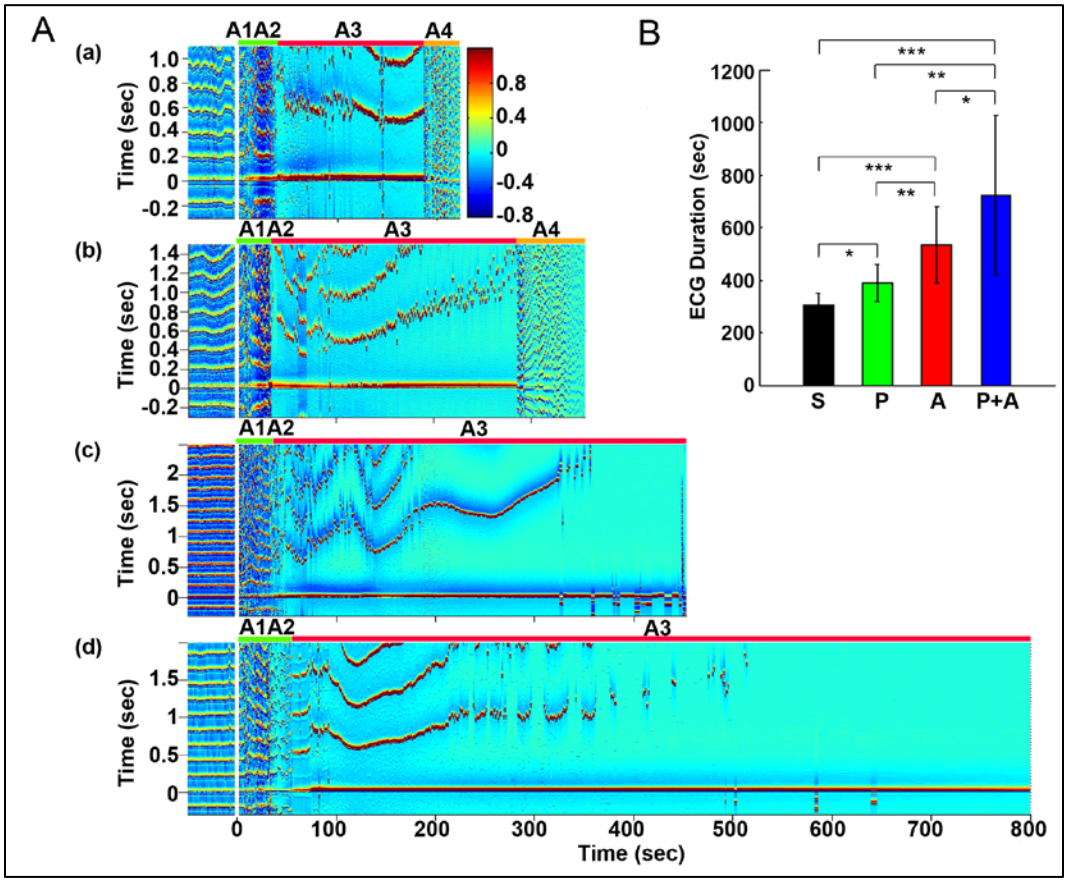

Figure 2.1 Adrenergic blockade prolongs cardiac survival. **(A)** Electrocardiomatrix (ECM) display of ECG signals before (50 sec) and after asphyxia in four groups of rats: (a) saline, (b) phentolamine, (c) atenolol, and (d) phentolamine plus atenolol. x axis shows time in seconds, y axis shows RR interval (RRI; in seconds), and z axis shows signal strength. Warmer color represents higher signal strength. Asphyxia was induced by CO_2 infusion at time 0 sec. **(B)** The mean and SD of ECG signal duration after asphyxia in four groups of rats: S (saline, n = 10), P (phentolamine, n = 7), A (atenolol, n = 8), and P+A (phentolamine plus atenolol, n = 11). Significant differences of ECG signal duration among 4 groups of rats are indicated using asterisks. Error bars denote SD (*$p < 0.05$, **$p < 0.01$, ***$p < 0.001$).

In contrast to the A1A2 period, the duration and cardiac arrhythmias in stages A3 and A4 varied significantly. During A3, all rats suffered bradycardia due to 2rd or 3rd degree atrioventricular blocks with sequential junctional and ventricular escape rhythms. RRI was expanded to as long as 1.4 sec (Figure 2.1Ab, stage A3), a 7-fold increase from the baseline values of 0.2 sec. This bradycardia period ended in sustained ventricular tachycardia (VT) during

A4 and VF during A5 period (not shown in ECM) in rats injected with saline and phentolamine. Interestingly, VT and VF were identified in only 1 of the 8 rats (12.5%) injected with atenolol and 2 of the 11 rats (18.2%) received phentolamine plus atenolol (Table 2.1). When VT and VF were blocked by these drugs, rats entered an isoelectric stage directly from the A3 stage, exhibiting 3rd degree heart block with ventricular escape beats. This result is consistent with the reported ability of beta blocker to reduce the incidence of ventricular arrhythmias in human patients [Patterson and Lucchesi, 1984; Bourque et al., 2007].

Table 2.1 Summary of ventricular tachycardia and ventricular fibrillation in four groups of asphyxic rats.

	Saline (n=10)	Phentolamine (n=7)	Atenolol (n=8)	Phentolamine + Atenolol (n=11)
V. Tachycardia	10/10 (100%)	7/7 (100%)	1/8 (12.5%)	2/11 (18.2%)
V. Fibrillation	10/10 (100%)	7/7 (100%)	1/8 (12.5%)	2/11 (18.2%)

To investigate the effects of adrenergic blockade on cardiac electrical activity, we compared the duration of ECG signals (that begins from the asphyxia onset to the beginning of the isoelectric state) in four groups of rats: saline (305 ± 45 sec; mean ± SD), phentolamine (389 ± 72 sec), atenolol (532 ± 145 sec), and phentolamine plus atenolol (723 ± 304 sec). We found a significant increase in the duration of ECG signals in rats received drugs (Figure 2.1B). Remarkably, rats received phentolamine plus atenolol had the most significant increase in the duration of ECG signals ($p < 0.001$).

2.3.2 Adrenergic blockade prolongs cortical functional connectivity

Cortical coherence (CCoh) was calculated before and after asphyxia (Figure 2.2). In all rats, EEG signals displayed intense coherence immediately after asphyxia for high gamma waves (> 150 Hz) and for theta waves. In addition, three distinct coherence clusters were noted in all rats:

gamma 3 (125-175 Hz), gamma 2 (65-115 Hz), and gamma 1 (25-55 Hz). Of these clusters, gamma 2 and 3 clusters occurred at the transitions between A1 and A2 stages, whereas the gamma 1 cluster occurred at the junction between the A2 and A3 states. The intensity and duration of these coherence clusters did not show significant differences among 4 groups of rats. During the bradycardia period (A3), EEG signals showed intense coherent activity at lower frequency ranges (5-55 Hz) with varying duration and intensity. In rats injected with saline and phentolamine, CCoh was intense and continuous. However, in rats injected with atenolol and phentolamine plus atenolol, CCoh was weaker and intermittent.

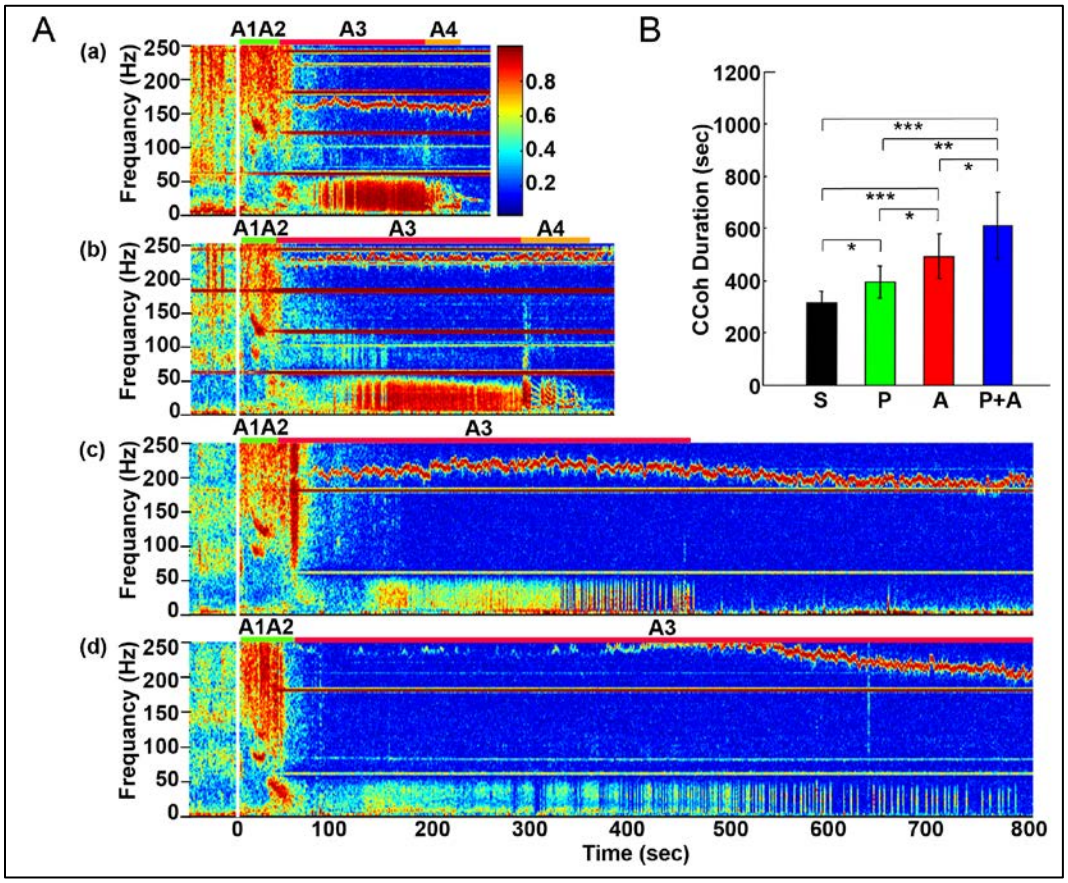

Figure 2.2 Adrenergic blockade prolongs cortical coherence (CCoh) duration. **(A)** CCoh (averaged over six EEG channels) before (50 sec) and after asphyxia in four groups of rats: (a) saline, (b) phentolamine, (c) atenolol, and (d) phentolamine plus atenolol. x axis shows time, y axis shows frequency, and z axis shows CCoh. Warmer color represents stronger CCoh. Asphyxia was induced at time 0 sec. **(B)** The mean and SD of CCoh duration after asphyxia in four groups of rats: S (saline, n = 10), P (phentolamine, n = 7), A (atenolol, n = 8), and P+A (phentolamine plus atenolol, n = 11). Significant differences of CCoh

duration among 4 groups of rats are indicated using asterisks. Error bars denote SD (*$p < 0.05$, **$p < 0.01$, ***$p < 0.001$).

To investigate the effects of adrenergic blockade on the length of functional activities of the brain, we compared the duration of CCoh in four groups of rats (Figure 2.2B): saline (314 ± 45 sec), phentolamine (394 ± 61 sec), atenolol (492 ± 86 sec), and phentolamine plus atenolol (608 ± 127 sec). We found significant increase in the duration of CCoh in all three drug groups from the saline treatment. Remarkably, rats received phentolamine plus atenolol had the most significant increase in the duration of CCoh ($p < 0.001$).

2.3.3 Adrenergic blockade abolishes cardiac event related potentials and cortical coherence during A3 specifically in the right hemisphere

To define the impact of the adrenergic drugs on local neuronal synchrony within the cortex, we analyzed cardiac event related potentials (CERP) [Li et al., 2015a] (Figure 2.3). EEG potentials (CERP) associated with ECG signals were seen in all rats during A3 phase of asphyxia, although they were undetectable in baseline or at early phase of asphyxia. CERP appeared evenly distributed among the 6 EEG electrodes in the saline treated rats, with slightly higher potential in the occipital lobes compared to the frontal lobes (Figure 2.3Aa). In the rat treated with both phentolamine and atenolol (Figure 2.3Ba), however, CERP was severely suppressed in all three electrodes specifically in the right hemisphere. This data demonstrates that adrenergic signaling underlies the CERP and its impact is dominant in the right cerebral hemisphere.

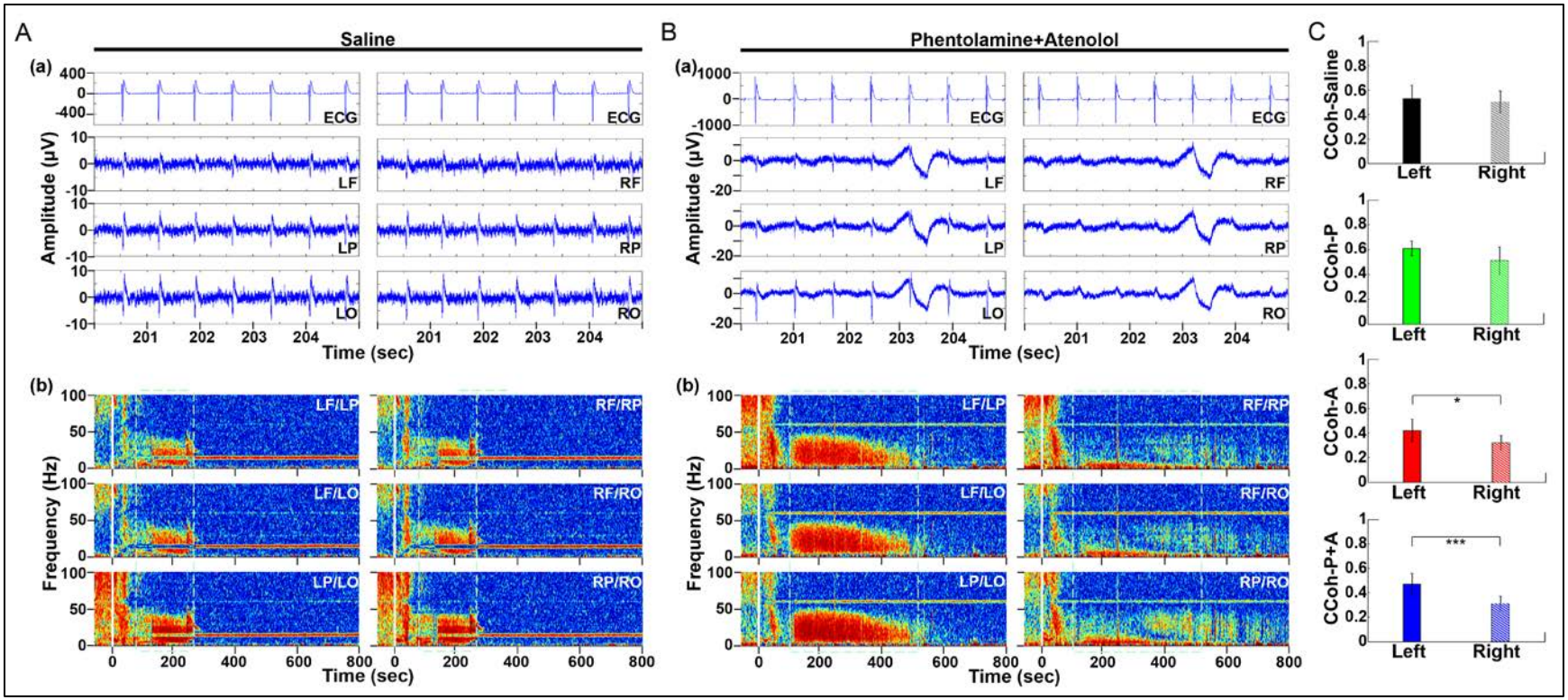

Figure 2.3 Adrenergic blockade leads to a marked hemispheric asymmetry of cardiac event related potential (CERP) and cortical coherence (CCoh). Raw ECG and EEG data (200-205 sec in A3), as well as CCoh raw data (50 sec before and 800 sec after asphyxia), for each hemispheric channel or channel-pair among the six EEG channels, is shown for one representative control rat **(A)** and a rat received phentolamine plus atenolol **(B)**. The blockers inhibit cardiac event related EEG potentials (Ba) and CCoh (Bb) specifically on the right hemisphere and the effects are more significant when phentolamine plus atenolol were used together **(C)**. Significant differences of mean pairs of CCoh, calculated for A3 at 5-55 Hz, are indicated using asterisks in panel C. LF: left frontal; RF: right frontal; LP: left parietal; RP: right parietal; LO: left occipital; RO: right occipital. Error bars denote SD (*$p < 0.05$, ***$p < 0.001$)

We also separated the coherence pairs formed between electrodes on the left hemisphere from those on the right hemisphere for both control and drug injected rats. Cortical coherence (CCoh) on the left cortex and the right cortex showed similar levels during A3 period (the white dashed boxes in Figure 2.3Ab) in a control rat. In a marked contrast, the CCoh on the right hemisphere was nearly abolished by the injected adrenergic blockers (Figure 2.3Bb). The drug-induced hemispheric asymmetry of CCoh during A3 was significant for rats when either atenolol or atenolol and phentolamine was used (Figure 2.3C). Importantly, when both phentolamine and atenolol were used together, the left and right asymmetry was more significant, compared to when either drug was used alone (Figure 2.3C). This data indicates that the drugs that do not penetrate the blood-brain-barrier can exert a major impact on the functional connectivity within the cerebral cortex during asphyxic cardiac arrest.

2.3.4 Brain functional connectivity parallels with cardiac electrical activity

Adrenergic blockade significantly prolonged both cardiac activity (Figure 2.1) and functional cortical connectivity (Figure 2.2) and longer survival was observed when both beta1- and alpha-adrenergic receptors were simultaneously inhibited. When ECG duration was compared with CCoh duration (Figure 2.4), a significance correlation between CCoh duration and ECG duration was found for each group of rats (saline: $r^2 = 0.974$, $p < 0.001$; phentolalamine: $r^2 = 0.969$, $p < 0.001$; atenolol: $r^2 = 0.731$, $p < 0.05$; phentolamine plus atenolol: $r^2 = 0.878$, $p < 0.01$). A significant correlation was found between CCoh duration and ECG duration ($r^2 = 0.983$, $p < 0.001$). Thus, the longer the brain was functioning, the longer the heart was signaling, despite a continued lack of oxygen supplies.

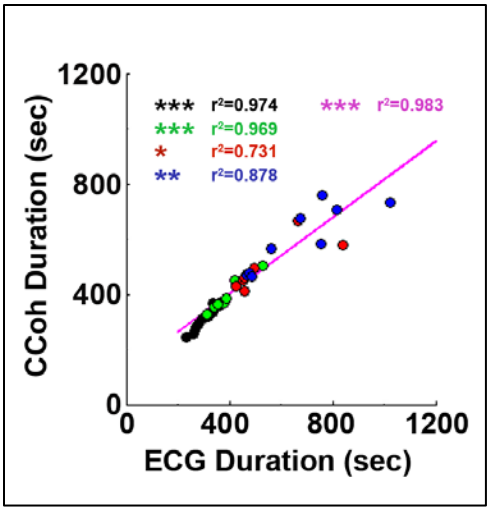

Figure 2.4 Cardiac survival parallels with cortical coherence (CCoh) duration. Each circle represents data from one rat. Linear regression line was plotted to show the correlation between ECG signal duration and CCoh duration for all four groups of rats. Significant correlations between ECG signal duration and CCoh duration are indicated using asterisks. Different color circles represent different treatment groups: saline control in black, phentolamine in green, atenolol in red and phentolamine plus atenolol in blue. The magenta color represents values obtained with all four groups of rats (n = 35). (*$p < 0.05$, **$p < 0.01$, ***$p < 0.001$).

2.3.5 Adrenergic blockade suppresses the initial heart-rate reduction induced by asphyxia

In Figure 2.1A, we noticed that during A1 and A2, the transient lengthening of RRI (i.e., reduction of heartrate) was less obvious in rats received atenolol and phentolamine plus atenolol than saline and phentolamine. To quantify these changes, we compared the initial rise of RRI in 4 groups of rats (Figure 2.5). Baseline RRI (RRI^{-CO2}) was obtained by averaging the RRI for 100 sec-long ECG data before asphyxia induction. RRI after asphyxia (RRI^{+CO2}) was defined by the first peak value of RRI after asphyxia. The RRI changes were expressed as percent changes of RRI after asphyxia versus baseline (RRI^{+CO2}*100/RRI^{-CO2}). We found that the initial increase of RRI was significantly suppressed by each drug (panel Ab), and that rats received both phentolamine and atenolol had the most significant suppression for RRI. When the extent of the RRI changes was compared with drug-dependent changes of ECG duration (Figure 2.5Ba) and CCoh duration (Figure 2.5Bb), significant correlations were found between RRI changes and

ECG duration (r^2 = -0.689, $p < 0.01$), and between RRI changes and CCoh duration (r^2 = -0.747, $p < 0.01$). These data demonstrate that a larger initial RRI expansion (thus a larger reduction of heart rate) was significantly associated with a shorter ECG duration and a shorter period of brain function.

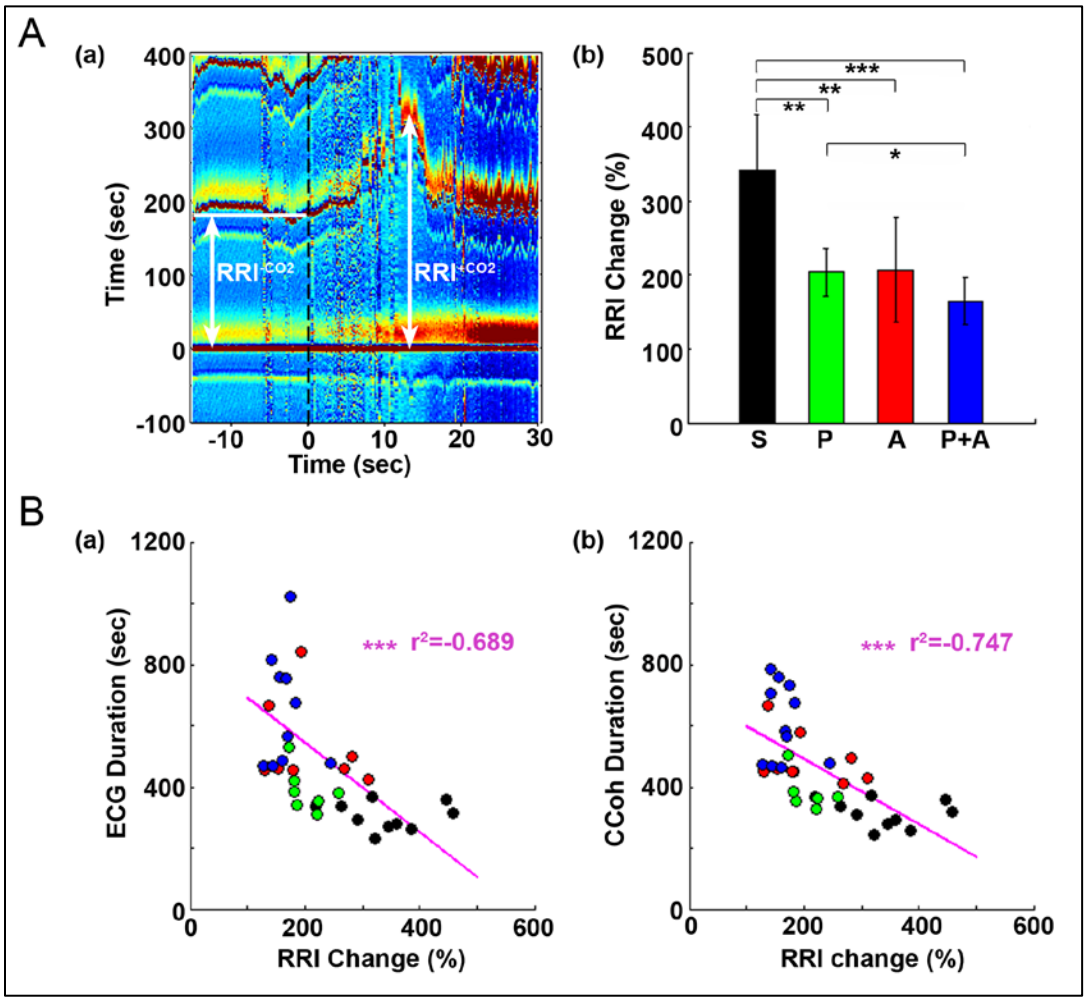

Figure 2.5 Adrenergic blockade suppresses the initial rise of RR interval (RRI), which negatively correlates with cardiac survival and cortical coherence (CCoh) duration. **(A)** Electrocardiomatrix (ECM) display of ECG signals -15 sec before and 30 sec after asphyxia for one control rat (panel a). RRI^{-CO2} represents the averaged baseline RRI (100 sec before asphyxia); RRI^{+CO2} indicates the peak amplitude of the first increase of RRI after asphyxia. The mean and SD of RRI change ($RRI^{+CO2}\times100/RRI^{-CO2}$) shows drug-specific changes (panel b). Significant differences of RRI among the rats are indicated using asterisks. Error bars denote SD (*$p < 0.05$, **$p < 0.01$, ***$p < 0.001$). **(B)** RRI changes are correlated with the survival times of both the heart (panel a) and the brain (panel b). Each circle represents data from one rat. Linear regression lines were plotted to show the correlation between RRI change and ECG duration (panel a), and between RRI change and CCoh duration (panel b) for all four groups of rats. Significant correlations between RRI change and ECG duration, or between RRI change and CCoh duration are indicated using asterisks (*$p < 0.05$, **$p < 0.01$, ***$p < 0.001$).

2.3.6 Adrenergic blockers suppress brain-heart communication

To explore the effects of adrenergic blockade on functional coupling between the brain and heart, we examined corticocardiac coherence (CCCoh) before and after asphyxia for all four groups of rats (Figure 2.6), a method developed in our previous study [Li et al., 2015a]. CCCoh was not detectable before asphyxia and during stages A1 and A2 in any of the rats. During bradycardia phase (A3), strong CCCoh at lower frequency (5-55 Hz) emerged with a delay, surged to its peak within 2 minutes of asphyxia, and persisted for as long as the ECG signal was detectable (Figure 2.6A). Similar to the CCoh examined earlier (Figure 2.2), CCCoh displayed different durations and distinct patterns among the different drug groups. In rats injected with saline and phentolamine, the duration of CCCoh was short, but the CCCoh was strong and continuous. However, in rats injected with atenolol and phentolamine plus atenolol, the duration of CCCoh was longer, but the CCCoh was weaker and intermittent.

To quantify the effects of adrenergic blockade on the functional coupling between the brain and the heart after asphyxia, we compared the mean intensity of CCCoh in four groups of rats (Figure 2.6B): saline (0.52 ± 0.068), phentolamine (0.55 ± 0.075), atenolol (0.38 ± 0.095), and phentolamine plus atenolol (0.41 ± 0.063). Since only a few of the rats treated with atenolol or atenolol with phentolamine exhibited ventricular tachycardia/fibrillation at the end of their lives (Table 1), we focused on the A3 period in all subsequent analysis. We found that the mean CCCoh levels was significantly lower in rats received either atenolol or phentolamine plus atenolol than saline or phentolamine alone. This data suggests that beta-adrenergic signaling plays a major role in mediating the brain and heart functional connectivity during asphyxic cardiac arrest. Interestingly, drug-dependent suppression of CCCoh was significantly higher on

the right hemisphere, compared to the left when rats received both alpha and beta-blockers (Figure 2.6C).

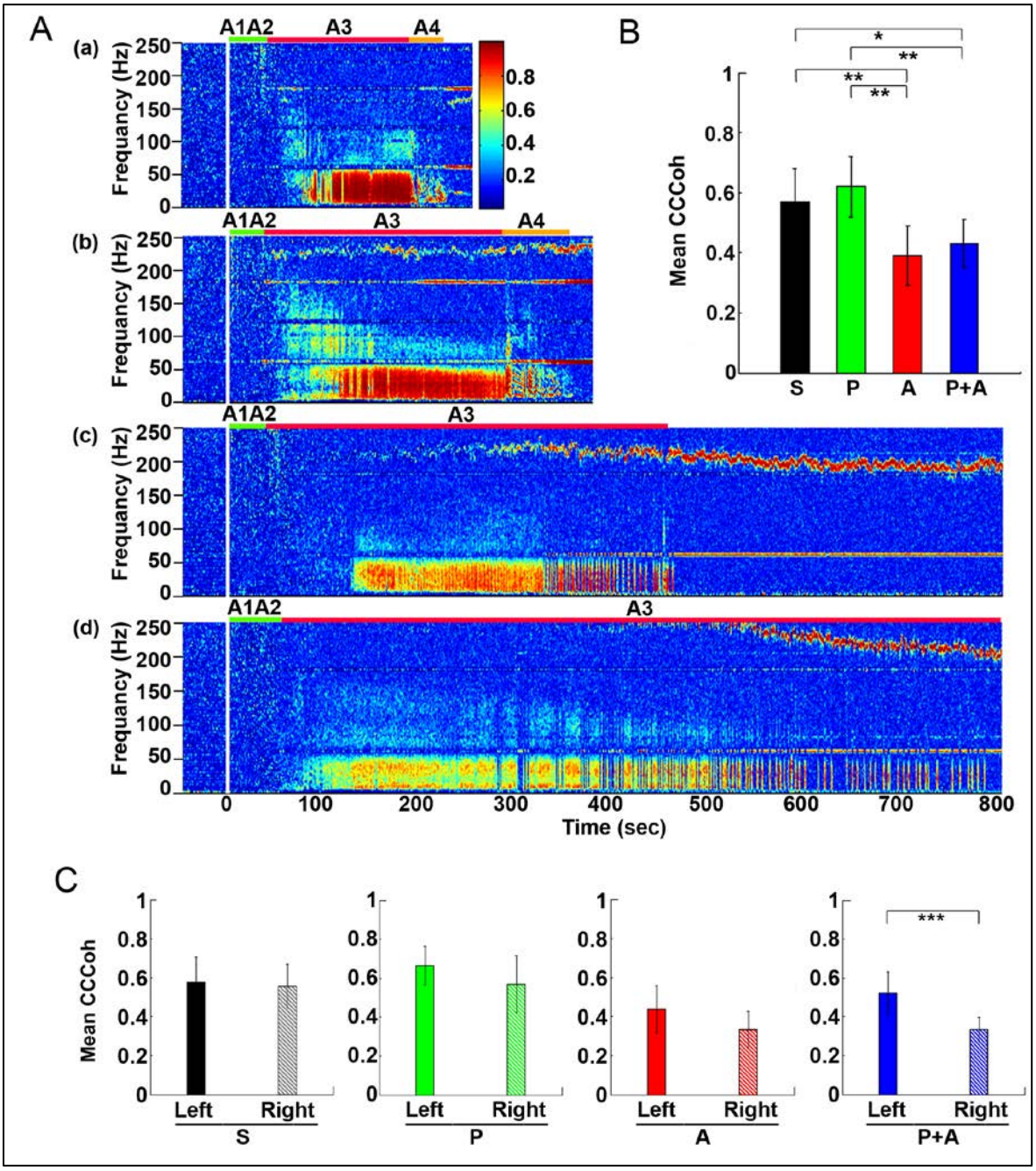

Figure 2.6 Adrenergic blockade decreases corticocardiac coherence (CCCoh). **(A)** CCCoh (averaged over all channel pairs) before (50 sec) and after asphyxia in four groups of rats: (a) saline, (b) phentolamine, (c) atenolol, and (d) phentolamine and atenolol. **(B)** The mean and SD of mean CCCoh (5-55Hz) after asphyxia in four groups of rats. **(C)** Impact of drugs on hemispheric asymmetry of CCCoh in four groups of rats. Significant differences of mean CCCoh among 4 groups of rats **(B)** or between the left and right side of the brain **(C)** are indicated using asterisks. Error bars denote SD (*p < 0.05, **p < 0.01, ***p < 0.001).

2.3.7 Adrenergic blockade results in marked asymmetry and regional specificity of heart-brain coupling

To further investigate the impact of adrenergic blockers on electrical coupling of the heart with the 6 different regions of the cortex, we examined the coherence between ECG signals and each of the six cortical signals (Figure 2.7). In rats received saline (panel Aa), CCCoh appeared equally strong at all brain sites and there were no apparent differences between the six cortical regions. In contrast, however, in rats received both phentolamine and atenolol (panel Ab), the right side of the cortex displayed marked reduction of CCCoh compared with the left side. Furthermore, there appeared to be a front-to-back gradient of CCCoh within the cortex, with frontal lobes exhibiting much weaker coupling with the heart than the occipital lobes (Figure 2.7A).

We quantified the differences in CCCoh among six cortical channels for each of the four groups of rats in A3 phase (Figure 2.7B). In general, the left side of the cortex appeared to have a stronger coupling with the heart than the right side of the brain, and the frontal lobes displaying lower coupling with the heart than the parietal and occipital lobes. In control rats, the CCCoh in occipital lobes was significantly higher than ipsilateral frontal lobes on both left and right hemispheres. In rats received atenolol, left frontal lobe shows higher CCCoh than the right frontal lobe, which shows lower CCCoh than both the parietal and occipital lobes of the same side. Remarkably, in rats received both phentolamine and atenolol, the CCCoh on the right side of the brain was significantly weaker than the left side of the brain, and the frontal lobe was significantly lower than parietal lobe, which was significantly lower than the occipital lobe. We also compared the CCCoh at each locus between the 4 groups of rats (Figure 2.7C). Significant differences on the left hemisphere between drug groups were identified only between rats treated

with phentolamine and atenolol. This effect appears to result from a slight increase of CCCoh by phentolamine and slight decrease by atenolol, though none of the drug treated groups had significant difference when compared with the control group (upper panels in Figure 2.7C). On the right hemisphere (lower panels in Figure 2.7C), however, beta-blockade significantly suppressed CCCoh compared to both control as well as alpha blocker-treated rats. The group treated with both alpha and beta blockers showed identical results with those treated with beta blocker alone, suggesting that alpha blocker had no effect for brain-heart coherence on the right hemisphere. Thus beta-blocker suppresses brain-heart coherence specifically and significantly on the right hemisphere of the brain.

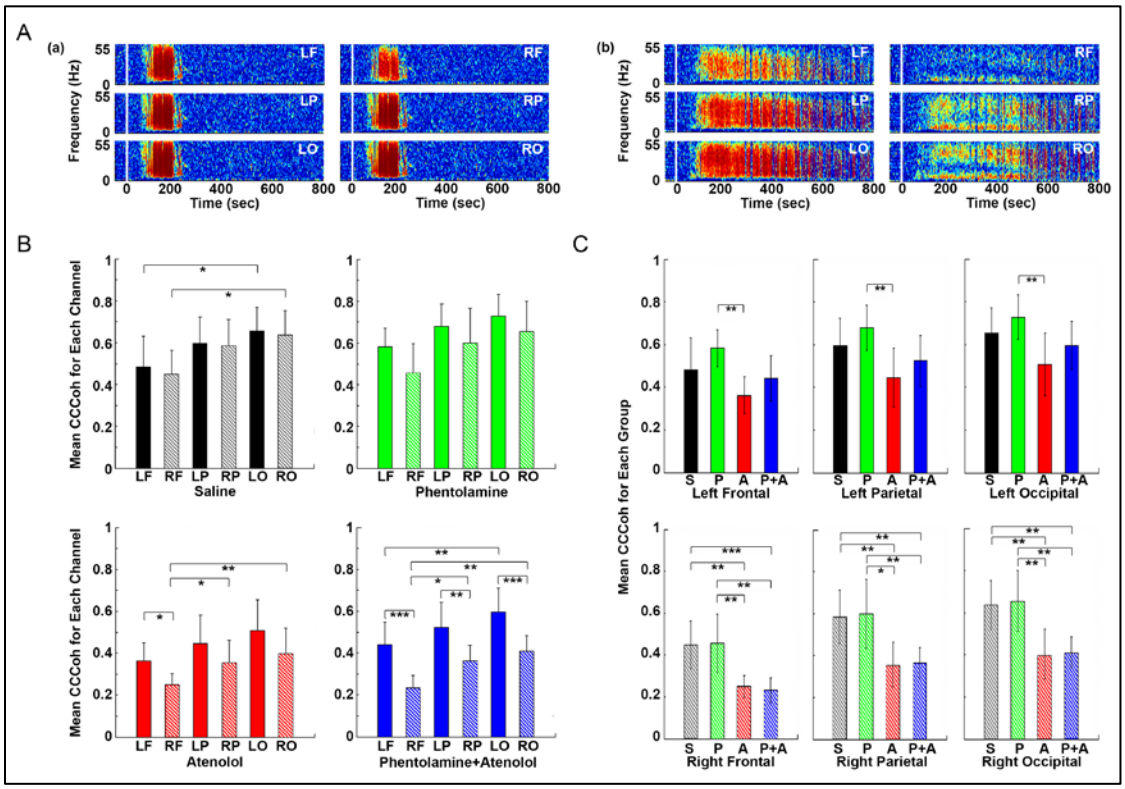

Figure 2.7 Adrenergic blockade leads to asymmetric corticocardiac coherence (CCCoh). **(A)** CCCoh raw data for each of the six EEG channels before (50 sec) and after asphyxia is shown for one representative control rat (panel a) and a rat received phentolamine plus atenolol (panel b). LF: left frontal; RF: right frontal; LP: left parietal; RP: right parietal; LO: left occipital; RO: right occipital. **(B)** CCCoh displays hemispheric asymmetry in rats treated with drugs. The mean and SD of CCCoh (5-55Hz) after asphyxia for each of the six EEG channels in four groups of rats. **(C)** Beta blocker inhibits CCCoh specifically on the right hemisphere. Significant differences of mean CCCoh among 6 EEG channels are indicated using asterisks in both panels B and C. Error bars denote SD (*$p < 0.05$, **$p < 0.01$, ***$p < 0.001$).

2.3.8 Beta blocker suppresses bi-directional effective communications between the brain and the heart

To explore the impact of adrenergic blockade on bi-directional brain-heart information transfer, we examined effective connectivity between the brain and heart (CCCon) in the four groups of rats (Figure 2.8). In all rats (panels Aa-Ad), connectivity remained at baseline levels during stages A1 and A2, the early phase of asphyxia. During bradycardia (A3), there was a delayed surge of connectivity in both afferent (feedforward or FF, from the heart to the brain) and efferent (feedback or FB, from the brain to the heart) directions, with efferent connectivity dominated in all rats (Figure 2.8A).

To quantify the effects of adrenergic blockade on directional information transfer between the brain and the heart following asphyxia, we examined brain-heart effective connectivity in both directions (Figure 2.8B). The mean CCCon was calculated in four groups of rats in both directions: saline (FF: 0.0159 ± 0.0020; FB: 0.0215 ± 0.0078), phentolamine (FF: 0.0148 ± 0.0017; FB: 0.0250 ± 0.0057), atenolol (FF: 0.0083 ± 0.0009; FB: 0.0101 ± 0.0029), and phentolamine plus atenolol (FF: 0.0090 ± 0.0012; FB: 0.0121 ± 0.0025). We found that the mean CCCon in both directions was significantly lower in rats received atenolol or both phentolamine plus atenolol than saline or phentolamine alone, indicating that blockade of beta-adrenergic signaling significantly decreased the brain and heart bi-directional information transfer during asphyxic cardiac arrest. Furthermore, phentolamine, when combined with atenolol, increased the efferent connectivity, but had no impact on the afferent connectivity, compared with atenolol alone where there was no feedback dominance of the brain-heart connectivity. Further analysis identified the impact of adrenergic drugs on the hemispheric asymmetry of brain-heart connectivity (Figure 2.8C): In rats treated with atenolol, afferent

connectivity (FF-CCCon) is stronger on the left side than on the right side, while in rats treated with phentolamine and phentolamine plus atenolol, efferent connectivity (FB-CCCon) on the right side of the brain is significantly suppressed than on the left side. Moreover, efferent connectivity was significantly stronger than afferent connectivity for control rats as well as rats injected with phentolamine or phentolamine plus atenolol and this effect is significant only on the left hemisphere. The alpha blocker elevated the efferent connectivity specifically on the left hemisphere when injected together with atenolol.

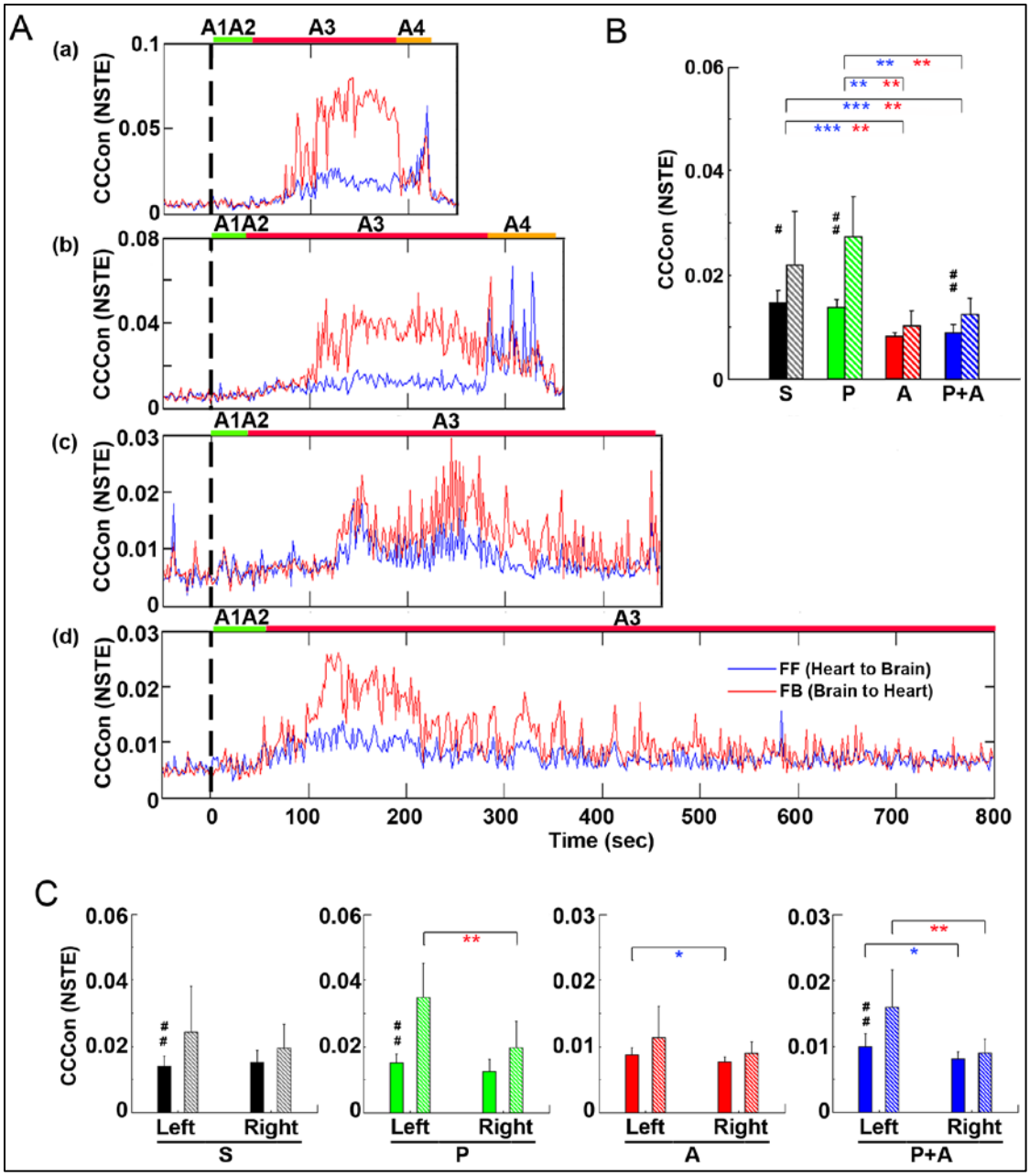

Figure 2.8 Adrenergic blockade decreases corticocardiac directional connectivity (CCCon). **(A)** CCCon, measured by the Normalized Symbolic Transfer Entropy (NSTE), shows high levels of feedback (from the brain to the heart or efferent) connectivity directed from the brain to the heart in 4 representative rats. CCCon (averaged over six EEG channels) before (50 sec) and after asphyxia in four representative rats: (a) saline, (b) phentolamine, (c) atenolol, and (d) phentolamine and atenolol. Red trace shows feedforward (from the brain to the heart) CCCon and blue trace shows feedback (from the heart to the brain) CCCon. **(B)** The mean and SD of CCCon (5-55Hz) during A3 phase (see panel A) in four groups of rats. Solid bars represent afferent CCCon and patterned bars represent efferent CCCon. Significant differences of afferent CCCon among 4 groups of rats are indicated using blue asterisks, and that of efferent CCCon among 4 groups are indicated using red asterisks. **(C)** Left and right asymmetry of afferent and efferent brain-heart connection in different drug groups. Significant differences between afferent and efferent CCCon are marked by pound signs. Error bars denote SD (*/#$p < 0.05$, **/##$p < 0.01$, ***$p < 0.001$).

2.3.9 Adrenergic blockade leads to marked hemispheric asymmetry and regional specificity of heart-brain effective connectivity

To investigate if adrenergic blockers affected brain-heart directional information transfer equally at the left and right, and at the front and back of the brain, we examined the effective connectivity between the heart and each of the six cortical loci (Figure 2.9). In rats received saline, the connectivity with the heart appeared slightly lower on the right side than the left side of the brain (panel Aa). However, in rats received both phentolamine and atenolol, the connectivity on the right side of the cortex was markedly reduced (panel Ab). Moreover, the connectivity in the frontal lobe appeared lower compared to the parietal and occipital lobes. In both rats, efferent connectivity (red tracings) appeared stronger than afferent connectivity (blue tracings).

Examination of the differences of brain-heart connectivity among six cortical channels for all four groups of rats revealed that the connectivity was affected by the drugs differentially at left and right side, and at the frontal and occipital regions of the brain (Figure 2.9B). Within each drug group and at each cortical location, connectivity is higher in the efferent direction from the left hemisphere than in the afferent direction, except the atenolol group. There was no directional asymmetry on the right hemisphere at any of the three cortical loci and within any of the 4 groups. Interestingly, no directional asymmetry was found in rats injected with atenolol at any of the 6 cortical regions. These data suggest that efferent signaling to the heart is more robust than afferent communication during asphyxia. Robust and significant efferent dominance over afferent connection was found at left frontal, left parietal, and left occipital lobes in saline, phentolamine, and phentolamine/atenolol treated rats ($p < 0.05$). In addition, all 4 groups of rats exhibited higher levels of afferent connectivity at occipital lobes than at the frontal lobes. In rats

treated with both phentolamine and atenolol, both afferent ($p < 0.05$) and efferent ($p < 0.01$) brain-heart connectivity was suppressed on the right side of the brain.

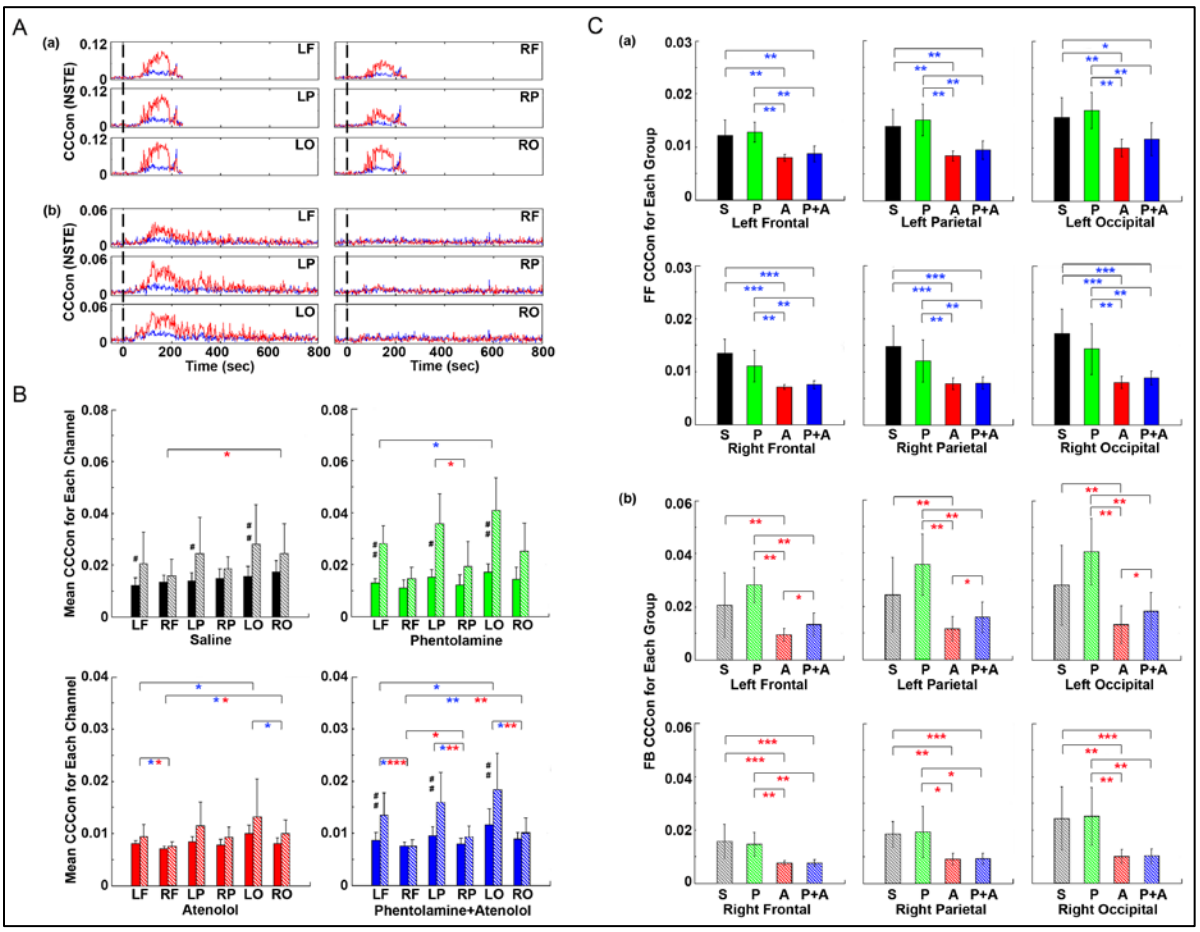

Figure 2.9 Adrenergic blockade affects corticocardiac connectivity (CCCon) with left and right hemispheric asymmetry, directional asymmetry, and regional specificity. **(A)** CCCon for each of the six EEG channels before (50 sec) and after asphyxia in one representative control rat (panel a) and a rat received phentolamine plus atenolol (panel b). Red trace shows afferent CCCon and blue trace shows efferent CCCon. **(B)** Regional differences on the effect of drugs on CCCon within each drug group. **(C)** Impact of drugs on hemispheric asymmetry, directional asymmetry, and regional specificity of CCCon compared between different drug groups. Solid bars represent afferent CCCon and patterned bars represent efferent CCCon. Significant differences in afferent CCCon among 4 groups of rats are indicated using blue asterisks, while that of efferent CCCon are indicated by the red asterisks. Significant differences between FF and FB CCCon are marked by pound signs. Error bars denote SD (*/#$p < 0.05$, **/##$p < 0.01$, ***$p < 0.001$).

The adrenergic blockers resulted in directional asymmetry (afferent vs. efferent), hemispheric asymmetry (left vs. right), and regional specificity (frontal vs. parietal vs. occipital) of brain-heart connectivity in the dying rats; and the effect was drug-specific. In each of the 6

cortical locations, atenolol significantly reduced the afferent brain-heart connectivity on both left ($p < 0.01$) and right ($p < 0.001$) hemisphere (panel Ca). Phentolamine had no effects on afferent connectivity to any of the 6 cortical loci. In addition, atenolol significantly suppressed efferent brain-heart connectivity in all 6 cortical regions ($p < 0.01$), while phentolamine displayed no significant impact on efferent connectivity on either hemisphere by itself (panel Cb). In rats treated with both atenolol and phentolamine, however, the efferent connectivity was significantly higher in rats treated with both alpha- and beta-blockers than in rats treated with the beta-blocker alone. Importantly this effect of phentolamine on brain-heart connectivity was limited to the efferent direction and exclusive to the left hemisphere (panel Cb).

2.3.10 Summary of the findings

Our data demonstrate that (1) simultaneous blockade of alpha- and beta-adrenergic signaling extends durations of both cardiac and cortical functional electrical activities and (2) beta-blocker suppresses bi-directional electrical communications between the heart and all regions of the cerebral cortex during asphyxic cardiac arrest. More specifically, beta blocker (1) nearly eliminated the occurrence of ventricular tachycardia and ventricular fibrillation induced by asphyxia, (2) significantly ($p < 0.01$) suppressed the initial and rapid decline of heart rate, (3) reduced the brain-heart coherence, significantly ($p < 0.01$) only on the right hemisphere, and (4) blocked both the efferent/feedback (brain-heart; $p < 0.01$) and afferent/feedforward (heart-brain; $p < 0.001$) signaling. Alpha blocker, on the other hand, (1) reduced the initial decline of heart rate ($p < 0.01$), (2) prolonged the duration of both cardiac ($p < 0.05$) and cortical ($p < 0.05$) functional electrical activities, and (3) when used in combination with beta blocker, reversed beta blocker-mediated significant suppression of efferent/feedback signaling significantly only on the left hemisphere. Importantly, when both alpha- and beta-adrenergic receptors were

simultaneously suppressed, ECG duration as well as cortical coherence duration were both lengthened and the combined drug effects were significantly higher than either drug used alone. Furthermore, the combined blockade of alpha and beta-receptors markedly suppressed cortical coherence, specifically on the right hemisphere.

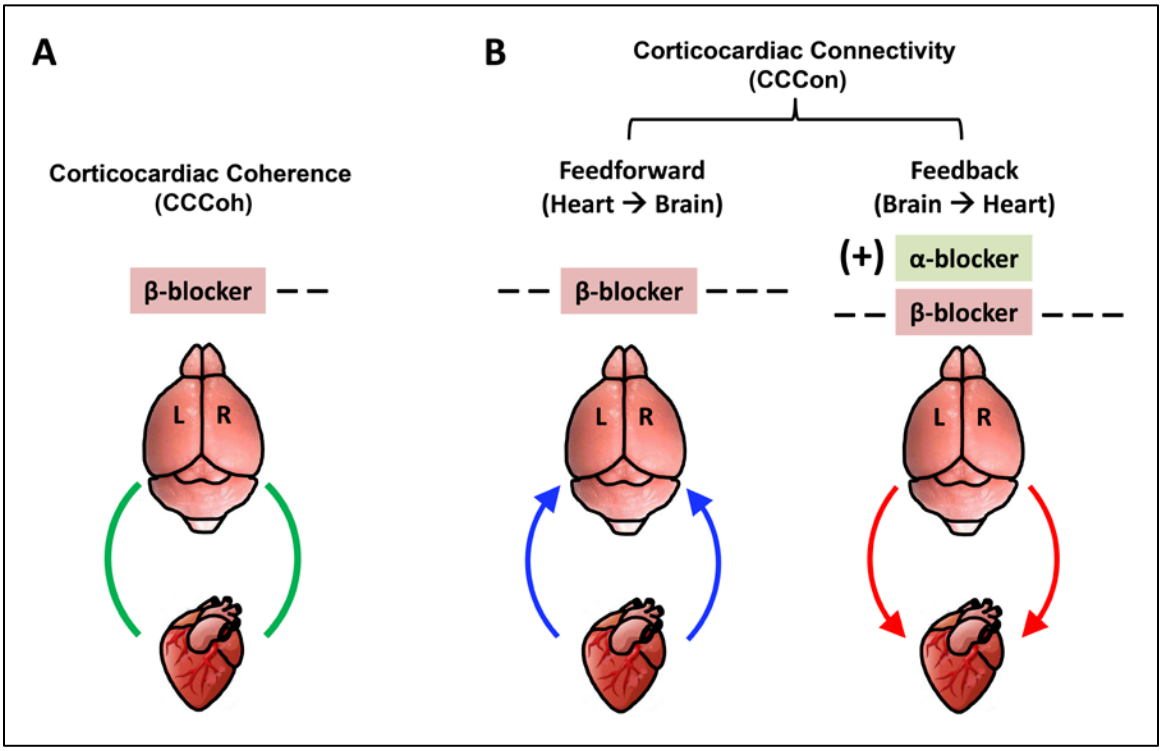

Figure 2.10 Adrenergic blockers bi-directionally and asymmetrically affect functional brain-heart communication. **(A)** Beta-adrenergic blockade markedly suppresses functional corticocardiac coherence (CCCoh) on the right hemisphere. **(B)** Beta-adrenergic blockade significantly suppresses both the afferent and efferent corticocardiac connectivity (CCCon), especially on the right hemisphere. Alpha-adrenergic blockade increases the efferent CCCon on the left hemisphere in the presence of atenolol. [--: decrease, $p < 0.01$; ---: decrease, $p < 0.001$; (+): significant increase only when atenolol was present; L: left; R: right]. The colored curved arrows indicate the direction of brain-heart communication.

The key findings on corticocardiac connectivity are illustrated in Figure 2.10. The beta blocker atenolol markedly suppressed brain-heart communications in asphyxic rats, by reducing the functional corticocardiac coherence (panel A) and effective corticocardiac connectivity (panel B). It is worth to note that atenolol's inhibitory actions on the brain-heart loop are significantly stronger on the right hemisphere for both coherence (panel A) and connectivity

(panel B) measures and that atenolol markedly suppresses both afferent (left panel in B) and efferent (right panel in B) communications between the cortex and the heart. Alpha blocker phentolamine, on the other hand, had no significant effect by itself for brain-heart communication. However, when used together with atenolol, phentolamine reversed the suppressive effects of atenolol on brain-heart connectivity. Importantly, this effect was limited to efferent signaling and unique to the left hemisphere (right panel in B). Taken together, these data suggest that beta blocker exerts its beneficial effects by reducing both afferent (feedforward) and efferent (feedback) communications with stronger impact on the right hemisphere.

2.4 Discussion

In this manuscript, we examined the impact of sympathetic blockers on the functional activities of the heart and the brain and functional interaction between the two vital organs in rats during asphyxic cardiac arrest. The results support our hypothesis [Li et al., 2015a] that the rapid cardiac demise by asphyxia stems from the sympathetic insult actively imposed by aroused brain.

2.4.1 Role of the brain during asphyxic cardiac arrest

Currently, very few studies have focused on the impact of the brain on the heart during cardiac arrest. We have shown that the brain is immediately aroused when rats are exposed to CO_2 [(Li et al., 2015a]; this study]. The brain activation, reflected by increased cortical coherence at high gamma and theta waves, was associated with an increased RRI (decreased heart rate) and a subsequent brief recovery of RRI within the first minute. Interestingly, there was no detectable electrical communication between the heart and the cortex during this period. A further increase of RRI was followed by a marked surge of brain-heart coherence and connectivity that lasted for the entire duration of ECG signals. These data lead to the following hypotheses: (1) asphyxia-

stimulated cortical signaling promotes autonomic activation during early phase of cardiac arrest via a homeostatic survival circuit, and the events in this early phase is likely mediated by subcortical players; (2) when the early rescue efforts fail, the brain mounts an intensive and sustained sympathetic activation, as reflected by the marked surge of corticocardiac coherence and bi-directional corticocardiac connectivity at later phase of cardiac arrest. The fact that adrenergic blockers suppressed the expansion of RRI during the early phase (Figure 2.5) supports the hypothesis #1 above. The data demonstrating reduced cortex-heart communication by beta-blocker atenolol during the later phase (Figures 2.7 and 2.9) supports the hypothesis #2. These data suggest that the rapid death by asphyxia is mediated by the overstimulation of the sympathetic system of the brain.

2.4.2 Animal models for cardiac arrest

Cardiac arrest kills more than 300,000 Americans each year and < 5% of out-of-hospital victims of cardiac arrest survive [Nolan et al., 2012]. Initial triggers that lead to cardiac arrest include sudden failures of cardiovascular, neurological, and pulmonary functions, accidents (drowning, choking, automobile accidents, etc), or drug overdose [Israel, 2014]. Most, if not all, of these sudden death occur in the absence of anesthesia. Of the various animal models used for cardiac arrest studies (intra-cardiac injection of toxins, electrical fibrillations, trachea occlusion, and non-oxygen gases induced asphyxiation), however, very few could be performed ethically in the absence of anesthesia. This issue is important, as anesthesia is well known to induce marked changes in autonomic functions [Farber et al., 1995] and can confound the interpretation of studies. Unlike other animal models, CO_2-mediated asphyxic cardiac arrest can be conducted easily in the absence of anesthesia and has been widely used to euthanize small laboratory rodents. This model has been used successfully to investigate brain-heart interactions during

asphyxia [Borovsky et al., 1998; Borjigin et al., 2013; Li et al., 2015a] and was the model of choice for our investigation of brain-heart communications in the present work. In future studies, non-oxygen gases, such as nitrogen [Borovsky et al., 1998], can be tested side-by-side with CO_2 to examine the impact of hypercapnea on brain-heart coupling. We also plan to monitor additional physiological parameters, such as blood pressure, pulse, and sympathetic nerve activity, in animal models of cardiac arrest.

2.4.3 Sympathetic toxicity and sudden death

Sudden death is associated with elevated sympathetic activities [Samuels, 2007; Sörös and Hachinski, 2012; Israel, 2014]. Elevated efferent sympathetic activity, measured by increased release of plasma norepinephrine, was detected in patients with sleep apnea [Baylor et al., 1995], myocardial damage [Mueller and Ayres, 1980], sustained ventricular arrhythmias [Meredith et al., 1991], and in rats dying from CO_2 inhalation [Borovsky et al., 1998]. Beta blockers reduce incidence of sudden cardiac death, cardiovascular death, and all-cause mortality [Yusuf et al., 1985; Al-Gobari et al., 2013]. Atenolol, a blocker of beta-adrenoceptor that does not pass through the blood-brain barrier, is used in human patients to treat a number of conditions including hypertension, angina, acute myocardial infarction, supraventricular tachycardia, and ventricular tachycardia [Patterson and Lucchesi, 1984; Draper et al., 1992]. Mechanisms for the beneficial effects of beta-blockers including atenolol, however, remain unclear [Yusuf et al., 1985; Bourque et al., 2007].

CO_2 results in cardiac arrest in less than five minutes [Coenen et al., 1995; Li et al., 2015a]. When the efferent neuronal signaling was blocked by cord transection, however, the duration of ECG and EEG signals was extended to more than 15 minutes in asphyxic rats, despite the continued absence of oxygen; and this effect was independent of atropine [Li et al.,

2015a]. This data suggests that the blockade of sympathetic action may be beneficial for prolonging the survival of both heart and brain in dying individuals, an idea tested in a rat model in the present work. Elevated sympathetic activity was reported in rats dying from CO_2-mediated asphyxiation [Borovsky et al., 1998]. Importantly the effect of CO_2 on norepinephrine release was shown to result from hypoxic rather than hypercapnic action of the gas and is independent of adrenally released epinephrine [Borovsky et al., 1998]. In our studies [Li et al., 2015a; this study], asphyxia induced a delayed surge of corticocardiac coherence and bi-directional connectivity between the brain and the heart. Atenolol, administered prior to asphyxia, significantly suppressed the brain-heart communication (Figures 2.7-2.9). In fact, the beta-blocker inhibits both efferent signaling from the brain to the heart and afferent signaling from the heart to the brain and extended the functional activity of both vital organs. In support of our finding, beta-blockers were shown to lower norepinephrine release in human subjects [Mueller and Ayres, 1980; Vincent et al., 1984; Packer, 1998] and rats [Berg, 2014]. Thus peripherally acting beta-blocker alters the feedback/efferent effective corticocardiac connectivity by inhibition of norepinephrine release at the presynaptic beta1-adrenoceptors [Berg, 2014]. These data indicate that the cerebral cortex is an essential part of a survival feedback loop and support the notion that sympathetic storm stimulated by a sudden drop of cardiovascular functions is the root cause of most, if not all, sudden cardiac arrest cases.

2.4.4 Cerebral asymmetry in autonomic control of the heart

Brain control of cardiac activity is lateralized, with left hemisphere associated with parasympathetic and right hemisphere with sympathetic functions [Wittling et al., 1998a; Wittling et al., 1998b; Critchley et al., 2005; Foster and Harrison, 2006]. Consistent with the right hemisphere predominance in sympathetically mediated cardiac control [Wittling, 1998b],

the beta-blocker specifically and significantly inhibited cortical coherence (Figure 2.3; in combination with phentolamine) and corticocardiac coherence (Figures 2.6 and 2.7) only on the right cerebral loci and inhibition of feedforward (afferent) corticocardiac directed connectivity by atenolol was more significant on the right hemisphere ($p < 0.001$) than the left hemisphere ($p < 0.01$) (Figure 2.9C). Interestingly, atenolol's suppressive effect on brain-heart coupling was not limited to the right hemisphere (Figure 2.9C); a significant ($p < 0.01$) inhibition of bi-directional effective brain-heart connectivity was detected on the left cortex. This data suggests that blockade of peripheral beta1-adrenergic receptors leads to downregulation of central sympathetic as well as parasympathetic signaling. These data are consistent with known mechanisms of autonomic regulation of the heart [Wehrwein et al., 2016]. Furthermore, they support the validity of our new approach for pharmacological dissection of signaling mechanisms within the cardiac survival circuit, to which the cerebral cortex is an essential player.

2.4.5 Dual alpha and beta blockers for lengthening the functional brain and heart activity

The two branches of the autonomic nervous system regulate cardiac functions through norepinephrine released by the sympathetic nerves and acetylcholine secreted by the vagal nerves. An extensive and reciprocal interaction, reflected by a prejunctional cholinergic modulation of adrenergic [Vanhoutte and Levy, 1980] and prejunctional adrenergic modulation of cholinergic [Akiyama and Yamazaki, 2000] neurotransmissions, exists between the two systems [Vizi, 1974; Vanhoutte and Levy, 1980; Wehrwein et al., 2016]. Specifically, norepinephrine, acting on the presynaptic adrenergic receptors inhibits acetylcholine release on postganglionic vagal nerve terminals, and this effect is abolished with phentolamine [Akiyama and Yamazaki, 2000]. In the present study, phentolamine, when used together with atenolol, had significantly more beneficial effects in prolonging functional activities of the brain and heart

than either drug alone (Figures 2.1 and 2.2). The dual blockers significantly ($p < 0.001$) increased the duration of functional activities of both the brain and the heart, and suppressed the initial expansion of RRI. Interestingly, the effect of the alpha blocker on brain-heart coupling was limited to the left cerebral hemisphere, in contrast to the right dominance of atenolol's effect. Furthermore, phentolamine's effect was more significant when both drugs were used together (Figures 2.3B, 2.3C, 2.6C, 2.7B, and 2.9B), and phentolamine significantly reversed the suppressive effect of atenolol on efferent corticocardiac connectivity, specifically on the left hemisphere (Figure 2.9Cb). These data suggest that phentolamine acts on the prejunctional alpha adrenoceptors to elevate the release of acetylcholine from cholinergic terminals in the myocardium, when beta1-adrenoceptors are blocked by atenolol.

2.4.6 Peripheral sympathetic blockade alters cortical and corticocardiac connectivity

Drugs used in this study, atenolol and phentolamine, are well known to affect cardiac functions. Consistent with their roles in the heart, the blockers (1) suppressed occurrence of VT/VF (Table 1 and Supplement Figure 1 in Appendix), (2) suppressed the initial drop of heart rate (Figure 2.5Ab), and (3) extended cardiac survival time (or the ECG duration; Figure 2.1B). More importantly, although having a minimum blood-brain barrier penetration [Neil-Dwyer et al., 1981; Nordling et al., 1981], they exerted marked impact on the dynamics of cortical functional connectivity (Figure 2.3) and corticocardiac coupling (Figures 2.6-2.9). We believe that this effect is due to the existence of a powerful corticocardiac loop (CCL), an extension of the autonomic nervous system that connects the heart with the cerebral cortex. Changes at either end of the CCL, in the heart or the cortex, can functionally influence the outcome at the other end. Thus, emotional trauma, a largely cerebral event, can precipitate a sudden arrest of the heart [Kassim et al., 2008; Sharkey et al., 2011], possibly via the ***efferent*** branch of this interconnected

CCL. Our data in this study provide evidence for the existence of the ***afferent*** branch of the CCL: blocking adrenergic receptors of the heart with drugs that do not penetrate the blood-brain barrier can powerfully alter the functional dynamics of cortical and corticocardiac connectivity. Further investigation of this intriguing loop may help elucidate (1) the role of the brain in cardiac diseases and (2) the impact of cardiac events on brain function. It should be noted that our finding that the functional connectivity within the brain and between the brain and heart is pharmacologically sensitive and hemispherically asymmetric alleviates the concern that ECG signals were artifactually detected in cortical electrodes.

2.4.7 A new tool for non-invasive investigation of brain-heart communications

Functional communications within the brain between two or more neuronal networks have been studied successfully using coherence [Sakkalis, 2011; Fries, 2015; Harris and Gordon, 2015] and connectivity metrics [Lee et al., 2009; Lee et al., 2015; Li et al., 2015a]. Similar methods have been developed for analysis of electrical signals encoding different forms of information. Coherence between EMG and EEG signals, for instance, has been analyzed as a measure for neural control of locomotion [Enders and Nigg, 2016]. We have pioneered the use of functional and effective connectivity measures to investigate neural control of cardiovascular functions [Li et al., 2015a]. Using this method, we have analyzed coherence and connectivity between heart and brain electrical signals and successfully demonstrated a surprisingly tight electrical communication between the heart and the cortex in dying rats [Li et al., 2015a]. While this mode of communication was undetected in healthy rats from the 6 cortical loci, it should be detectable in normal individuals when EEG electrodes are placed directly within brain regions with known involvement in the autonomic control of cardiac functions such as insular cortex, paraventricular nucleus, etc. Our ongoing research in human patients also identified a surge of corticocardiac

coherence and connectivity when their cardiac functions failed suddenly (manuscript in preparation). In the present manuscript, we have further expanded the utility of this novel approach to probing the signaling mechanisms of bi-directional brain-heart communication. We plan to apply this approach extensively in future studies to probe the mechanisms of various cardiogenic drugs currently used in clinic.

2.5 Acknowledgements

This work was supported by the Department of Molecular and Integrative Physiology at the University of Michigan and American Heart Association Predoctoral Fellowship (to FT). We thank Drs. Louis D'Alecy, Richard Keep, Daniel Beard, Anuska Andjelkovic-Zochowska, and UnCheol Lee for their helpful discussions and comments.

2.6 References

Akiyama, T., & Yamazaki, T. (2000). Adrenergic inhibition of endogenous acetylcholine release on postganglionic cardiac vagal nerve terminals. Cardiovascular Research, 46(3), 531-538.

Al-Gobari, M., El Khatib, C., Pillon, F., & Gueyffier, F. (2013). β-Blockers for the prevention of sudden cardiac death in heart failure patients: a meta-analysis of randomized controlled trials. BMC cardiovascular disorders, 13, 52. doi:10.1186/1471-2261-13-52

Baylor, P., Mouton, A., Shamoon, H. H., & Goebel, P. (1995). Increased norepinephrine variability in patients with sleep apnea syndrome. The American Journal of Medicine, 99(6), 611-615.

Berg, T. (2014). β1-blockers lower norepinephrine release by inhibiting presynaptic, facilitating β1-adrenoceptors in normotensive and hypertensive rats. 1-10. doi:10.3389/fneur.2014.00051/abstract

Borjigin, J., Lee, U., Liu, T., Pal, D., Huff, S., Klarr, D., . . . Mashour, G. A. (2013). Surge of neurophysiological coherence and connectivity in the dying brain. Proceedings of the National Academy of Sciences of the United States of America, 110(35), 14432-14437. doi:10.1073/pnas.1308285110/-/DCSupplemental

Borovsky, V., Herman, M., & Dunphy, G. (1998). CO2 asphyxia increases plasma norepinephrine in rats via sympathetic nerves. American Journal of ….

Bourque, D., Daoust, R., Huard, V., & Charneux, M. (2007). β-Blockers for the treatment of cardiac arrest from ventricular fibrillation? Resuscitation, 75(3), 434-444. doi:10.1016/j.resuscitation.2007.05.013

Chugh, S. S., Reinier, K., Teodorescu, C., Evanado, A., Kehr, E., Al Samara, M., . . . Jui, J. (2008). Epidemiology of Sudden Cardiac Death: Clinical and Research Implications. Progress in Cardiovascular Diseases, 51(3), -. doi:10.1016/j.pcad.2008.06.003

Coenen, A. M. L., Drinkenburg, W. H. I. M., Hoenderken, R., & van Luijtelaar, E. L. J. M. (1995). Carbon dioxide euthanasia in rats: oxygen supplementation minimizes signs of agitation and asphyxia. Laboratory animals, 29(3), 262-268. doi:10.1258/002367795781088289

Critchley, H. D., Wiens, S., Rotshtein, P., Öhman, A., & Dolan, R. J. (2004). Neural systems supporting interoceptive awareness. Nature Neuroscience, 7(2), 189-195. doi:10.1038/nn1176

Dhalla, N. S., Adameova, A., & Kaur, M. (2010). Role of catecholamine oxidation in sudden cardiac death. Fundamental & Clinical Pharmacology, 24(5), 539-546. doi:10.1111/j.1472-8206.2010.00836.x

Draper, A. J., Kingsbury, M. P., Redfern, P. H., & Todd, M. H. (1992). Effects of chronic administration of atenolol on the in situ perfused mesentery of normotensive and hypertensive rats. Journal of autonomic pharmacology, 12(2), 89-96.

Enders, H., & Nigg, B. M. (2016). Measuring human locomotor control using EMG and EEG: Current knowledge, limitations and future considerations. European journal of sport science, 16(4), 416-426. doi:10.1080/17461391.2015.1068869

Farber, N. E., Samso, E., Kampine, J. P., & Schmeling, W. T. (1995). The effects of halothane on cardiovascular responses in the neuraxis of cats. Influence of background anesthetic state. Anesthesiology, 82(1), 153-165.

Foley, P. J., Tacker, W. A., Wortsman, J., Frank, S., & Cryer, P. E. (1987). Plasma catecholamine and serum cortisol responses to experimental cardiac arrest in dogs. The American journal of physiology, 253(3 Pt 1), E283-289.

Foster, P. S., & Harrison, D. W. (2006). Magnitude of cerebral asymmetry at rest: Covariation with baseline cardiovascular activity. Brain and Cognition, 61(3), 286-297. doi:10.1016/j.bandc.2006.02.004

Freemantle, N., Cleland, J., Young, P., Mason, J., & Harrison, J. (1999). beta Blockade after myocardial infarction: systematic review and meta regression analysis. BMJ (Clinical research ed.), 318(7200), 1730-1737.

Fries, P. (2015). Rhythms for Cognition: Communication through Coherence. Neuron, 88(1), 220-235. doi:10.1016/j.neuron.2015.09.034

Harris, A. Z., & Gordon, J. A. (2015). Long-Range Neural Synchrony in Behavior. Annual Review of Neuroscience, 38(1), 171-194. doi:10.1146/annurev-neuro-071714-034111

Israel, C. W. (2014). Mechanisms of sudden cardiac death. Indian Heart Journal, 66(S1), S10-S17. doi:10.1016/j.ihj.2014.01.005

Kassim, T. A., Clarke, D. D., Mai, V. Q., Clyde, P. W., & Mohamed Shakir, K. M. (2008). Catecholamine-induced cardiomyopathy. Endocr Pract, 14(9), 1137-1149. doi:10.4158/EP.14.9.1137

Kew, H.-P., & Jeong, D.-U. (2011). Variable threshold method for ECG R-peak detection. Journal of Medical Systems, 35(5), 1085-1094. doi:10.1007/s10916-011-9745-7

Lahousse, L., Niemeijer, M. N., van den Berg, M. E., Rijnbeek, P. R., Joos, G. F., Hofman, A., . . . Brusselle, G. G. (2015). Chronic obstructive pulmonary disease and sudden cardiac death: the Rotterdam study. European heart journal, 36(27), 1754-1761. doi:10.1093/eurheartj/ehv121

Lee, U., Blain-Moraes, S., & Mashour, G. A. (2014). Assessing levels of consciousness with symbolic analysis. Philosophical Transactions of the Royal Society A: Mathematical, Physical and Engineering Sciences, 373(2034), 20140117-20140117. doi:10.1073/pnas.1308285110

Lee, U., Kim, S., Noh, G.-J., Choi, B.-M., Hwang, E., & Mashour, G. A. (2009). The directionality and functional organization of frontoparietal connectivity during consciousness and anesthesia in humans. Consciousness and Cognition, 18(4), 1069-1078. doi:10.1016/j.concog.2009.04.004

Li, D., Mabrouk, O. S., Liu, T., Tian, F., Xu, G., Rengifo, S., . . . Borjigin, J. (2015a). Asphyxia-activated corticocardiac signaling accelerates onset of cardiac arrest. Proceedings of the National Academy of Sciences, 201423936. doi:10.1073/pnas.1423936112

Li, D., Tian, F., Rengifo, S., Xu, G., M Wang, M., & Borjigin, J. (2015b). Electrocardiomatrix: A new method for beat-by-beat visualization and inspection of cardiac signals. Journal of Integrative Cardiology, 1(5). doi:10.15761/JIC.1000133

Meredith, I. T., Broughton, A., Jennings, G. L., & Esler, M. D. (1991). Evidence of a selective increase in cardiac sympathetic activity in patients with sustained ventricular arrhythmias. New England Journal of Medicine, 325(9), 618-624. doi:10.1056/NEJM199108293250905

Mueller, H. S., & Ayres, S. M. (1980). Propranolol decreases sympathetic nervous activity reflected by plasma catecholamines during evolution of myocardial infarction in man. Journal of Clinical Investigation, 65(2), 338-346. doi:10.1172/JCI109677

Neil-Dwyer, G., Bartlett, J., McAinsh, J., & Cruickshank, J. M. (1981). Beta-adrenoceptor blockers and the blood-brian barrier. Br J Clin Pharmacol, 11(6), 549-553.

Nolan, J. P., Soar, J., Wenzel, V., & Paal, P. (2012). Cardiopulmonary resuscitation and management of cardiac arrest. Nature reviews. Cardiology, 9(9), 499-511. doi:10.1038/nrcardio.2012.78

Nordling, J., Meyhoff, H. H., & Hald, T. (1981). Sympathetic influence on striated urethral sphincter in urinary incontinence. Prog Clin Biol Res, 78, 101-103.

Norris, R. M., Barnaby, P. F., Brown, M. A., Geary, G. G., Clarke, E. D., Logan, R. L., & Sharpe, D. N. (1984). Prevention of ventricular fibrillation during acute myocardial infarction by intravenous propranolol. Lancet, 2(8408), 883-886.

Packer, M. (1998). Beta-adrenergic blockade in chronic heart failure: principles, progress, and practice. Prog Cardiovasc Dis, 41(1 Suppl 1), 39-52.

Packer, M. (1998). Beta-adrenergic blockade in chronic heart failure: principles, progress, and practice. Progress in Cardiovascular Diseases, 41(1 Suppl 1), 39-52.

Patterson, E., & Lucchesi, B. R. (1984). Antifibrillatory properties of the beta-adrenergic receptor antagonists, nadolol, sotalol, atenolol and propranolol, in the anesthetized dog. Pharmacology, 28(3), 121-129.

Ram, C. V., & Kaplan, N. M. (1979). Alpha- and beta-receptor blocking drugs in the treatment of hypertension. Current Problems in Cardiology, 3(10), 1-53.

Rydén, L., Ariniego, R., Arnman, K., Herlitz, J., Hjalmarson, A., Holmberg, S., . . . Yamamoto, M. (1983). A double-blind trial of metoprolol in acute myocardial infarction. Effects on ventricular tachyarrhythmias. New England Journal of Medicine, 308(11), 614-618. doi:10.1056/NEJM198303173081102

Sakkalis, V. (2011). Review of advanced techniques for the estimation of brain connectivity measured with EEG/MEG. Computers in Biology and Medicine, 41(12), 1110-1117. doi:10.1016/j.compbiomed.2011.06.020

Samuels, M. A. (2007). The Brain-Heart Connection. Circulation, 116(1), 77-84. doi:10.1161/CIRCULATIONAHA.106.678995

Silvani, A., Calandra-Buonaura, G., Dampney, R. A. L., & Cortelli, P. (2016). Brain–heart interactions: physiology and clinical implications. Philosophical Transactions of the Royal Society A: Mathematical, Physical and Engineering Sciences, 374(2067), 20150181. doi:10.1161/01.CIR.93.5.1043

Sörös, P., & Hachinski, V. H. (2012). Cardiovascular and neurological causes of sudden death after ischaemic stroke. The Lancet Neurology, 11(2), 179-188. doi:10.1016/S1474-4422(11)70291-5

Stecker, E. C., Reinier, K., Marijon, E., Narayanan, K., Teodorescu, C., Uy-Evanado, A., . . . Chugh, S. S. (2014). Public Health Burden of Sudden Cardiac Death in the United States. Circulation: Arrhythmia and Electrophysiology, 7(2), 212-217. doi:10.1161/CIRCEP.113.001034

Taggart, P., Critchley, H., & Lambiase, P. D. (2011). Heart-brain interactions in cardiac arrhythmia. Heart, 97(9), 698-708. doi:10.1136/hrt.2010.209304

Vanhoutte, P. M., & Levy, M. N. (1980). Prejunctional cholinergic modulation of adrenergic neurotransmission in the cardiovascular system. American Journal of Physiology- ….

Vincent, H. H., Boomsma, F., Man in't Veld, A. J., Derkx, F. H., Wenting, G. J., & Schalekamp, M. A. (1984). Effects of selective and nonselective beta-agonists on plasma potassium and norepinephrine. Journal of cardiovascular pharmacology, 6(1), 107-114.

Vizi, E. S. (1974). Interaction between adrenergic and cholinergic systems: presynaptic inhibitory effect of noradrenaline on acetylcholine release. Journal of Neural Transmission, Suppl 11(0), 61-78.

Wehrwein, E. A., Orer, H. S., & Barman, S. M. (2016). Overview of the Anatomy, Physiology, and Pharmacology of the Autonomic Nervous System. Comprehensive Physiology, 6(3), 1239-1278. doi:10.1002/cphy.c150037

Wittling, W., Block, A., Genzel, S., & Schweiger, E. (1998a). Hemisphere asymmetry in parasympathetic control of the heart_1997_Wittling. Neuropsychologia, 36(5), 461-468.

Wittling, W., Block, A., Schweiger, E., & Genzel, S. (1998b). Hemisphere asymmetry in sympathetic control of the human myocardium. Brain Cogn, 38(1), 17-35. doi:10.1006/brcg.1998.1000

Wong, G. W. K., Laugerotte, A., & Wright, J. M. (2015). Blood pressure lowering efficacy of dual alpha and beta blockers for primary hypertension. The Cochrane database of systematic reviews(8), CD007449. doi:10.1002/14651858.CD007449.pub2

Yusuf, S., Peto, R., Lewis, J., Collins, R., & Sleight, P. (1985). Beta blockade during and after myocardial infarction: an overview of the randomized trials. Progress in Cardiovascular Diseases, 27(5), 335-371.

Chapter 3 Corticocardiac coupling in dying human patients

3.1 Introduction

Sudden cardiac death remains a major public health problem, accounting for 300,000-400,000 deaths in the United States annually [Stecker et al., 2014]. A recent North American analysis showed that the overall survival rate of sudden cardiac arrest was 4.6% [Nichol et al., 2008]. Sudden cardiac death is often the first manifestation of coronary heart disease or other structural heart disease, and is responsible for about 50% of the mortality from cardiovascular diseases in the United States and other developed countries [Myerburg and Castellanos, 2015]. However, sudden cardiac arrest could also be induced by non-cardiac causes, which include epilepsy, ischemic stroke, intracranial bleeding, traumatic heard injury, and asphyxia [Papadakis et al., 2009; Finsterer and Wahbi, 2014]. The multi-factorial properties of sudden cardiac death make its prediction, prevention, and management a challenging task. Given the high incidence and low survival rate of sudden cardiac arrest, a better understanding on the mechanism underlying sudden cardiac arrest is in urgent need.

Recent studies from our laboratory demonstrate that asphyxia induced sudden cardiac arrest lead to a rapid surge of functional connectivity (CCoh) and effective connectivity (CCon) in the dying brain [Li et al., 2015a]. In addition, asphyxia activates a surge of brain-heart coupling, a novel form of communication, between the brain and heart, measured by corticocardiac coherence (CCCoh) and directional corticocardiac connectivity (CCCon), prior to sudden death [Li et al., 2015a]. A dramatic release of a set of key cortical transmitters that are

important for the regulation of cardiovascular system is also identified during the dying process [Li et al., 2015a]. Based on these data, we hypothesized that the stimulated brain functions to resuscitate the heart during cardiac arrest, and the strong brain-heart coupling may be a potential biomarker to predict sudden death. However, this hypothesis has never been tested in human patients that suffered from sudden cardiac arrest.

The objective of current study is to investigate the dynamic changes and functional interactions between the brain and the heart in patients died from cardiac arrest using the same signal processing approach we developed in previous studies [Brojigin et al., 2013; Li et al., 2015a]. This study is expected to improve our understanding on how the brain and the heart interact during cardiac arrest in human.

3.2 Materials and method

3.2.1 Patient information and data collection

This 25-year-old woman had generalized epilepsy for 1 year and long QT syndrome for 2 years. The patient was admitted to the intensive care unit (ICU) at the University of Michigan and was treated with hypothermia with long-term video, EEG (19 channels, Fpz was used as reference), and ECG (2 channels, lead II was used for data analysis) monitoring. The sampling frequency for both EEG and ECG signal was 512 Hz. Cardiac arrest was revealed to be the cause of death for the patient.

3.2.2 Construction of electrocardiomatrix (ECM) and EEG matrix (electroencephalomatrix, EEM)

The construction of ECM and EEM (Figure 3.1B and 3.5) begins with R-peak detection in ECG signal. To avoid the influence of baseline wandering, baseline drift correction was first

performed using second-order Butterworth high-pass filtering with a cutoff frequency of 0.5 Hz (butter.m and filtfilt.m in Matlab signal processing toolbox; MathWorks Inc., Natick, MA). R peaks of ECG signals were then detected using variable threshold method [Kew and Jeong, 2011]. Specifically, an amplitude threshold in each nonoverlapping 1 second epoch was applied to select the candidates for R peaks, which can be verified only if the RRI value exceeds a predefined threshold. In this study, the interval threshold was selected as half of the median value of the RR interval (RRI) values in the last 1 second epoch. The automatically detected R peaks were manually validated through a custom user interface developed in Matlab (MathWorks Inc., Natick, MA).

For construction of ECM [Li et al., 2015b] , a window centered on the detected R peaks was extracted from the ECG signal after baseline drift correction. All ECG windows were then sorted in the order of R-peak time and plotted as parallel colored lines to form a colored rectangular image. To construct EEM, a window centered on the ECG R peaks was extracted from the EEG signal. All EEG epochs were then sorted according to R-peak time and plotted as parallel colored lines. For both ECM and EEM, the intensity of signals was denoted on z axis, with warmer color indicating positive peaks with higher voltage, and cooler colors indicating lower-voltage peaks. The color scheme can be adjusted as needed.

3.2.3 Analysis of power spectrum

EEG power was analyzed using short time Fourier transform based on discrete Fourier transform with 10-second segment size and no overlapping (spectrogram.m in Matlab signal processing toolbox; MathWorks Inc., Natick, MA). Each segment was windowed with a Hamming window. The absolute power was expressed in log scale (Figure 3.2A). The averaged power for each stage was calculated for five frequency bands: delta (1-4 Hz), theta (4-8 Hz), alpha (8-13 Hz), beta

(13-25 Hz), and gamma (25-55 Hz). The scalp power distribution was calculated using the topoplot function in EEGLAB (Figure 3.2B) [Delorme and Makeig, 2004].

3.2.4 Analysis of CCoh and CCCoh

To measure the CCoh among 19 EEG channels and the CCCoh between 1 ECG and each of the 19 EEG channels, EEG and ECG signals were first segmented into non-overlapping 10-second epochs. For each 10-second epoch, mean coherence was calculated based on magnitude squared coherence estimate using Welch's averaged periodogram method with 0.5 Hz frequency bin (mscohere.m in Matlab signal processing toolbox; MathWorks Inc., Natick, MA). The magnitude squared coherence estimate $C_{xy}(f)$ is a function of frequency with values between 0 and 1 that indicates how well signal x corresponds to signal y at each frequency:

$$C_{xy}(f) = \frac{|P_{xy}(f)|^2}{P_{xx}(f)P_{yy}(f)}, 0 \leq C_{xy}(f) \leq 1 \qquad (1)$$

where $P_{xx}(f)$ and $P_{yy}(f)$ are the power spectral density of x and y, and $P_{xy}(f)$ is the cross power spectral density.

The coherence between every two EEG channels (Figure 3.3A) or between 1 EEG and 1 ECG channel (Figure 3.6A) was plotted for frequencies from 0-55Hz. The averaged coherence for each studied stage was calculated at five frequency bands: delta (1-4 Hz), theta (4-8 Hz), alpha (8-13 Hz), beta (13-25 Hz), and gamma (25-55 Hz). The topographical distribution of CCoh was represented in graph, with the width of edge indicating the level of coherence (Figure 3.3B). The scalp distribution of CCCoh was plotted using the topoplot function in EEGLAB (Figure 3.6B) [Delorme and Makeig, 2004].

3.2.5 Analysis of CCon and CCCon

Twelve EEG channels and 1 ECG channel were selected for connectivity calculation. The 12 EEG channels were divided into 4 clusters: left frontal (LF: Fp1, F7, and F3), right frontal (RF: F8, Fp2, and F4), left posterior (LP: T5, P3, and O1), and right posterior (RP: T6, P4, and O2). The CCon between the 3 pairs of channels in LF and RP, as well as the 3 pairs of channels between RF and LP was calculated. For CCCon, the bidirectional information flow between each of the 12 EEG channels and ECG signal was calculated. Both CCon and CCCon were measured by modified [Li et al., 2015a] Normalized Symbolic Transfer Entropy (NSTE) [Lee et al., 2009], which is a nonlinear and model-free estimation of directional functional connection based on information theory. STE measures the amount of information provided by the additional knowledge from the past of the source signal $X(X^P)$ in the model describing the information between the past $Y(Y^P)$ and the future $Y(Y^F)$ of the target signal Y, which is defined as following:

$$STE_{X\to Y} = I(Y^F; X^P|Y^P) = H(Y^F|Y^P) - H(Y^F|X^P, Y^P) \qquad (2)$$

where $H(Y^F|Y^P)$ is the entropy of the process Y^F conditional on its past. Each vector for $Y^F, X^P \text{ and } Y^P$ is a symbolized vector point. The potential bias of STE was removed with a shuffled data, and the unbiased STE is normalized as follows:

$$NSTE_{X\to Y} = \frac{STE_{X\to Y} - STE_{X\to Y}^{Shuffled}}{H(Y^F|Y\ )} \in [0, 1] \qquad (3)$$

where $STE_{X\to Y}^{Shuffled} = H(Y^F|Y^P) - H(Y^F|X_{Shuff}^P, Y^P)$. X_{Shuff}^P is a shuffled data created by dividing the data into sections and rearranging them at random. Therefore, NSTE is normalized STE (dimensionless), in which the bias of STE is subtracted from the original STE and then divided by the entropy within the target signal, $H(Y^F|Y^P)$.

For CCoh, the feedback connectivity ($\overline{NSTE}_{FB}$) was calculated over the 3 pairs of EEG channels from the frontal (f) channels (LF/RF cluster) to the parietal (p) and occipital (o) channels (RP/LP cluster), which are defined as following:

$$\overline{NSTE}_{FB} = \frac{1}{n_f . n_{p,o}} \sum_{(i,j)=1}^{n_f, n_{p,o}} NSTE_{i \to j} \qquad (4)$$

where $n_f = 3$ and $n_{p,o} = 3$. The feedforward connectivity ($\overline{NSTE}_{FB}$) from the parietal and occipital channels (LP/RP cluster) to the frontal channels (RF/LF cluster) is vice versa.

For CCCon, the feedback connectivity ($\overline{NSTE}_{EEG \to EKG}$) was calculated by averaging NSTE over 12 pairs of EEG channels to ECG channel, which are defined as follows:

$$\overline{NSTE}_{EEG \to EKG} = \frac{1}{n_{EEG}} \sum_{i=1}^{n_{EEG}} NSTE_{i \to EKG} \qquad (5)$$

where $n_{EEG} = 12$. The feedforward connectivity ($\overline{NSTE}_{EKG \to EEG}$) from the ECG to 12 EEG channels is vice versa.

EEG and ECG signals were first filtered into five frequency bands, delta (1-4 Hz), theta (4-8 Hz), alpha (8-13 Hz), beta (13-25 Hz), and gamma (25-55 Hz), and then segmented into 10-second long epochs with 5-second long overlapping. The feedback and feedforward CCon and CCCon were sequentially calculated for each epoch. Three parameters: embedding dimension (d_E), time delay (τ), and prediction time (δ), are required for calculation. In this study, we selected the parameter setting that could yield maximum $NSTE_{X \to Y}$ by fixing the embedding dimension (d_E) at 3, and optimizing prediction time δ (from 1 to 30, corresponding to 2-60 ms with the sampling frequency of 512 Hz) and time delay τ (from 1 to 125, 1-250 ms). The same procedure was used to calculate $NSTE_{Y \to X}$, provided that the information between two signals is transferred through different neuronal pathways. The averaged CCon (Figure 3.4) and CCCon (Figure 3.7) for each stage were calculated and plotted for five frequency bands.

3.3 Results

3.3.1 EEG and ECG displayed series of activity with distinct features during the dying process

To explore the electrophysiological state of the brain and the heart during the dying process, raw EEG and ECG signals were first analyzed. Unprocessed EEG signals from 19 cortical channels (Figure 3.1C) and ECG data (lead II), as well as the RRI for the last hour are shown in Figure 3.1A. According to the features of signals, six representative stages were selected for detailed analysis. Stage 1 (S1: 700-800 second) is characterized by normal EEG, ECG, and RRI and is considered as baseline. Stage 2 (S2: 2760-2890 second) is comprised of high amplitude EEG signal and normal ECG signal. In stage 3 (S3: 2890-2990 second), EEG activity became weaker and both the EEG and ECG signals exhibited relatively normal morphology. Stage 4 (S4: 3050-3160 second) is marked by a reduction in the amplitude of EEG signals. During this stage, cardiac pacing rhythm dominated ECG. Interestingly, despite the pacing, the RRI jumped from 0.81 second to 1.62 second in the middle of pacing (3115 seconds), which ended at 15.62 second as soon as the pacing stopped (3160 seconds). Stage 5 (S5: 3160-3260 second) is consisted of further reduced amplitude of EEG and ECG signals that were associated with third-degree heart blocks. During this phase, P-waves were undetectable. In stage 6 (S6: 3260-3420 second), there is a further attenuation of EEG signal and a partial recovery of heart rate from the stage 5 in ECG signal. It is worth mentioning that, the patient already had multiple episodes of cardiac arrest and was on life support by the end of S4 in this terminal cardiac arrest. The subtle increase of RRI between S3 and S4 was associated with the activation of cardiac pacemakers, which stopped momentarily. An additional mild increase of RRI preceding S4 was followed by a much longer duration of cardiac pacemaker activity during S4. The life support was removed at the end of S4,

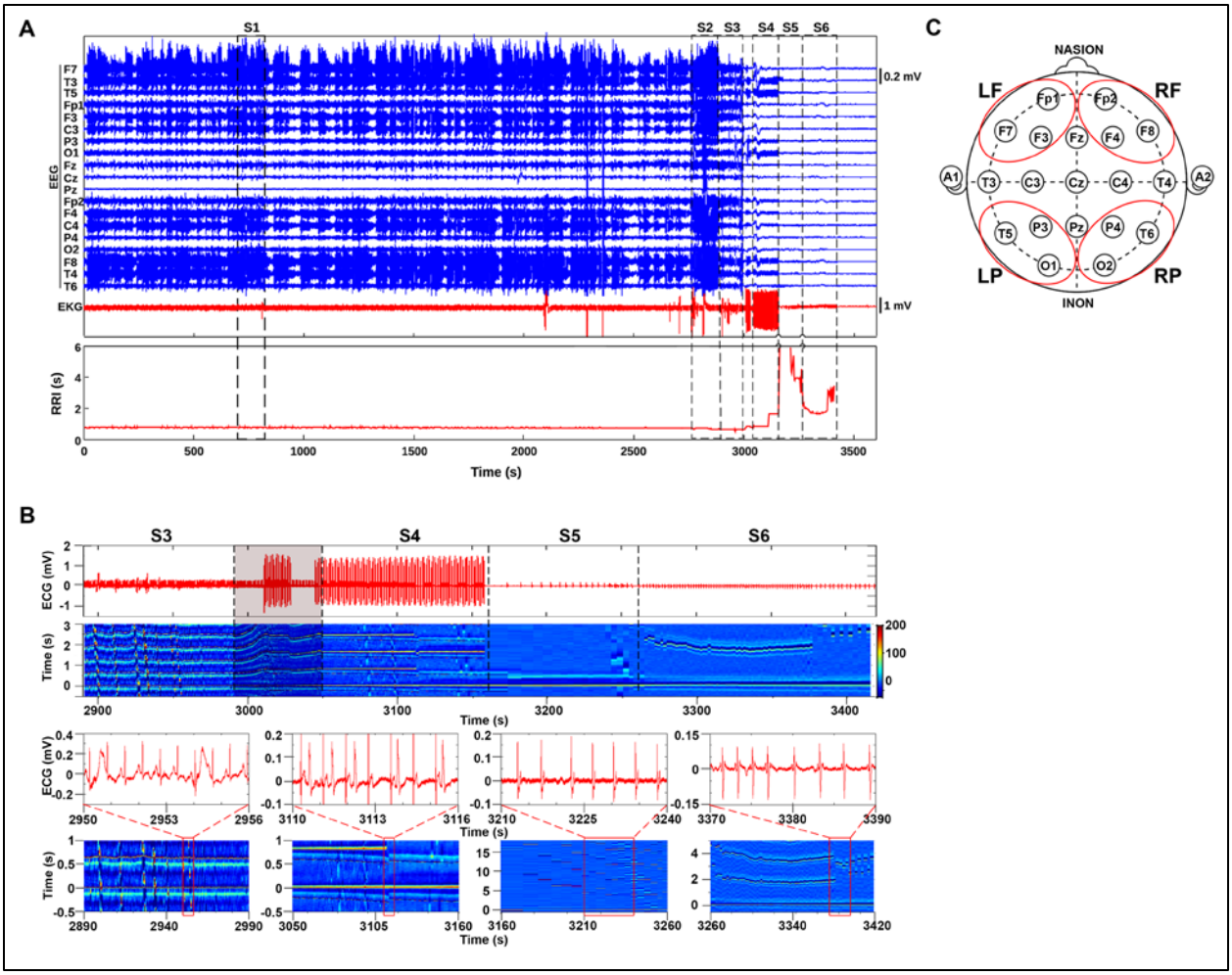

Figure 3.1 EEG and ECG displayed series of activity with distinct features during the dying process. **(A)** EEG (from 19 cortical locations), ECG (lead II), and RR interval (RRI) during 1-hour terminal stage in the patient. The whole dying process was divided into 6 stages: stage 1 (S1: 700-800 sec), stage 2 (S2: 2760-2890 sec), stage 3 (S3: 2890-2990 sec), stage 4 (S4: 3050-3160 sec), stage 5 (S5: 3160-3260 sec), and stage 6 (S6: 3260-3420 sec). **(B)** ECG and ECM display of raw signal from S3 to S6 (upper panels) and representative cardiac arrhythmias (middle panels) for each stage (lower panels). **(C)** Placement of 19 EEG electrodes and classification of 12 channels into 4 clusters. LF: left frontal, RF: right frontal, LP: left posterior, RP: right posterior.

which was associated with a sudden onset of bradycardia, with RRI rising from 1.62 seconds to 15.62 seconds (see bottom panel in Figure 3.1A). From S5 onward, this patient was no longer on life support. Because the internal interactions between the brain and the heart is the focus of current study, S5 and S6 are the stages of major interests. To facilitate visualization, ECG signal from S3 to S6 was enlarged and aligned together with its corresponding ECM (Figure 3.1B). The

ECM for each stage (S3, S4, S5, and S6) is displayed in the lower panel of Figure 3.1B. Representative cardiac rhythms, which include peaked T wave in S3, cardiac pacing rhythm in S4, third-degree heart blocks in S5, and bradycardia in S6, were plotted and placed above the ECM (4 middle panels, Figure 3.1B).

3.3.2 Recovery of EEG power at near-death

EEG power analysis was conducted to investigate the dynamic changes of electrical activity in 19 different cortical regions during the dying process. The temporal changes of EEG power from S2 to S6 for 4 representative channels F8, T5, Pz, and T6 are shown in Figure 3.2A. In S2, high level of EEG power was detected in right frontal channel F8, whereas relatively low level of EEG power was detected in left and right posterior channels T5 and T6. The EEG power for channel Pz located in the posterior midline is the lowest in S2. From S3 to S6, there was a large decrease of overall EEG power for all 4 channels compared to S2. For channel F8, there was a modest recovery of EEG power during the late S5 at high frequency ranges, as well as during S6 for low frequencies. The EEG power for both T5 and T6 showed mild reduction in S3, and a transient recovery at late S4, and the early phase of S5 compared to S2. The EEG power showed further decline from the mid-S5 for high frequency rhythm for both channels, while the EEG power for low frequency showed a slight increase than previous stages. The EEG power for channel Pz was maintained at lowest level from S3 until asystole.

To obtain a comprehensive understanding on the changes of EEG power for all 19 channels during cardiac arrest, EEG power topography was plotted for each of the 6 stages (Figure 3.2B). As shown in the figure, during S1 and S2, high level of EEG power was detected for all 5 frequencies. The left and right frontal regions displayed higher EEG power than other regions. From S3 to S6, there was a dramatic decrease of overall EEG power for all frequencies.

Interestedly, on S4, there was still detectable EEG power on the left parietal and the right frontal regions for all frequency bands. On S5 and S6, EEG power was nearly undetectable for all channels at all frequencies except for S6 at theta rhythm, which showed an increase of EEG power on the left posterior and right frontal regions.

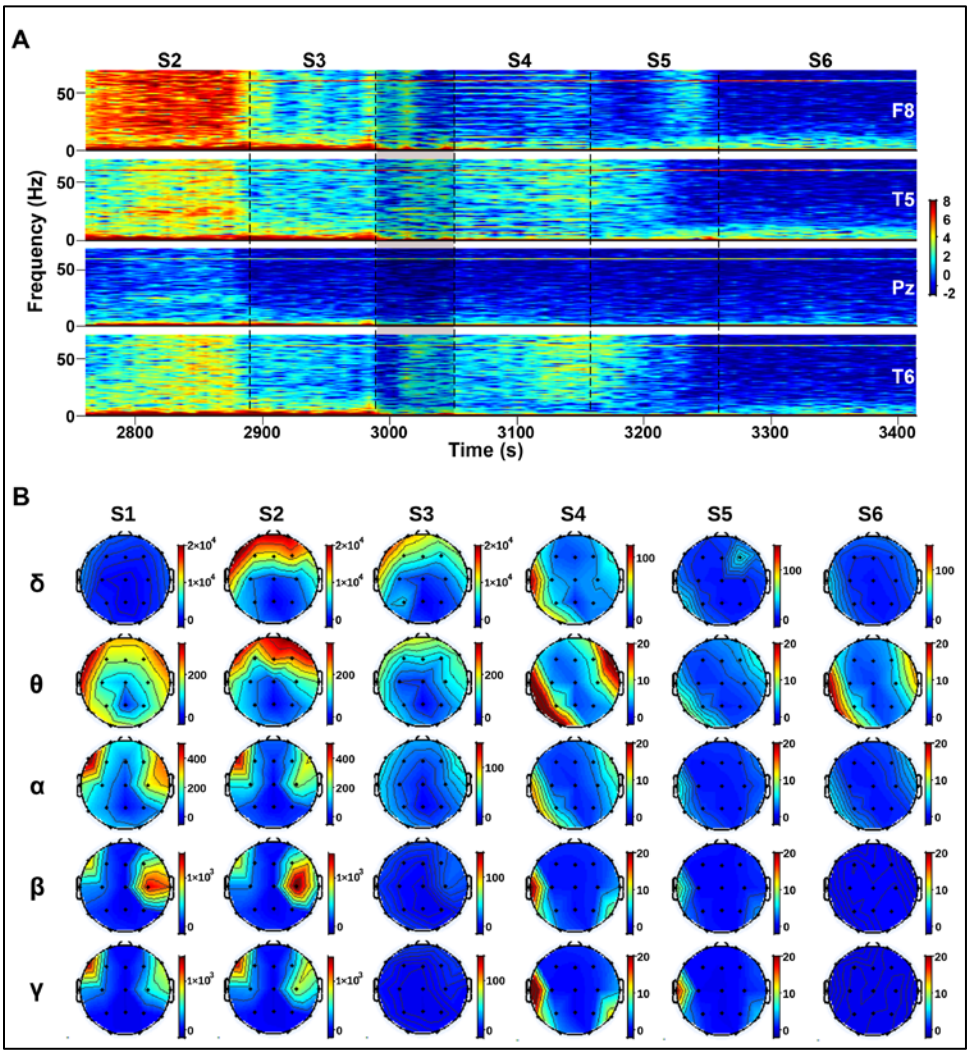

Figure 3.2 Recovery of EEG power at near-death. **(A)** The spectrogram of EEG power for 4 representative channels (F8, T5, Pz, and T6) from S2 to S6. **(B)** Topographic distribution of EEG power for 6 stages at 5 different frequency bands: delta (1-4Hz), theta (4-8Hz), alpha (8-13Hz), beta (13-25Hz), and gamma (25-55 Hz).

3.3.3 Increase of interhemispheric CCoh during cardiac arrest

To investigate the functional synchronization between different cortical regions during cardiac arrest, CCoh analysis was performed for every 2 cortical channels. Figure 3.3A shows the temporal changes of CCoh for 4 representative cortical channel pairs during cardiac arrest. Functional connectivity in the dying brain exhibited clear spatial distribution. At lower frequency range (<30 Hz), the CCoh between F8 and Fp2 increases from S2 to S3, which further increases in S4 and S6. CCoh surge at higher range (30-65 Hz) in S4 coincided with the cardiac pacing. Intriguingly, the disappearance of this high frequency CCoh between F8 and Fp2 preceded the transition of ECG from sinus rhythms to 2^{nd} degree heart block (Fig. 3.1B). The right posterior CCoh between T6 and P4 channels demonstrated a pattern nearly complementary to the right frontal CCoh, with much weaker CCoh at lower frequency (<25 Hz) in stages 4-6 and a stronger CCoh at higher frequency (>25 Hz) during S3 and the second half of S4 (Fig. 3.3A). In contrast, the left posterior CCoh between T5 and P3 channels, hemispherically symmetric to the CCoh between T6 and P4, demonstrated highest values at all five (S2-S6) stages. It is worth noticing that high levels of CCoh is not universally found in all regions of the brain, as the CCoh between right frontal channel F8 and posterior midline channel Pz was nearly undetectable during the entire process (Fig. 3.3A). These data demonstrate that functional connectivity within the cerebral cortex displays temporal and spatial specificity in dying human brain.

To obtain a global view of the dynamic changes of CCoh during cardiac arrest, the mean coherence between every two of the 19 cortical channels was plotted for each of the 6 stages at 5 frequencies. The CCoh displayed channel, frequency, and stage dependent changes. As shown in Figure 3.3B, from S1 to S3 at delta, theta, and alpha frequencies, the CCoh between adjacent channels was stronger than from distant channels, and the CCoh for lateral channels was stronger

than central channels. However, from S4 to S6, this ring-shaped coherence transformed into strong interhemispheric coupling between 3 channels in right frontal (F8, Fp2, and F4) and 3 channels in left posterior regions (T5, O1, and P3). The 3 channels within each cluster also exhibited intense synchronization with each other. The interhemispheric coherence during S4-S6 stages was stronger at theta and alpha frequencies and weaker at beta and gamma frequencies.

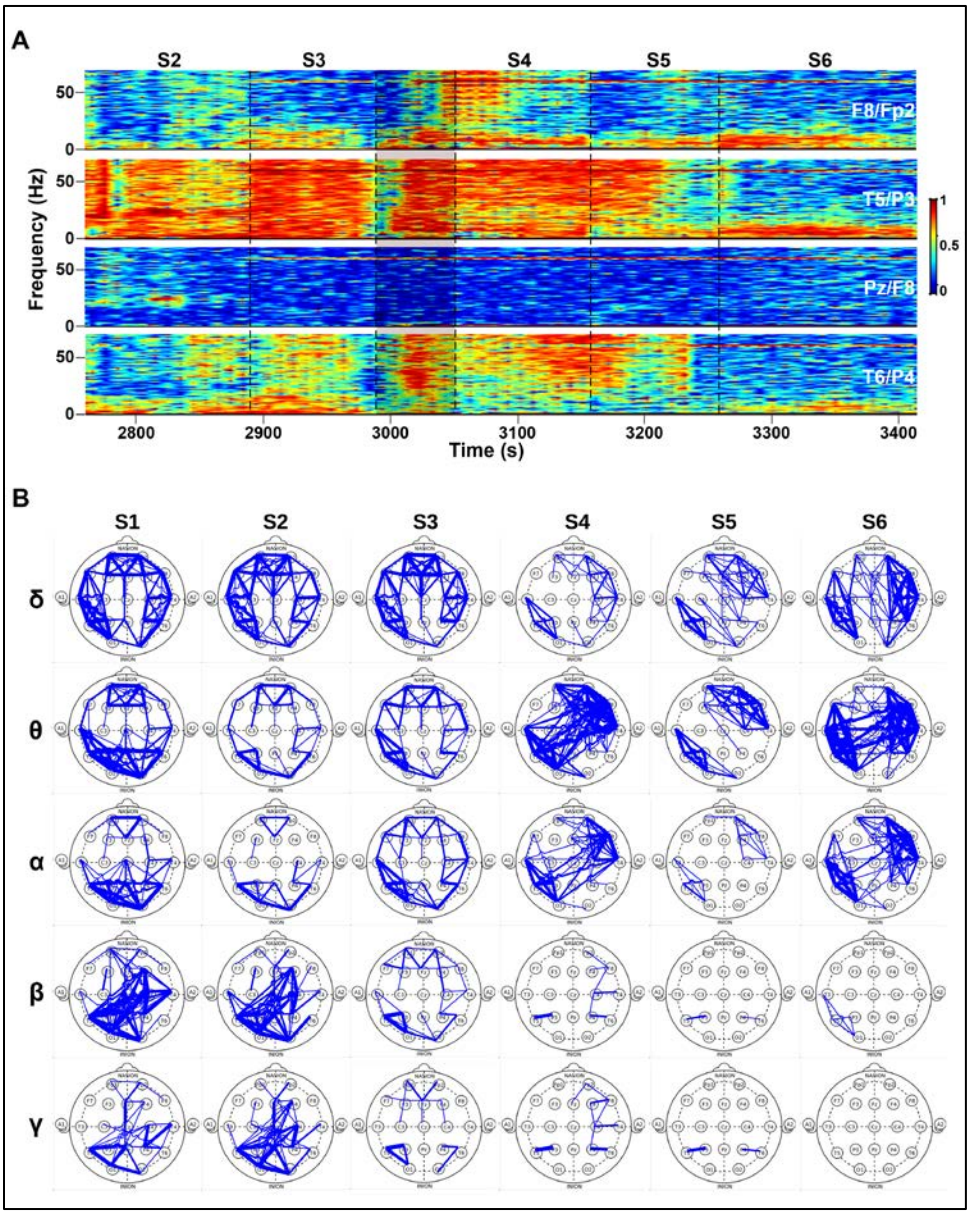

Figure 3.3 Increase of interhemispheric cortical coherence (CCoh) at dear-death. **(A)** CCoh for 4 pairs of cortical channels (F8/Fp2, T5/P3, Pz/F8, and T6/P4) from S2 to S6. **(B)** Topographic distribution of CCoh for 6 stages at 5 different frequency bands: delta (1-4Hz), theta (4-8Hz), alpha (8-13Hz), beta (13-25Hz), and gamma (25-55 Hz). The width of edge indicates the level of coherence (0.4-0.9).

3.3.4 Increase of CCon at near-death

To investigate how different cortical region communicates with each other during the dying process, feedforward (FF, from occipital/parietal to frontal regions) and feedback (FB, from frontal to parietal/occipital regions) CCon was measured for 12 pairs of cortical channels. The 12 channels were first divided into 4 clusters (LF, RF, LP, and RP), each of which contains 3 channels (Figure 3.1C). The FF and FB CCon between the 3 channels in LF and RP, as well as between the 3 channels in RF and LP was calculated. Figure 3.4A shows the FF and FB CCon for 2 representative cortical channel pairs. As shown in the left panel (F8/T5), there was increase during S6 in both FF and FB CCon between F8 and left posterior channel T5 during S6 for delta, theta, and gamma rhythm. In alpha frequency, the stage that showed high level of CCon was S4, whereas CCon for beta rhythm showed elevated levels only during S2 phase, which remained rather flat for the remainder of the recording. For gamma rhythms, however, even though coherence value was relatively low between F8 and T5, the causal connectivity (CCoh) reached the highest levels in stage S6, immediately before cardiac arrest. The FB and FF CCon for right frontal channel F8 and left posterior channel O1 exhibited similar dynamic as F8 and T5.

FF and FB CCon between every 2 channels from diagonal clusters for each stage exhibit dynamic changes in the dying brain (Fig. 3.4B). At delta frequency, FF and FB CCon were maintained at low level with small fluctuations from S1 to S6. For theta and alpha bands, there were active FF and FB communications between the 4 clusters in S1, S2 (only alpha), S4, and S6. During other stages, only sporadic activity was detected in a few channels, including Fp1/T6, O2/F7 (FB), F8/T5 (FF), and Fp1/P4 (FF). In addition, the CCon surge in S1, S2, and S6 demonstrated distinct patterns. In S1 and S2, the most active channels are O1/F8 (FB), F8/T5 (FF), Fp1/O2 (FF), Fp1/T6 (FF), F7/O2 (FF), P3/F4, and T5/F4. In S6, the most active channels

are F8/T5 (FF), T6/Fp1 (FB), F3/P4 (FF), F3/T6 (FF), Fp1/P4 (FF), and Fp1/T6 (FF). For beta and gamma oscillations, FF and FB CCon between F4 and 3 channels in LP clusters was high during S1 and S2. The CCon for all the channels at beta frequency then declined from S3 to S6. At gamma band, the CCon was low from S3 until S5. However, at S6, there was a marked surge of FB CCon between LP and RF clusters.

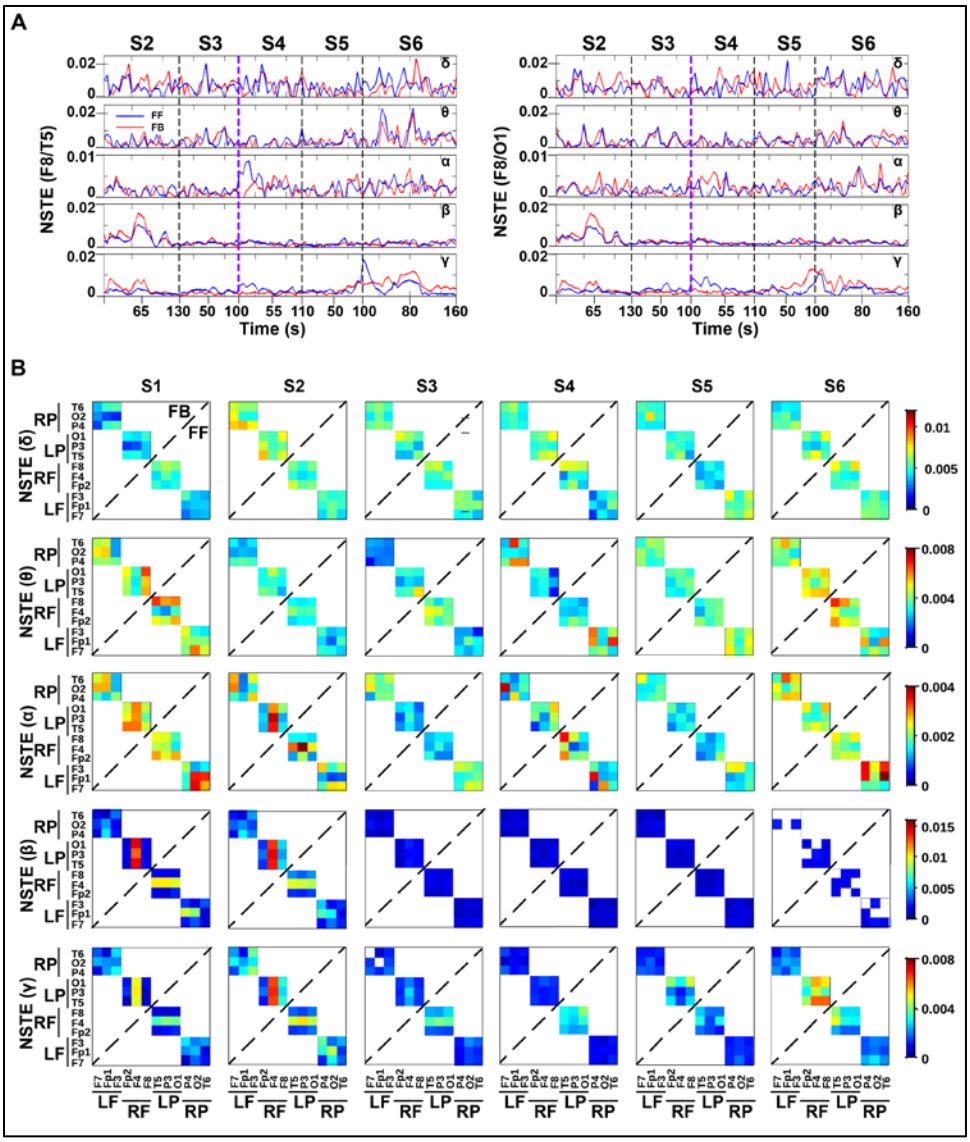

Figure 3.4 Increase of cortical directional connectivity (CCon) at near-death. **(A)** CCon for 2 pairs of cortical channels (F8/T5 and F8/O1) from S2 to S6 at 5 different frequencies: delta (1-4Hz), theta (4-8Hz), alpha (8-13Hz), beta (13-25Hz), and gamma (25-55 Hz). FF: feedforward (occipital/parietal to frontal regions). FB: feedback (frontal to parietal/occipital regions). **(B)** The CCon between 12 EEG channels for 6 stages at 5 different frequencies.

3.3.5 Surge of cardiac event-related potential (CERP) at near-death

To investigate the possible interactions between the brain and the heart during cardiac arrest, raw EEG and ECG signals were first converted into matrix format (Li et al., 2015a; 2015b) and aligned together. Figure 3.5A shows the ECM and EEM for 4 representative cortical channels, F8, T5, Pz, and T6, from S2 to S6. No obvious phase relationships were identified between ECM and EEM for all 4 cortical channels during S2 and S3. From S4 to S6, however, signals from right frontal channel F8 and left posterior channel T5 synchronized with ECG signal and showed cardiac event-related potential (CERP), which was strongest during S6. In contrast, CERP was undetectable for channel Pz located in posterior midline from S4 to S6 and was only identifiable for right posterior channel T6 during S6. To make a clearer comparison between the CERP from F8 and T5, two 40-second-long epochs were selected from S4 and S6 (red bars in Figure 3.5A) and placed side by side with the ECM (Figure 3.5B). As shown in the figure, ECG and F8 displayed positive peaks with similar amplitude during S4. However, during S6, the R-peak of F8 was much more positive than the corresponding ECG signal. For both S4 and S6, left posterior channel T5 exhibited strong negative peaks. When the raw ECG and EEG signals were averaged over the 40 sec epoch and plotted together (right panels in Figure 3.5B), similar amplitude relationship among ECG, F8, and T5 were found for both S4 (top graph) and S6 (bottom graph). Interestingly, ECG and EEG signals demonstrated distinctive phase relationship at two different stages. During S4, very little time delay was found for peak potentials from F8 and T5 channels compared to the peak of heartbeat, whereas an 18-ms time delay was identified for peak potentials from both F8 and T5 during S6. EEM for all 19 EEG channels arranged according to their locations on the skull during S4 and S6 is shown in Supplement Figure 2 and Supplement Figure 3 in Appendix.

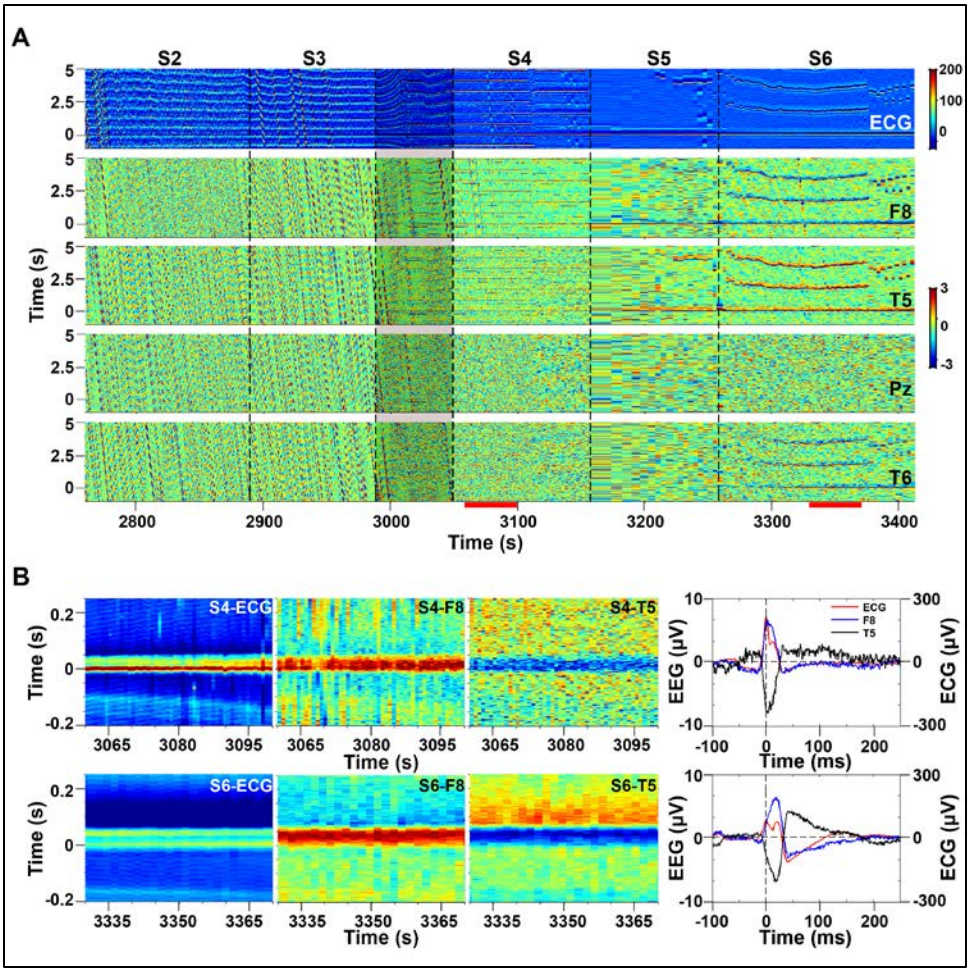

Figure 3.5 Surge of cardiac event-related potential (CERP) at near-death. **(A)** ECM and EEM for ECG and 4 representative cortical channels (F8, T5, Pz, and T6) from S2 to S6. **(B)** Alignment of ECM (left panel) with EEM for 2 cortical channels, F8 (middle left) and T5 (middle right), for 2 epochs (red bars in A, S4: 3060-3100 sec, S6: 3330-3370 sec). CERP for F8 (blue trace) and T5 (black trace) was averaged and displayed along with the averaged heartbeat (red trace) in right panel.

3.3.6 Surge of CCCoh at near-death

The detection of CERP stimulated the investigation on the functional coupling between the brain and the heart at near-death. CCCoh was calculated between each of the 19 EEG channels and the ECG signal. Figure 3.6A shows the temporal dynamics of the functional connectivity between ECG and 4 representative EEG channels F8, T5, Pz, and T6. In S2 and S3, very little CCCoh was detected between the 4 cortical channels and the ECG. From S4 until cardiac asystole, there is a dramatic surge of CCCoh at low frequencies (<30 Hz) for both right frontal channel F8 and left posterior channel T5, with higher frequency (>30 Hz) CCCoh seen during S4 for both channels. For channel Pz located in the posterior midline, no CCCoh was identified during the entire process. A weak CCCoh was detected for right posterior channel T6 at S4 and S6 at low frequency ranges. To obtain a comprehensive understanding on the dynamic changes of CCCoh between 19 cortical regions and the heart during the dying process, CCCoh for 19 channels was calculated for each of the 6 stages and plotted in a topographic format for 5 frequencies (Figure 3.6B). No detectable or marginal level of CCCoh was identified for all the channels from S1 to S3. Remarkable level of CCCoh was identified at 3 near-death stages: S4, S5, and S6. Among all 19 cortical regions, the left parietal, left occipital, and right frontal lobes are the main cortical regions that synchronize with the cardiac signals during cardiac arrest. In addition of exhibiting temporal (S1-S6) and spatial (channels 1-19) specificity, CCCoh is also frequency specific. In high frequency bands (beta and gamma), only low level of CCCoh was detected for a few channels (F8/ECG and T5/ECG) during S4. High level of CCCoh was clustered mainly at theta and alpha frequencies.

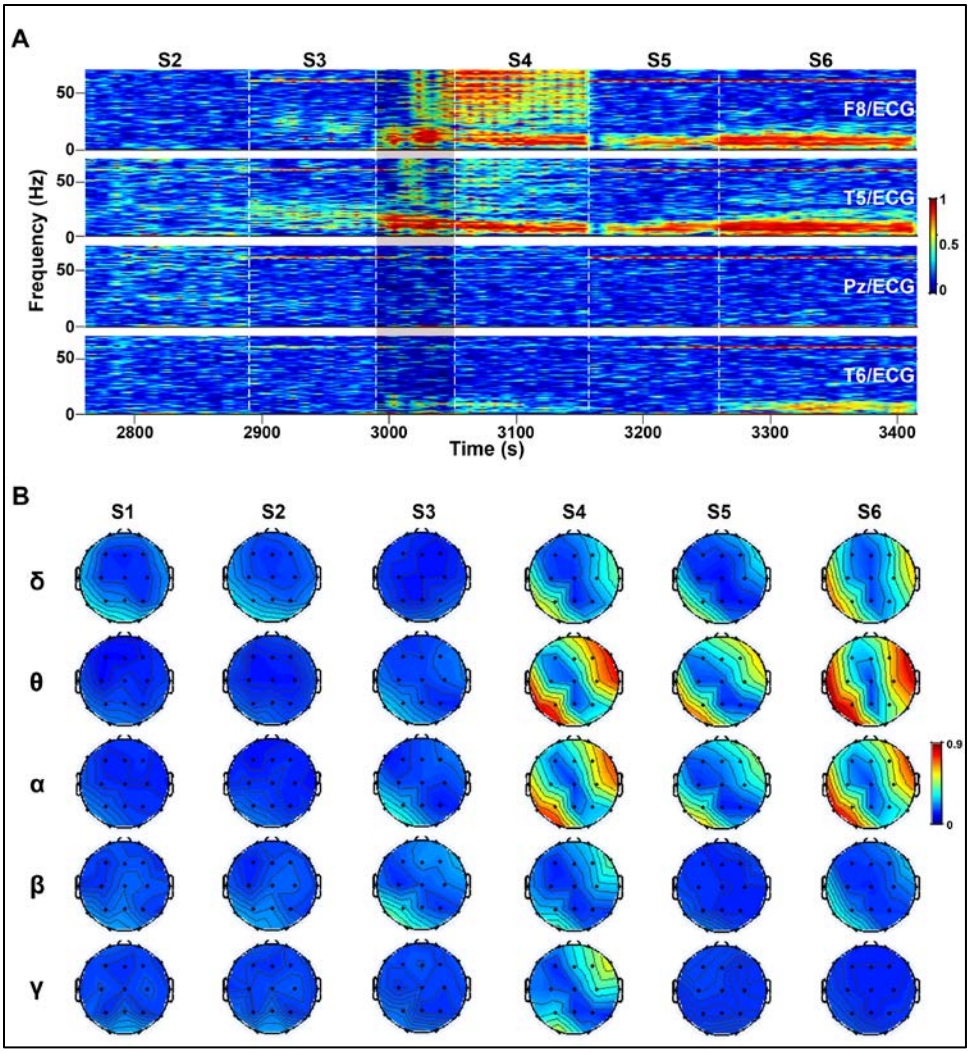

Figure 3.6 Surge of corticocardiac coherence (CCCoh) at near-death. **(A)** CCCoh between 4 cortical channels (F8, T5, Pz, and T6) and ECG from S2 to S6. **(B)** Topographic distribution of CCCoh for 6 stages at 5 different frequency bands: delta (1-4Hz), theta (4-8Hz), alpha (8-13Hz), beta (13-25Hz), and gamma (25-55 Hz).

3.3.7 Surge of CCCon at near-death

To investigate the directional information flow between the brain and the heart during the dying process, CCCon analysis was conducted between each of the 12 EEG channels and ECG signal. Figure 3.7A shows the CCCon between representative cortical channels (F8 and T5) and the ECG signal. Afferent connectivity (from the heart to the brain, or feedforward, or FF) to the right frontal cortex (F8) from the heart is strong at both delta and theta frequency bands specifically at the terminal S6 stage, and is evident for alpha and beta bands only during the early phase of S4

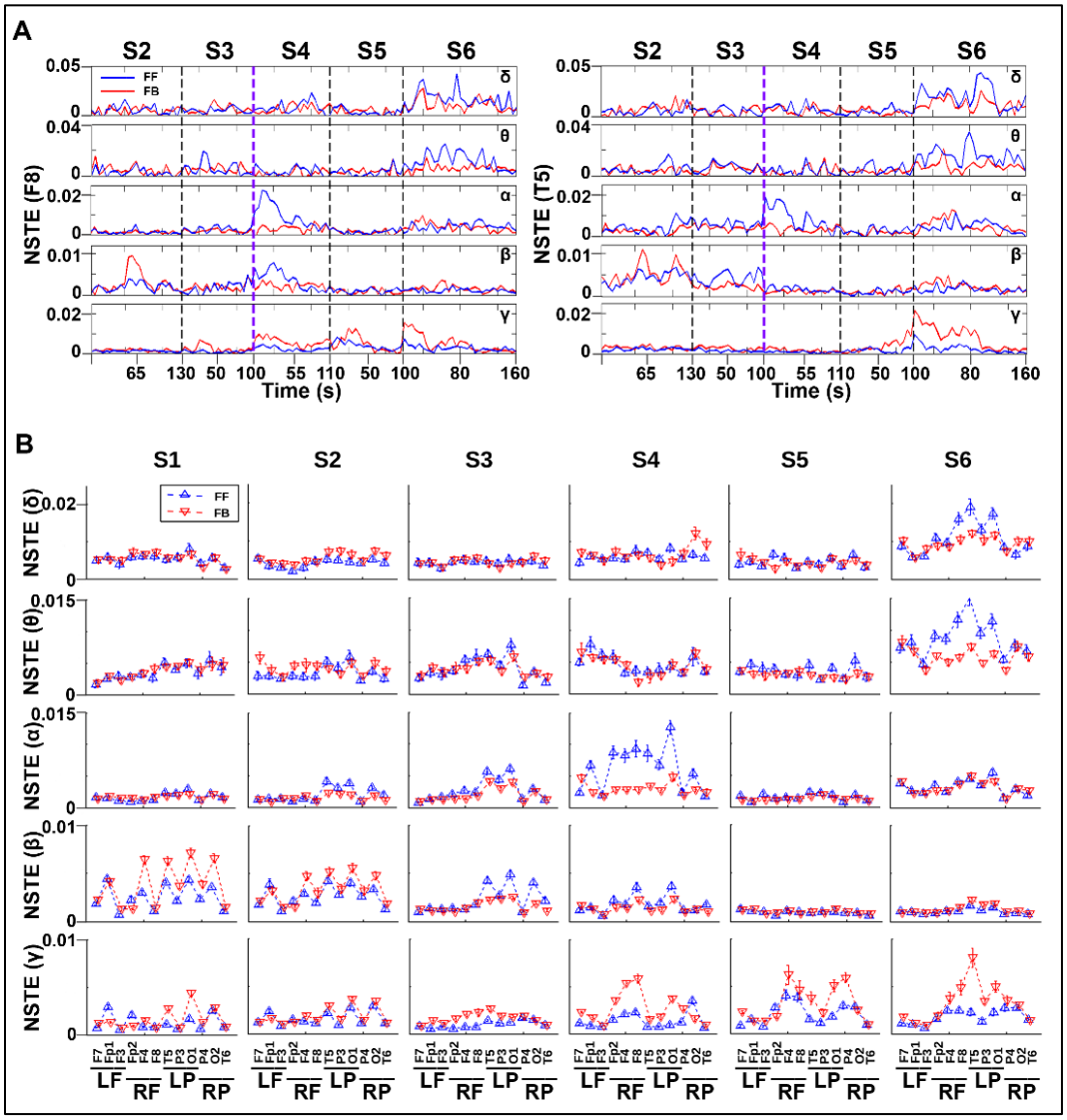

Figure 3.7 Surge of corticocardiac directional connectivity (CCCon) at near-death. **(A)** CCCon between 2 cortical channels (F8 and T5) and ECG from S2 to S6 at 5 different frequencies: delta (1-4Hz), theta (4-8Hz), alpha (8-13Hz), beta (13-25Hz), and gamma (25-55 Hz). FF: feedforward (heart to brain). FB: feedback (brain to heart). **(B)** The CCCon between 12 EEG channels and ECG for 6 stages at 5 different frequency bands.

prior to the onset of 2nd degree heart block. Efferent connectivity (from the brain to the heart, or feedback, or FB) is elevated during stage 6 for multiple frequency bands below alpha bands and uniquely seen for beta bands in S1 and for gamma band at multiple time points (S3-S6). Afferent signaling from the heart to the left posterior cortex at T5 (Figure 3.7A, right panels) exhibited a pattern similar to that of F8. Notable exception was the temporal distribution of CCCoh at

gamma frequency, which is specific for S6 states in both directions at T5 locus, whereas a wider distribution of gamma connectivity across stages S3-S6 is found at F8 locus (Figure 3.7A, left panels). Additional notable feature includes that (1) efferent brain-heart connectivity dominates over afferent heart-brain connectivity for gamma band and (2) at lower frequency bands (lower than beta frequency), opposite appears to be true: afferent connectivity is more dominant. The CCCon between each of the 12 cortical channels and the heart were calculated for each stage at 5 frequencies (Figure 3.7B). FF and FB CCCon exhibited stage-, frequency-, and channel-dependent changes during cardiac arrest. As shown in the figure, marked surge of CCCon was detected at S6 for delta and theta bands, S4 for alpha band, S1 and S2 for beta band, and S4, S5, S6 for gamma frequency. From S1 to S2, CCCon on both directions was maintained at similar basal level for all the channels at delta, theta, alpha, and gamma frequencies. On beta band, the FB CCCon was higher for right frontal and left posterior channel F4, T5, O1, and O2 than other channels. During S3, the FF CCCon for left posterior channels T5 and O1 was higher than other channels from theta to beta rhythm. The CCCon on delta and gamma bands remained at low level for all channels. From S4 to S6, there was a gradual decline of CCCon for all the channels at beta rhythm. In contrast, there is a dramatic surge of CCCon for delta, theta, and alpha oscillations occur at S6, S6, and S4, respectively, with FF CCCon domination. The most active channels are right frontal and left posterior channel F8, T5, and O1 for FF CCCon and left frontal and posterior channel F7, T5, and O1 for FB CCCon. However, for high frequency gamma rhythm, the surge of CCCon was identified during S4, S5, and S6 with FB domination. The most active FB channels are right frontal and left posterior channel F4, F8, and O1, whereas the most active FF channels are right frontal and right posterior channel F4, T5, and O2.

3.3.8 Summary of findings

During cardiac arrest, there are ordered change of RRI and decrease of EEG power. A marked surge of coherence and connectivity both within the brain and between the brain and the heart are identified at near-death stages. Marked increase of cortical coherence and connectivity indicates that the brain is internally highly activated. Marked increase of corticocardiac coherence and connectivity indicates that there are strong electrical signal coupling and communication between the brain and the heart in the dying phase. The brain regions that are mainly responsible for cortical control of cardiac function during sudden cardiac arrest appear to include the right frontal and left parietal lobes.

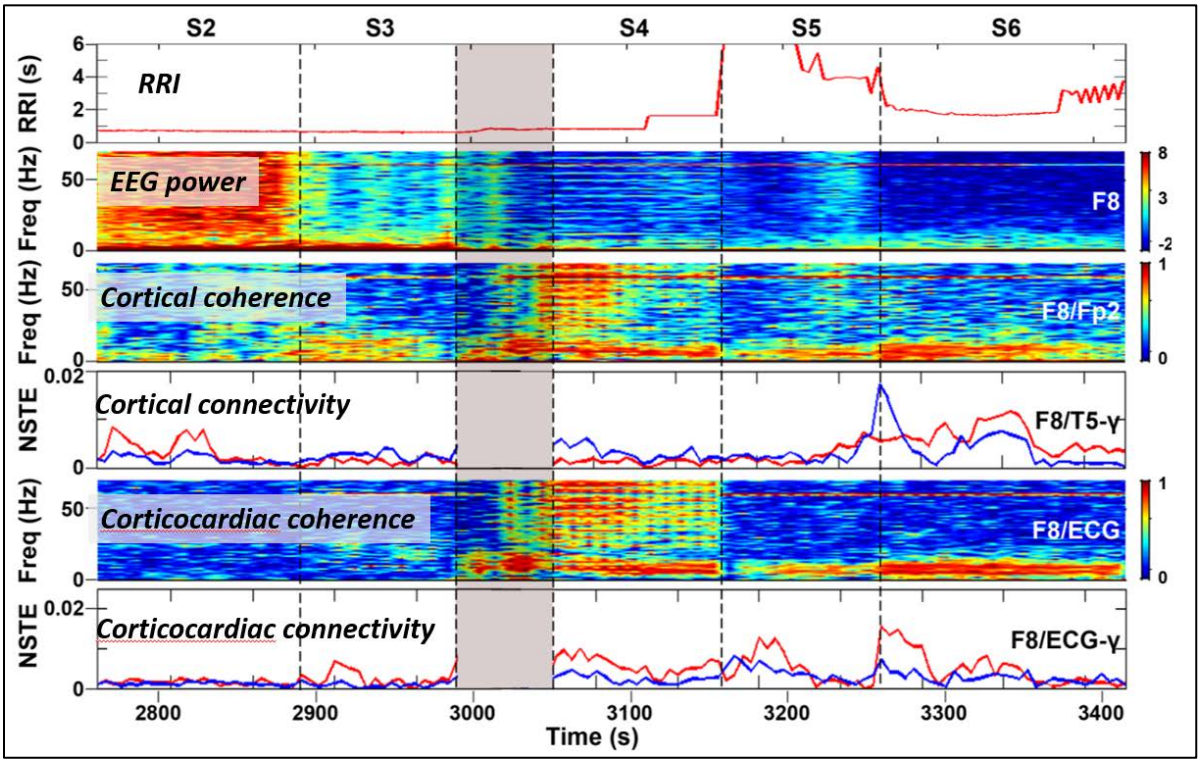

Figure 3.8 Summary of findings. RRI: RR interval, NSTE: normalized symbolic transfer entropy.

3.4 Discussion

In this study, we investigated the dynamic changes of electrical activities of the brain, the heart, and the functional electrical interactions between the brain and the heart in a human patient before and after sudden cardiac failure. Consistent with previous findings in asphyxia cardiac arrest rat model, a marked surge of coherence and connectivity was identified both within the brain and between the brain and the heart in this human patient at near-death. However, different from the rat model, coherence and connectivity in human patient showed changes unique to particular frequency ranges and cortical areas, especially the low frequencies in right frontal and left posterior lobes, suggesting that the low frequency oscillations in these two brain regions may play an important role in cortical control of the cardiac function during sudden cardiac arrest. This result indicates that strong brain-heart connection might be a common mechanism for sudden cardiac arrest in both rats and human.

3.4.1 Deterioration of the heart and activation of the brain at near-death

Many previous studies suggest that the abnormal interactions between the brain and the heart may be the mechanism underlying sudden cardiac arrest [Samuels, 2007; Dorrance and Fink, 2015; Gonzales-Portillo et al., 2016]. However, the dynamic changes of the brain, the heart, and interactions between the two vital organs have not been studied in any human cardiac arrest cases before. In current study, we monitored the electrical activity of the brain and the heart simultaneously during sudden cardiac failure in a human patient, and investigated the functional changes as well as the potential interactions between the brain and the heart during the dying process. Analysis of the RRI and cardiac arrhythmias revealed that the heart underwent similar changes at near-death in human patients as in asphyxic cardiac arrest rat models.

EEG signals of this patient displayed a series of dynamic functional changes before asystole. The functional coupling and directional information transfer between different cortical region was investigated. Consistent with earlier findings from KCl injection and asphyxia-induced cardiac arrest rat model [Borjigin et al., 2013; Li et al., 2015a], a marked surge of coherence and directional connectivity was identified within the brain at near-death. Unlike rat studies, however, the CCoh and CCon in the human patient showed a remarkable spatial specificity. Upon progressing to S4 from S3, the CCoh transitioned from intra-hemispheric to strong interhemispheric patterns of coherence between left posterior and right frontal regions at delta, theta, and alpha frequency. During the same transition, the CCon also showed a surge between left and right frontal region at delta, theta, alpha, and gamma oscillations. In contrast, in KCl injection-induced cardiac arrest model, the surge of CCoh and CCon was only identified in theta and gamma frequency band. In addition, in asphyxic cardiac arrest model, there is a dramatic increase of CCoh and CCon from theta to gamma rhythm. Currently, it is still unknown how the cortical signal communication switched from a diffused pattern to strong interhemispheric coherence and connectivity. Nevertheless, the recovery of EEG power, and marked surge of CCoh and CCon indicates that a highly-activated brain at near-death is conserved between rats and human.

3.4.2 Asymmetrical distribution of CERP during sudden cardiac arrest

To investigate the coupling between the brain and the heart, raw EEG and ECG signals were converted into a matrix format and aligned together to facilitate identification of interesting patterns. We found a surge of CERP at near-death stages. Interestingly, the CERP demonstrated asymmetrical patterns over the cerebral cortex. On the right side of the brain, the CERP displayed positive relationship with ECM, whereas on the left side of the brain, the CERP

showed negative relationship with ECM. And the right frontal and left parietal regions showed the most positive and negative CERPs. The asymmetrical distribution of CERP among the cortex may be associated with the hemisphere asymmetry in autonomic control of the heart. It is known that neural control of the heart is mediated by the sympathetic and parasympathetic nervous pathways innervating the heart [Schwartz and De Ferrari, 2011]. Evidence suggests that the right hemisphere of the brain is predominantly concerned with sympathetic activity, whereas the left hemisphere is predominantly concerned with parasympathetic activity [Lane and Jennings, 1995; Wittling et al., 1998]. Autonomic nerves from the brain to the heart are mostly symmetrical [Levy et al., 1966; Yanowitz et al., 1966; Randall and Ardell, 1990]. These form the basis for the laterality hypothesis whereby central neural processes may be represented asymmetrically on the heart [Lane and Jennings, 1995; Lane et al., in press]. However, in rat models, CERP did not display asymmetrical distribution among the cortex. The spatial specificity of CERP in human brain may due to the fact that the human brain is more evolved than rats, so that different cortical regions in human brain may be specialized to exert limited functions or perform specific tasks, which include the regulation of cardiac function through the autonomic nervous pathways. Except for hemispheric specificity, CERP also demonstrated distinct temporal patterns at different stages. A 18-ms time delay was identified for the CERP from both right frontal channel F8 and left posterior channel T5 in middle cardiac arrest S4 than later cardiac arrest S6. Based on these results, we made the hypothesize that the afferent information from the heart may be first received by the right side of the brain, and the efferent information to the heart may be sent out from the left side of the brain. The strong coherence and directional connectivity between the left posterior and right frontal region may be explained by that the brain is integrating and processing the cardiac information in order to perform internal resuscitation to save the heart. With the

progression of cardiac arrest, the brain-heart communicating is becoming less effective, which is indicated by a longer time-delay in later cardiac arrest S6.

3.4.3 Role of left posterior and right frontal regions in cortical control of cardiac function

Using the same signal processing approaches in rat models, we identified a dramatic increase of coherence and directional connectivity between the brain and the heart at near-death in human patient. The consistency of current study with previous study indicates that corticocardiac coupling may be a common mechanism underlying sudden cardiac arrest in human and rats. However, there are differences of CCCoh and CCCon between asphyxic cardiac arrest rat model and human patient. While no hemispheric specificity was identified for CCCoh and CCCon in rat models, CCCoh and CCCon in human patient is clustered in left posterior and right frontal regions. In addition, the surge of CCCoh and CCCon was detectable from delta to gamma frequencies in rat models. However, in human patient, CCCoh and CCCon mainly appeared at theta and alpha frequencies. The asymmetrical topographic distribution and frequency specificity of CCCoh and CCCon suggest a different and potentially more complex mode of interaction between the brain and the heart in humans than in rats. Till now, it is unclear how the right frontal and left posterior regions communicate with the heart at near-death. But these two brain regions are close to the insular cortex and prefrontal cortex, which have been shown to be involved in the cortical control of the cardiac function using fMRI or cortical stimulation [Napadow et al., 2008; Oppenheimer et al., 1990; Critchley et al., 2003; Palma and Benarroch, 2014; Thayer and Lane, 2009; Gianaros and Sheu; 2009]. More recently, another study demonstrated that in humans, neural events locked to heartbeats before stimulus onset predict the detection of visual grating in the posterior right inferior parietal lobule and the ventral anterior cingulate cortex [Park et al., 2014], which is near to the right frontal region in our study. Another

study measuring the changes in cardiac response in patients with established ventricular dysfunction demonstrated that the amplitude of heart-beat-evoked potential at left temporal and lateral frontal regions correlated with stress-induced changes in cardiac output, which is consistent with the two super-activated cortical regions we identified at near-death. In addition, the amplitude of the heart-beat-evoked potential in the left temporal region reflected the pro-arrhythmic status of the heart [Gray et al., 2007]. Results from the above studies suggest that left posterior and right frontal regions may play an important role for cortical control of the heart. Future studies with multiple electrodes implanted in cortical and subcortical regions, as well as brainstem may provide a more precise estimation of key regions or pathways that mediate brain-heart connection during the dying process.

3.4.4 Corticocardiac coupling as a conserved mechanism for sudden cardiac arrest

In previous studies, we showed that both experimental cardiac arrest and ischemic cardiac arrest stimulated a marked surge of coherence and connectivity in the brain as well as between the brain and the heart before sudden death in rat models [Borjigin et al., 2013; Li et al., 2015a]. Combined with the microdialysis results, we proposed that during the asphyxic cardiac arrest, the right hemisphere of the brain sends strong electrical signals to the heart and causes premature and rapid deterioration of the cardiac function via the activated sympathetic nervous system. In human patient, we found that there are ordered change of RRI and decrease of EEG power in the dying process. A recovery of EEG power and marked surge of coherence and connectivity both within the brain and between the brain and the heart are identified at near-death. Marked increase of CCoh and CCon indicates that the brain is internally highly activated. Marked increase of CCCoh and CCCon indicates that there are strong electrical signal coupling and communication between the brain and the heart in the dying process. The brain regions that are mainly

responsible for cortical control of cardiac function during sudden cardiac arrest are the right frontal and left parietal lobes. Current study in human patient successfully reproduced the results obtained in rat models, suggesting that corticocardiac coupling may be a conserved mechanism for sudden cardiac arrest induced by different causes. Nevertheless, the asymmetrical topographic distribution of CCCoh and CCCon suggest a potentially more complex mode of interaction between the brain and the heart in humans than in rats. As the next step, we plan to perform signal analysis for more human patients to further validate our hypothesis.

3.5 Acknowledgement

This work was supported by the Department of Molecular and Integrative Physiology at the University of Michigan and American Heart Association Predoctoral Fellowship (to FT). We thank Dr. Duan Li for helping analyzing the data in this Chapter. We also thank Drs. Richard Keep, Daniel Beard, Anuska Andjelkovic-Zochowska, and UnCheol Lee for their helpful discussions and comments.

3.6 References

Borjigin, J., Lee, U., Liu, T., Pal, D., Huff, S., Klarr, D., . . . Mashour, G. A. (2013). Surge of neurophysiological coherence and connectivity in the dying brain. Proc Natl Acad Sci U S A, 110(35), 14432-14437. doi:10.1073/pnas.1308285110

Critchley, H. D., Mathias, C. J., Josephs, O., O'Doherty, J., Zanini, S., Dewar, B. K., . . . Dolan, R. J. (2003). Human cingulate cortex and autonomic control: converging neuroimaging and clinical evidence. Brain, 126(Pt 10), 2139-2152. doi:10.1093/brain/awg216

Delorme, A., & Makeig, S. (2004). EEGLAB: an open source toolbox for analysis of single-trial EEG dynamics including independent component analysis. J Neurosci Methods, 134(1), 9-21. doi:10.1016/j.jneumeth.2003.10.009

Dorrance, A. M., & Fink, G. (2015). Effects of Stroke on the Autonomic Nervous System. Compr Physiol, 5(3), 1241-1263. doi:10.1002/cphy.c140016

Finsterer, J., & Wahbi, K. (2014). CNS-disease affecting the heart: brain-heart disorders. J Neurol Sci, 345(1-2), 8-14. doi:10.1016/j.jns.2014.07.003

Gianaros, P. J., & Sheu, L. K. (2009). A review of neuroimaging studies of stressor-evoked blood pressure reactivity: emerging evidence for a brain-body pathway to coronary heart disease risk. Neuroimage, 47(3), 922-936. doi:10.1016/j.neuroimage.2009.04.073

Gonzales-Portillo, C., Ishikawa, H., Shinozuka, K., Tajiri, N., Kaneko, Y., & Borlongan, C. V. (2016). Stroke and cardiac cell death: Two peas in a pod. Clin Neurol Neurosurg, 142, 145-147. doi:10.1016/j.clineuro.2016.01.001

Gray, M. A., Taggart, P., Sutton, P. M., Groves, D., Holdright, D. R., Bradbury, D., . . . Critchley, H. D. (2007). A cortical potential reflecting cardiac function. Proc Natl Acad Sci U S A, 104(16), 6818-6823. doi:10.1073/pnas.0609509104

Kew, H. P., & Jeong, D. U. (2011). Variable threshold method for ECG R-peak detection. J Med Syst, 35(5), 1085-1094. doi:10.1007/s10916-011-9745-7

Lane, R. D., and Jennings, J. R. (1995). Hemispheric asymmetry, autonomic asymmetry and the problem of sudden death, in Brain Asymmetry, eds R. J. Davidson and K. Hugdahl (Cambridge, MA: The MIT Press), 271-304.

Lane, R. D., Critchley, H. D., and Taggart, P. (2011). Asymmetric autonomic innervation, in Handbook of Cardiovascular Behavioral Medicine, eds S. Waldstein, W. Kop, and L. Katzel (New York: Springer).

Lee, U., Kim, S., Noh, G. J., Choi, B. M., Hwang, E., & Mashour, G. A. (2009). The directionality and functional organization of frontoparietal connectivity during consciousness and anesthesia in humans. Conscious Cogn, 18(4), 1069-1078. doi:10.1016/j.concog.2009.04.004

Levy, M. N., Ng, M. L., & Zieske, H. (1966). Functional distribution of the peripheral cardiac sympathetic pathways. Circ Res, 19(3), 650-661.

Li, D., Mabrouk, O. S., Liu, T., Tian, F., Xu, G., Rengifo, S., . . . Borjigin, J. (2015a). Asphyxia-activated corticocardiac signaling accelerates onset of cardiac arrest. Proc Natl Acad Sci U S A, 112(16), E2073-2082. doi:10.1073/pnas.1423936112

Li, D., Tian, F., Rengifo, S., Xu, G., M Wang, M., & Borjigin, J. (2015b). Electrocardiomatrix: A new method for beat-by-beat visualization and inspection of cardiac signals. Journal of Integrative Cardiology, 1(5). doi:10.15761/JIC.1000133

Myerburg R.J., Castellanos A (2015). Cardiac arrest and sudden cardiac death, in: Heart Disease: A Textbook of Cardiovascular Medicine, eds E. Braunwald, chap. 39;821-860.

Napadow, V., Dhond, R., Conti, G., Makris, N., Brown, E. N., & Barbieri, R. (2008). Brain correlates of autonomic modulation: combining heart rate variability with fMRI. Neuroimage, 42(1), 169-177. doi:10.1016/j.neuroimage.2008.04.238

Nichol, G., Thomas, E., Callaway, C. W., Hedges, J., Powell, J. L., Aufderheide, T. P., . . . Resuscitation Outcomes Consortium, I. (2008). Regional variation in out-of-hospital cardiac arrest incidence and outcome. JAMA, 300(12), 1423-1431. doi:10.1001/jama.300.12.1423

Oppenheimer, S. M., & Cechetto, D. F. (1990). Cardiac chronotropic organization of the rat insular cortex. Brain Res, 533(1), 66-72.

Palma, J. A., & Benarroch, E. E. (2014). Neural control of the heart: recent concepts and clinical correlations. Neurology, 83(3), 261-271. doi:10.1212/WNL.0000000000000605

Papadakis, M., Sharma, S., Cox, S., Sheppard, M. N., Panoulas, V. F., & Behr, E. R. (2009). The magnitude of sudden cardiac death in the young: a death certificate-based review in England and Wales. Europace, 11(10), 1353-1358. doi:10.1093/europace/eup229

Park, H. D., Correia, S., Ducorps, A., & Tallon-Baudry, C. (2014). Spontaneous fluctuations in neural responses to heartbeats predict visual detection. Nat Neurosci, 17(4), 612-618. doi:10.1038/nn.3671

Randall, W. C., and Ardell, J. L. (1990). Nervous control of the heart: anatomy and pathophysiology, in Cardiac Electrophysiology: From Cell to Bedside, eds D. P. Zipes and J. Jalife (Philadelphia: W. B. Saunders), 291-299.

Samuels, M. A. (2007). The brain-heart connection. Circulation, 116(1), 77-84. doi:10.1161/CIRCULATIONAHA.106.678995

Schwartz, P. J., & De Ferrari, G. M. (2011). Sympathetic-parasympathetic interaction in health and disease: abnormalities and relevance in heart failure. Heart Fail Rev, 16(2), 101-107. doi:10.1007/s10741-010-9179-1

Stecker, E. C., Reinier, K., Marijon, E., Narayanan, K., Teodorescu, C., Uy-Evanado, A., . . . Chugh, S. S. (2014). Public health burden of sudden cardiac death in the United States. Circ Arrhythm Electrophysiol, 7(2), 212-217. doi:10.1161/CIRCEP.113.001034

Thayer, J. F., & Lane, R. D. (2009). Claude Bernard and the heart-brain connection: further elaboration of a model of neurovisceral integration. Neurosci Biobehav Rev, 33(2), 81-88. doi:10.1016/j.neubiorev.2008.08.004

Tian, F., Liu, T., Xu, G., Li, D., Ghazi, T., Shick, T., . . . Borjigin, J. (2018). Adrenergic blockade bi-directionally and asymmetrically alters functional brain-heart communication

and prolongs electrical activities of the brain and heart during asphyxic cardiac arrest. Frontiers in Physiology, 9, 99.

Wittling, W., Block, A., Genzel, S., & Schweiger, E. (1998). Hemisphere asymmetry in parasympathetic control of the heart. Neuropsychologia, 36(5), 461-468.

Yanowitz, F., Preston, J. B., & Abildskov, J. A. (1966). Functional distribution of right and left stellate innervation to the ventricles. Production of neurogenic electrocardiographic changes by unilateral alteration of sympathetic tone. Circ Res, 18(4), 416-428.

Chapter 4 Intermittent surge of corticocardiac coupling preceding to sudden death in ischemic rats

4.1 Introduction

Sudden death is an important but under-recognized consequence of stroke [Sörös and Hachinski, 2012]. Despite major improvements in stroke diagnosis and treatment, 2-6% of patients suffer from sudden, unexpected death within the first 3 months after ischemic stroke [Prosser et al., 2007; Sörös and Hachinski, 2012]. In addition, about 19% of patients have fatal or serious non-fatal cardiac events, such as ventricular arrhythmias, which greatly increase the risk of sudden death [Prosser et al., 2007; Frangiskakis et al., 2009; Sörös and Hachinski, 2012]. The mechanisms of ischemic stroke-induced sudden death remain unclear. As a consequence, identification of patients at risk and prevention of stroke-induced sudden death present a major challenge.

Our laboratory has discovered that the brain is highly activated immediately following global ischemia induced by experimental cardiac arrest [Borjigin et al., 2013]. More recently, we reported a marked surge of functional connectivity (cortical coherence, CCoh) and directional connectivity (CCon) in the dying brain of rats following asphyxia, which paralleled with excessive cortical release of a set of core neurotransmitters [Li et al., 2015a]. In addition to the changes within the brain, a surge of corticocardiac coherence (CCCoh) and directional connectivity (CCCon), indicator for strong brain-heart connection, emerged after the onset of asphyxia with a reliable time delay [Li et al., 2015a]. These data suggest that sudden death in rats

that suffered global ischemia is tightly associated with the surge of functional connectivity within the cortex as well as between the cortices and the heart. Whether this association exists in dying rats with forebrain ischemia is unknown.

Bilateral common carotid artery ligation (BCCAL) in stroke-prone spontaneously hypertensive rat (SHRSP) is a well-established model for forebrain ischemia [Kakihana et al., 1983; Lobanova et al., 2008]. The cerebrovascular architecture and risk factors in SHRSP resemble with stroke in human patients, which makes SHRSP, derived from the normotensive Wistar-Kyoto (WKY) rat, a suitable model for studying ischemic stroke in rats [Yamori et al., 1976]. Compared to asphyxic cardiac arrest rat model used in our previous studies, in which the entire body, including the brain and heart, is globally affected, the forebrain ischemia model (BCCAL) tests the direct influence of brain ischemia on cortical/cardiac functions, and permits the dissection of functional communication between the two vital organs. In this study, we use advanced signal processing techniques to functionally characterize the brain and the heart in the BCCAL model. Our goal is to understand how neurological injuries lead to abnormal brain-heart connection, autonomic dysfunction, cardiac damage, and sudden death. Ultimately, we hope this line of investigation will contribute to better understanding of the dying brain and the development of novel non-invasive biomarkers for prediction of risk for sudden death.

4.2 Materials and methods

4.2.1 Animals

Inbred SHRSP and WKY rats were acclimatized in our housing facility for at least 1 week before implantation of electrodes. Following electrode implantation, rats were allowed to recover for 1 week before online recording. The experimental procedures were approved by the University of

Michigan Committee on Use and Care of Animals. All experiments were conducted using adult rats (300-400 g) maintained on a light: dark cycle of 12: 12 hour (lights on at 6:00 am) and provided with ad libitum food and water.

4.2.2 Electrode implantation and configuration

Rats were implanted with electrodes for EEG signal recording under surgical anesthesia [1.8% (vol/vol) isoflurane]. The EEG signals were recorded through screw electrodes implanted bilaterally on the frontal [anteroposterior (AP): + 3.0 mm; mediolateral (ML): ± 2.5 mm, bregma], parietal (AP: -3.0 mm; ML ± 2.5 mm, bregma), and occipital (AP: -8.0 mm; ML: ± 2.5 mm, bregma) cortices. The ECG signals were recorded through flexible and insulated (except at the tip) multi-stranded wires (Cooner Wires, Chatsworth, CA) inserted into subcutaneous muscles flanking the heart. The EEG and ECG electrodes were interfaced with two six-pin pedestals (Plastics One, Roanoke, VA), and the entire assembly was secured on the skull using dental acrylic.

4.2.3 Signal acquisition and stroke surgeries

Prior to data collection, rats were acclimatized in the recording chamber. EEG and ECG signals were recorded using Grass Model 15LT physiodata amplifier (15A54 Quad amplifiers) system (Astro-Med, Inc., Quincy, MA) interfaced with BIOPAC MP-150 data acquisition unit and AcqKnowledge software (version 4.1.1, BIOPAC systems, Inc., Goleta, CA). The signals were filtered between 0.1 and 300 Hz and sampled at 1,000 Hz. EEG and ECG recordings were initiated consistently at 10:00 am to control for circadian factors. Baseline signals were recorded for 1 hour. At the end of this baseline recording, permanent BCCAL was performed for SHRPS and WKY rats under surgical anesthesia [Ogata et al., 1976]. After BCCAL, recording was continued until sudden death for SHRSP rats and for at most 24 hours for WKY rats.

4.2.4 Analysis of RR interval (RRI), cardiac arrhythmias, and heart rate variability (HRV)

To analyze the RRI, baseline drift correction was first implemented using second-order Butterworth high-pass filtering with a cutoff frequency at 1 Hz (butter.m and filtfilt.m in Matlab Signal Processing Toolbox; MathWorks Inc., Natick, MA). R peaks of ECG signals were then detected using variable threshold method [Kew and Jeong, 2011]. Specifically, an amplitude threshold in each nonoverlapping 1 second epoch was applied to select the candidates for R peaks, which can be verified only if the RRI value exceeds a predefined threshold. In this study, the interval threshold was selected as half of the median value of the RRI values in the last 1 second epoch. The automatically detected R peaks were manually validated through a custom user interface developed in Matlab (MathWorks Inc., Natick, MA). As the next step, outliers were removed from the validated RRI using threshold and sliding window averaged filter. RRI was then interpolated using linear interpolation for every 1 minute and plotted for SHRSP and WKY rats (Figure 4.1B). The mean and standard deviation of RRI during baseline (1 hour before BCCAL), first hour (1st hour after BCCAL), and last hour (1.5-0.5 hour before death) were calculated for all SHRPS (n=9) and WKY (n=8) rats (Figure 4.1C). To analyze the number and types of cardiac arrhythmias, ECG signals were examined and cardiac arrhythmias were manually labeled and counted using a custom user interface developed in Matlab (MathWorks Inc., Natick, MA).

HRV was analyzed to study the interactions between the sympathetic and parasympathetic nervous system. While high frequency (HF) is considered to reflect parasympathetic activity, low frequency (LF) is thought to be affected by both the sympathetic and parasympathetic activity [Kuwahara et al., 1994]. The ratio between LF and HF (LF/HF) reflects the relative balance of sympatho-vagal influences on the heart. Frequency domain

analysis of HRV was performed using Fast Fourier transform for LF (0.25-0.8 Hz) and HF (0.8-3 Hz). Frequency selection was based on previous works in rats [Fauchier et al., 2006; Barbosa et al., 2013]. The power spectrum of HRV was calculated and expressed in log scale for SHRSP and WKY rats (Figure 4.6A). The mean and standard deviation of power spectral density for LF, HF, and LF/HF during baseline (1 hour before BCCAL), first hour (1st hour after BCCAL), and last hour (1.5-0.5 hour before death) were calculated for all SHRPS (n=9) and WKY rats (n=8) (Figure 4.6B).

4.2.5 Construction of electrocardiomatrix (ECM)

The ECM is designed to facilitate the visualization of RRI, the amplitude, and the morphology of ECG signals. For construction of ECM [Li et al., 2015b] , a window centered on the detected ECG R peaks (for example, from -0.1 second to 0.3 second, with 0 corresponding to the time of R-peak) was extracted from the ECG signal after baseline drift correction. All ECG windows were sorted according to the order of R-peak time and then plotted as parallel colored lines to form a colored rectangular image. The intensity of ECG signal was denoted on *z*-axis, with warmer color indicates positive peaks with higher voltage, while cooler color indicates negative peaks with lower voltage. The color scheme could be adjusted according to the need.

4.2.6 Analysis of EEG power

The original sampling frequency of 1,000 Hz was first down-sampled to 500 Hz to reduce computing time. A notch filter was used to remove the 60 Hz artifact and its possible super-harmonics. Then EEG power was analyzed using short time Fourier transform based on discrete Fourier transform with 2-second segment size and 1 second overlapping for each frequency bin (0.5-250 Hz with 0.5 Hz bin size; spectrogram.m in Matlab Signal Processing Toolbox,

MathWorks Inc., Natick, MA). Each segment was windowed with a Hamming window. The absolute EEG power was expressed on a log scale for SHRSP and WKY rats (Figure 4.2A). The absolute EEG power on gamma 1 frequency was summed up and plotted for SHRSP and WKY rats (Figure 4.2B). The mean and standard deviation of absolute EEG power during baseline (1 hour before BCCAL), first hour (1st hour after BCCAL), and last hour (1.5-0.5 hour before death) was calculated for six frequency bands: delta (0.5-5 Hz), theta (5-10 Hz), alpha (10-15 Hz), beta (15-25 Hz), gamma 1 (25-55 Hz), and gamma 2 (65-115 Hz) for all SHRPS (n=9) and WKY (n=8) rats (Figure 4.2C).

4.2.7 Analysis of CCoh and CCCoh

The coherence between 6 EEG channels (CCoh), or between 1 ECG and 6 EEG channels (CCCoh) was measured by amplitude squared coherence ($C_{xy}(f)$) (mscohere.m in Matlab Signal Processing Toolbox, MathWorks Inc., Natick, MA), which is a coherence estimate of the input signals x and y using Welch's averaged, modified periodogram method. The magnitude squared coherence estimate $C_{xy}(f)$ is a function of frequency with values between 0 and 1 that indicates how well signal x corresponds to signal y at each frequency:

$$C_{xy}(f) = \frac{|P_{xy}(f)|^2}{P_{xx}(f)P_{yy}(f)}, 0 \leq C_{xy}(f) \leq 1 \qquad (1)$$

where $P_{xx}(f)$ and $P_{yy}(f)$ are the power spectral density of x and y, and $P_{xy}(f)$ is the cross power spectral density.

In current study, a notch filter was used to remove the 60 Hz artifact and its possible super-harmonics. EEG or ECG signals were then segmented into 2-second epochs with 1-second overlap. The magnitude squared coherence was calculated at each epoch and frequency bin (0.5-250 Hz with 0.5 Hz bin size). The mean coherence between 6 EEG channels (Figure 4.3A) and

among 1 ECG and 6 EEG channels (Figure 4.4A) were calculated and plotted for frequencies from 0.5 to 250 Hz for SHRSP and WKY rats. The mean CCoh (Figure 4.3B) and CCCoh (Figure 4.4B) for gamma 1 frequency band were also plotted for SHRSP and WKY rats. The mean and the standard deviation of coherence among 15 pairs of 6 EEG channels during baseline (1 hour before BCCAL), first hour (1st hour after BCCAL), and last hour (1.5-0.5 hour before death) were calculated for frequencies from delta to gamma 2 for all SHRPS (n=9) and WKY (n=8) rats (Figure 4.3C). The mean and the standard deviation of percent changes on the amplitude of CCCoh over baseline were calculated for each hour after BCCAL and compared between SHRSP (n=9) and WKY (n=8) rats (Figure 4.4C, left panel). The duration of epochs with CCCoh 2 times higher than baseline was summed up for each rat and expressed as a percentage of the total duration for that rat. Comparison was then made between SHRSP (n=9) and WKY (n=8) rats for all 6 frequencies (from delta to gamma 2) (Figure 4.4C, right panel).

4.2.8 Analysis of CCCon

The directional connectivity between EEG and ECG signals was measured by modified [Li et al., 2015a] Normalized Symbolic Transfer Entropy (NSTE) [Lee et al., 2009], which is a nonlinear and model-free estimation of directional functional connection based on information theory. STE measures the amount of information provided by the additional knowledge from the past of the source signal $X(X^P)$ in the model describing the information between the past $Y(Y^P)$ and the future $Y(Y^F)$ of the target signal Y, which is defined as following:

$$STE_{X\to Y} = I(Y^F; X^P|Y^P) = H(Y^F|Y^P) - H(Y^F|X^P, Y^P) \qquad (2)$$

where $H(Y^F|Y^P)$ is the entropy of the process Y^F conditional on its past. Each vector for $Y^F, X^P \; and \; Y^P$ is a symbolized vector point. The potential bias of STE was removed with a shuffled data, and the unbiased STE is normalized as follows:

$$NSTE_{X\to Y} = \frac{STE_{X\to Y} - STE_{X\to Y}^{Shuffled}}{H(Y^F|Y^P)} \in [0,1] \qquad (3)$$

where $STE_{X\to Y}^{Shuffled} = H(Y^F|Y^P) - H(Y^F|X_{Shuff}^P, Y^P)$. X_{Shuff}^P is a shuffled data created by dividing the data into sections and rearranging them at random. Therefore, NSTE is normalized STE (dimensionless), in which the bias of STE is subtracted from the original STE and then divided by the entropy within the target signal, $H(Y^F|Y^P)$.

For CCCon, the feedback connectivity ($\overline{NSTE}_{EEG\to EKG}$) was calculated by averaging NSTE over 6 pairs of EEG channels to ECG channel, which are defined as follows:

$$\overline{NSTE}_{EEG\to EKG} = \frac{1}{n_{EEG}} \sum_{i=1}^{n_{EEG}} NSTE_{i\to EKG} \qquad (4)$$

where $n_{EEG} = 6$. The feedforward connectivity ($\overline{NSTE}_{EKG\to EEG}$) from the ECG to 6 EEG channels is vice versa.

Specifically, we first filtered EEG and ECG signals into 6 frequency bands (from delta to gamma 2), and then segmented the filtered signals into 2-second long epochs with 1-second overlapping. The mean CCCon ($\overline{NSTE}_{EEG\to EKG}$ and $\overline{NSTE}_{EKG\to EEG}$) were sequentially calculated for each epoch and each frequency band. Three parameters: embedding dimension (d_E), time delay (τ), and prediction time (δ), were required in the calculation. In this study, we selected the parameter setting that could yield maximum $NSTE_{X\to Y}$ by fixing the embedding dimension (d_E) at 3, and optimizing prediction time δ (from 1 to 50, corresponding to 1-50 ms with the sampling frequency of 1,000 Hz) and time delay τ (1-300 ms). The same procedure was used to calculate $NSTE_{Y\to X}$, provided that the information between two signals is transferred through different neuronal pathway. The feedback and feedforward CCCon were plotted for theta and gamma 1 frequency for a sample epoch that shows a surge of CCCoh (Figure 4.5A). The mean and standard deviation of CCCon epochs during baseline (1 hour before BCCAL), first hour (1st

hour after BCCAL), and last hour (1.5-0.5 hour before death) was calculated for six frequency bands for all SHRPS (n=9) rats (Figure 4.5B).

4.2.9 Statistical analysis

For all the statistical analyses, Shapiro-Wilk normality test was first implemented to determine if the data was normally distributed. To test the differences of RRI (Figure 4.1C), EEG power (Figure 4.2C), CCoh (Figure 4.3C), CCCon (Figure 4.5B), and HRV (Figure 4.6C) among baseline, first hour, and last hour, repeated measures ANOVA with post hoc Pair-Sample T-test (for normally distributed data) or Friedman Test with Wilcoxon post hoc comparisons (for non-normally distributed data) were conducted. To analyze the differences of CCCoh between SHRSP and WKY (Figure 4.4C), and the differences between feedback and feedforward CCCon (Figure 4.5B), independent-sample T-test (for normally distributed data) or Mann-Whitney (for non-normally distributed data) test was used. For all the comparisons, $p < 0.05$ was considered as statistically significant. Statistical analyses were performed using the software SPSS (version 19.0; IBM SPSS Statistics).

4.3 Results

4.3.1 Forebrain ischemia claimed 100% mortality in SHRSP rats within 14 hours

A total of 9 SHRSP and 8 WKY rats underwent BCCAL procedure, which caused 100% mortality in SHRSP rats within 14 hours. In contrast, no mortality was observed in WKY control rats. The survival length of SHRSP rats ranged from 2.89 hours to 13.92 hours, with a mean length of 8.13 hours.

4.3.2 SHRSP rats suffering from forebrain ischemia exhibited a marked decrease in RRI and increase in cardiac arrhythmias

The effects of forebrain ischemia on cardiac function was investigated. ECM was first generated to facilitate a comprehensive understanding on the dynamic changes of RRI and cardiac arrhythmias before and after BCCAL procedure in representative SHRSP and WKY rats (Figure 4.1A). Figure 4.1B shows the RRI plot for the same pair of SHRSP and WKY rats. As we can see in Figure 4.1A and 4.1B, during baseline (-1-0 hour) condition, SHRSP and WKY rats displayed similar RRI of about 0.2 seconds [heart rate of 300 beats/minute (bpm)]. After BCCAL, RRI for SHRSP rat continued to decline until the sudden collapse of cardiac function at 7^{th} hour after ischemic stroke, as indicated by the large increase of RRI in the ending phase. In sharp contrast, RRI for WKY rat showed mild fluctuations during the entire process. These features are conserved for all SHRSP and WKY rats (Figure 4.1C). As shown in the left panel of Figure 4.1C, the RRI for SHRSP rats was significantly lower in first hour after ischemia (0.17±0.02 second [353 bpm]) than the baseline (0.19±0.01 second [316 bpm]). Moreover, SHRSP rats showed a further significant reduction of RRI in the last hour (1.5-0.5 hour before sudden death) (0.13±0.01 second [462 bpm]) compared to baseline and first hour after BCCAL. However, no significant differences on RRI were found for WKY rats among baseline, first hour after BCCAL, and last hour before sudden death (right panel in Figure 4.1C).

Cardiac arrhythmias before and after forebrain ischemia are summarized in Table 4.1. A total of 9 common arrhythmias were identified. Among them, the average hourly occurrence of premature ventricular contraction (PVC), sinus pause (SP), junctional rhythm (JR), and second-degree heart block (2HB) significantly increased after ischemic stroke for both SHRSP and WKY rats. However, significant increase in average hourly occurrence for premature atria

contraction (PAC), third-degree heart block (3HB), junctional escape beat (JEB), ventricular escape beat (VEB), and marked sinus bradycardia (MSB) over baseline was only observed in SHRSP rats. In addition, during the last 30 minutes (ending phase) before death, agonal signals including 2HB, 3HB, JEB, VEB, and MSB remarkably increased for SHRSP rats, but were not identified in any WKY rats.

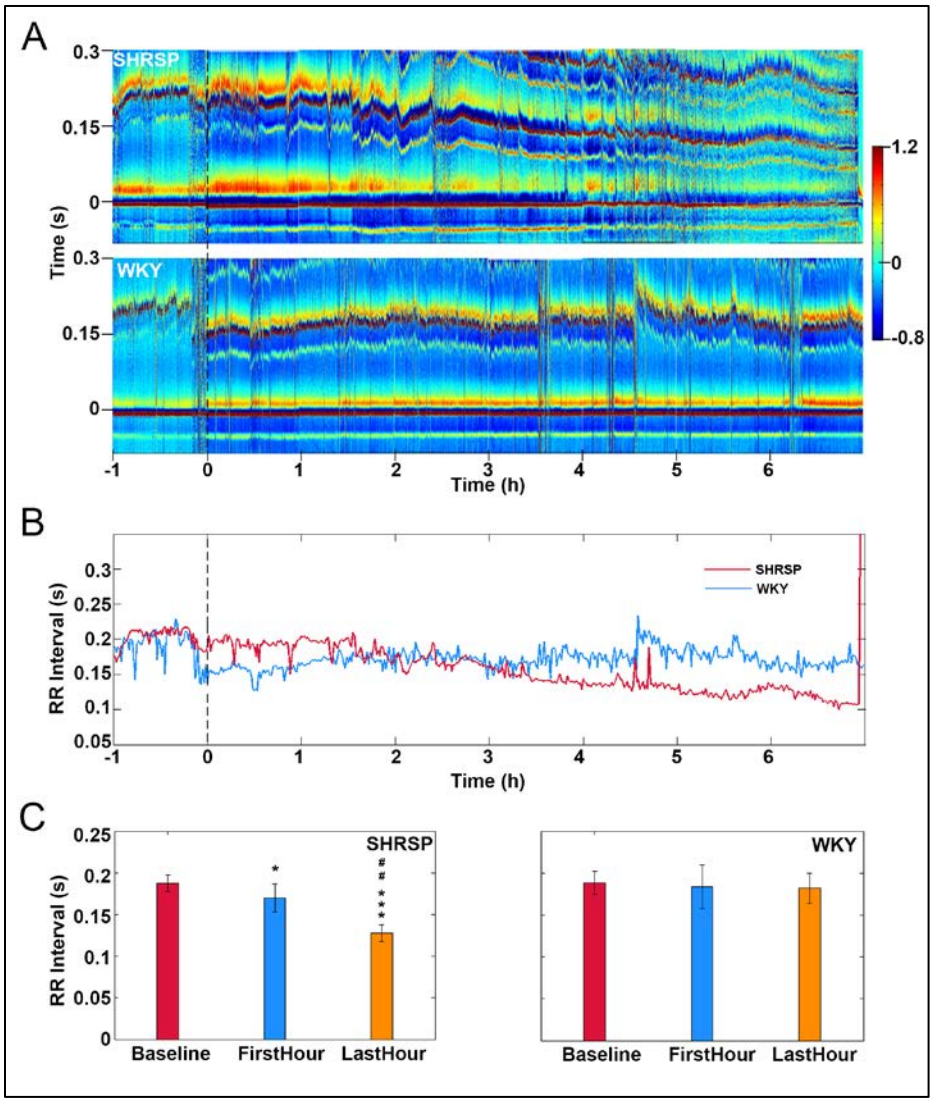

Figure 4.1 BCCAL results in marked reduction of RRI in SHRSP rats. **(A)** Electrocardiomatrix (ECM) display of ECG signals before and after BCCAL (time 0 sec) for representative rats. **(B)** RRI before and after BCCAL for representative rats. **(C)** RRI during baseline (-1-0 hour), first hour (0-1 hour), and last hour (1.5-0.5 hour before death) for all SHRSP (n=9) and WKY (n=8) rats. Data expressed as mean±SD. *Significant differences over baseline, ##significant differences between first and last hour (*/#$p < 0.05$, **/##$p < 0.01$, ***/###$p < 0.001$).

Table 4.1 Hourly occurrence of cardiac arrhythmias per rat.

	Time	PAC	PVC	SP	JR	2HB	3HB	JEB	VEB	MSB
SHRSP	Baseline	1.4±0.4	0.2±0.1	0.7±0.4	0.0	0.0	0.0	0.0	1.9±1.9	0.0
	First Hour	4.4±1.1	17.0±5.9 **	0.3±0.2	35.1±26.2	0.0	0.0	0.0	0.0	0.0
	Last Hour	1.2±0.6	5.2±2.6 *	6.3±3.6	17.4±15.1	5.9±5.9	0.0	11.7±8.9	24.9±19.1	0.2±0.2
	Ending Phase	6.2±4.5	6.0±3.0	56.4±48.8 #	66.9±48.5	60.7±33.4 *#	28.0±15.1 *#^	260.4±69.8 **##^^	106.2±22.5 **##^	255.6±90.1 *#^
	Average	5.2±1.4 **	13.8±2.7 **	14.0±8.4 **	42.6±16.5 *	3.6±1.4 *	1.5±0.7 *	25.2±12.1 **	23.5±7.2 *	23.8±10.1 *
WKY	Baseline	0.4±0.4	0.3±0.2	0.0	9.0±4.8	0.0	0.0	0.0	0.0	0.0
	First Hour	1.6±0.6	3.4±1.1 *	2.9±1.3	18.9±8.2	1.4±0.8	0.0	0.0	0.0	0.0
	Last Hour	0.5±0.4	1.5±0.4 *	5.8±2.6	118.3±96.2	0.4±0.3	0.0	0.0	0.0	0.0
	Ending Phase	2.0±1.5	0.8±0.4	10.0±5.1	195.3±152.6 *	0.0	0.0	0.0	0.0	0.0
	Average	1.2±0.3	2.0±0.4 *	6.9±3.1 *	131.0±110.5 *	0.8±0.3 *	0.0	0.0	0.0	0.0

PAC: premature atria contraction, PVC: premature ventricular contraction, SP: sinus pause, JR: junctional rhythm, 2HB: second-degree heart block, 3HB: third-degree heart block, JEB: junctional escape beat, VEB: ventricular escape beat, MSB: marked sinus bradycardia, baseline: 1 hour before BCCAL, first hour: 1st hour after BCCAL, last hour: 1.5-0.5 hour before death, ending phase: 0.5-0 hour before death. Data expressed as mean±SDE. *Significant differences over baseline, #significant differences over first hour, ^significant differences over last hour (*/#/^$p < 0.05$, **/##/^^$p < 0.01$).

4.3.3 SHRSP rats exhibited a marked reduction of EEG power following forebrain ischemia

To explore the influence of forebrain ischemia on the electrical activity of the brain, average EEG power across all 6 cortical channels before and after BCCAL was analyzed. Figure 4.2A shows the EEG power spectrum for all frequencies (0-250 Hz) in representative SHRSP and WKY rats. As shown in the figure, EEG power was dramatic reduced for SHRSP rat immediately after BCCAL and maintained at low levels until sudden death for all frequency bands (upper panel in Figure 4.2A). However, EEG power for WKY rat did not exhibit obvious changes over the entire process (lower panel in Figure 4.2A). Figure 4.2B displays the changes of EEG power at gamma 1 frequency before and after BCCAL for the same pair of SHRSP and WKY rats. In contrast to the nearly stable EEG power in control WKY rat, EEG power for SHRSP rat demonstrated a dramatic reduction immediately following forebrain ischemia, which then continued to decline until sudden death. Statistical analyses were conducted to compare the changes of EEG power among baseline, first hour after BCCAL, and last hour (0.5-1.5 hour before sudden death) in all SHRSP and WKY rats. As shown in Figure 4.2C, the significant reduction of EEG power in both first hour after BCCAL and last hour before sudden death compared to baseline are consistent for all SHRSP rats across all 6 frequencies, which include delta, theta, alpha, beta, gamma 1, and gamma 2 (left panel in Figure 4.2C). Additionally, the EEG power for last hour was also significantly lower than first hour for delta, theta, alpha, beta, and gamma 1 frequencies. In contrast, while showing significant reduction of EEG power in the first hour after forebrain ischemic stroke in most frequencies (delta, theta, alpha, beta, and gamma 1), WKY rats demonstrated a rebound increase of EEG power in the last hour for all frequencies (right panel in Figure 4.2C). EEG power changes for each channel during baseline,

first hour, and last hour for all frequencies in SHRSP and WKY rats are shown in Supplement Figure 4 in Appendix.

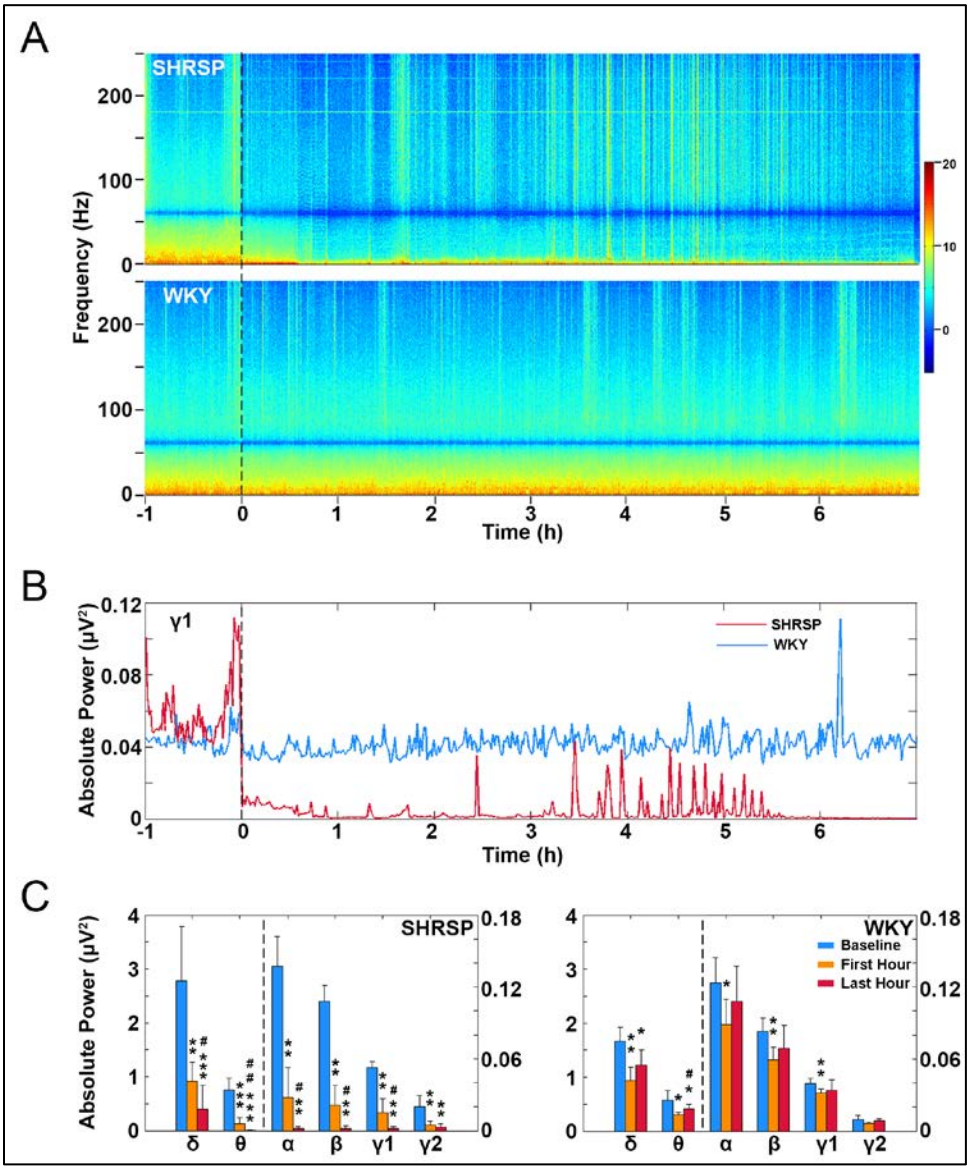

Figure 4.2 BCCAL results in marked reduction of EEG power in SHRSP rats. **(A)** EEG power spectrum before and after BCCAL (at time 0) for all frequencies in representative rats. **(B)** EEG power before and after BCCAL at gamma 1 frequency in representative rats. **(C)** EEG power during baseline (-1-0 hour), first hour (0-1 hour), and last hour (1.5-0.5 hour before death) for all SHRSP (n=9) and WKY (n=8) rats. Data expressed as mean±SD. *Significant differences over baseline, ##significant differences between first and last hour (*/#$p < 0.05$, **/##$p < 0.01$, ***/###$p < 0.001$).

4.3.4 SHRSP rats exhibited a significant increase of CCoh following forebrain ischemia

To explore the influence of forebrain ischemia on functional connectivity (coherence) of the brain, CCoh before and after BCCAL was analyzed. Figure 4.3A shows the CCoh before and after BCCAL for all frequencies in representative SHRSP and WKY rats. As shown in the figure, there is a marked decrease of CCoh at low frequencies (0-55 Hz) and increase of CCoh for high frequencies (65-250 Hz) within 1 hour after BCCAL in SHRSP rat (upper panel in Figure 4.3A). After this early phase reduction of low frequency CCoh, CCoh for all frequencies demonstrated a dramatic and sustained increase until sudden death. However, for WKY rats, while the CCoh at high frequency (65-250 Hz) showed sporadic increases after BCCAL, the CCoh for low frequency bands (0-55 Hz) decreased after ischemic stroke (lower panel in Figure 4.3A). Figure 4.3B displays the CCoh at gamma 1 frequency for the same pair of SHRSP and WKY rats. In SHRSP rat, the CCoh for gamma 1 frequency showed a marked reduction within the first hour of ischemia, which immediately increased to values that are greater than the baseline and persisted for the rest of the recording. In contrast, WKY rat showed a small reduction of CCoh after BCCAL and remained at low values for the remaining of the ischemic period. Statistical analyses were conducted to compare the CCoh changes among baseline, first hour after BCCAL, and last hour (0.5-1.5 hour before sudden death) for both SHRSP and WKY rats. As shown in Figure 4.3C, in both SHRSP (left panel) and WKY (right panel) rats, there was a dramatic reduction of CCoh in first hour after forebrain ischemic stroke than baseline for 5 frequencies (delta to gamma 1). In last hour, however, CCoh increased to a level that was significantly greater than baseline for SHRSP rats (delta to gamma 1), whereas in WKY rats, CCoh in last hour was recovered to a level that is higher than first hour but lower than baseline

level. CCoh between each of the 6 cortical channels during baseline, first hour, and last hour for all frequencies was shown in Supplement Figure 5 in Appendix.

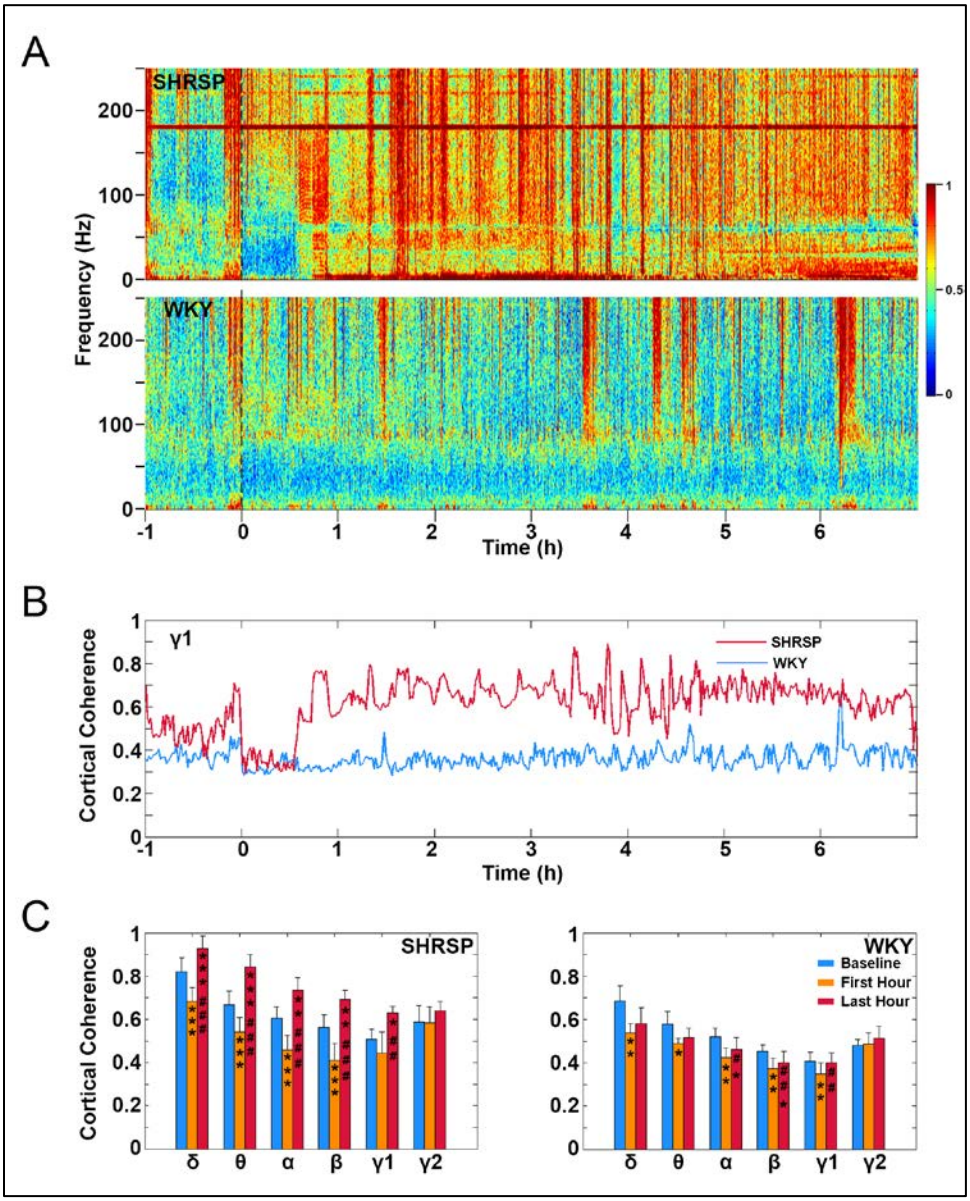

Figure 4.3 BCCAL results in marked increase of CCoh in SHRSP rats. **(A)** CCoh before and after BCCAL (at time 0) for all frequencies in representative SHRSP and WKY rats. **(B)** CCoh before and after BCCAL for gamma 1 frequency in representative SHRSP and WKY rats. **(C)** CCoh during baseline (-1-0 hour), first hour (0-1 hour), and last hour (0.5-1.5 hour before death) all SHRSP (n=9) and WKY (n=8) rats. Data expressed as mean±SD. *Significant differences over baseline, ##significant differences between first and last hour (*/#$p < 0.05$, **/##$p < 0.01$, ***/###$p < 0.001$).

4.3.5 Intermittent surge of functional connectivity between the heart and the brain in SHRSP rats following forebrain ischemia

To investigate the impact of forebrain ischemia on the electrical signal synchronization between the brain and the heart, CCCoh before and after BCCAL was calculated. Figure 4.4A shows the CCCoh for all frequencies in representative SHRSP and WKY rats. Intermittent surge of CCCoh was observed for SHRSP rats after BCCAL (upper panel in Figure 4.4A). However, the CCCoh for WKY rats was nearly undetectable in both baseline and after BCCAL procedure (lower panel in Figure 4.4A). Figure 4.4B displays the CCCoh at gamma 1 frequency for the same pair of SHRSP and WKY rats. In contrast to WKY rat, which demonstrated no obvious changes in CCCoh before and after BCCAL, SHRSP rat showed a dramatic surge of CCCoh at gamma 1 frequency within the first hour of ischemic injury, and a continued and intermittent surge of CCCoh throughout the remainder of the recorded period. Statistical analyses were conducted to compare the changes on the amplitude of CCCoh and the duration of high CCCoh epochs after BCCAL between SHRPS and WKY rats (Figure 4.4C). As shown in figure, a large increase in the amplitude of CCCoh after BCCAL over baseline (0.50-1.21-fold increase) was identified for SHRSP rats for all frequencies, but was not observed for WKY rats, as indicated by the 0.01-0.11-fold change of CCCoh amplitude before and after BCCAL among all frequencies (left panel in Figure 4.4C). Statistical analysis suggests that the increase of CCCoh amplitude after BCCAL was significantly higher in SHRSP than WKY rats. Right panel shows the percentage of signal duration with CCCoh amplitude 2 times higher than baseline level over the total duration of the signal in all SHRSP and WKY rats. While 13-32% of signals after BCCAL had CCCoh that is 2 times higher than baseline in SHRSP rats, the CCCoh for WKY maintain at low level after BCCAL, with less than 5% of the signals that has CCCoh that is 2 times higher than baseline.

Statistical analysis suggests that the percentage of CCCoh epochs that are 2 times larger than baseline after BCCAL was significantly larger in SHRSP than WKY rats (right panel in Figure 4.4C). CCCoh between each of the 6 cortical channels and the heart during baseline, first hour, and last hour for all frequencies was shown in Supplement Figure 6 in Appendix.

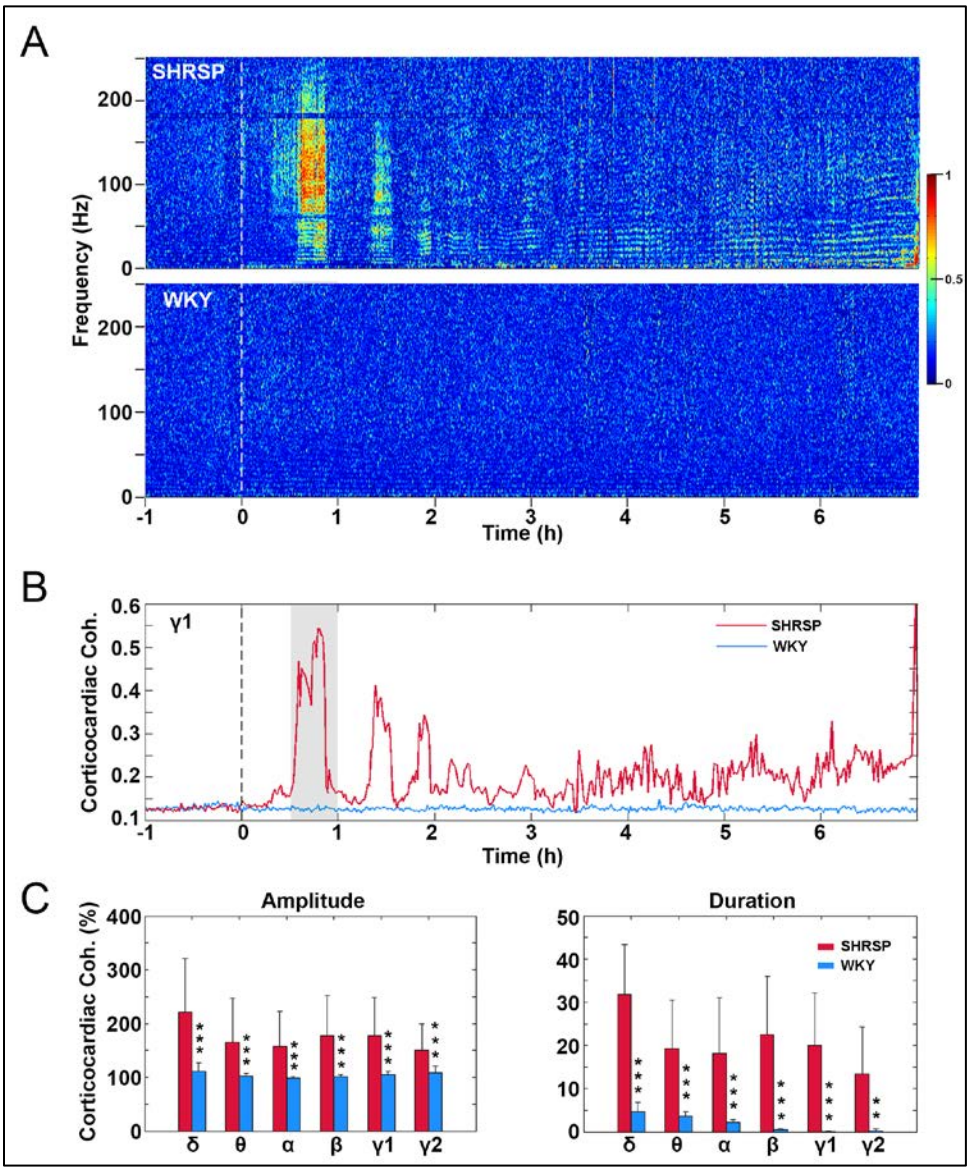

Figure 4.4 BCCAL results in intermittent surge of CCCoh in SHRSP rats. **(A)** CCCoh before and after BCCAL (at time 0) for all frequencies in representative SHRSP and WKY rats. **(B)** CCCoh before and after BCCAL at gamma 1 frequency in representative rats. (**C)** Percent changes on the amplitude of CCCoh over baseline between all SHRSP (n=9) and WKY (n=8) rats (left panel), percent of signal duration with 2 times higher than baseline CCCoh between all SHRSP (n=9) and WKY (n=8) rats (right panel). Data expressed as mean±SD. *Significant differences between SHRSP and WKY rats (*$p < 0.05$, **$p < 0.01$, ***$p < 0.001$).

4.3.6 Intermittent surge of directional connectivity between the heart and the brain in SHRSP rats following forebrain ischemia

To examine the impact of forebrain ischemia on the directional communication between the brain and the heart, CCCon before and after forebrain ischemia was analyzed. Figure 4.5A shows the feedback (from the brain to the heart or efferent) and feedforward (from the heart to brain or afferent) CCCon in a sample epoch that has high CCCoh (corresponding to the shaded region in Figure 4.4A) within the first hour after BCCAL in representative SHRSP rat. As shown in the figure, a marked surge of connectivity in both theta and gamma 1 frequencies was detected in feedforward as well as feedback directions when CCCoh was elevated. However, when the CCCoh was low, the heart-brain connectivity was low in both directions for both theta and gamma 1 frequencies. Statistical analyses were conducted to compare the changes of feedforward and feedback CCCoh for all frequencies among epochs selected from baseline, first hour (0-1 hour or first few hours after BCCAL), and last hour (0-0.5 hour before sudden death) (Figure 4.5B). As shown in the figure, the significant increase of CCCon after forebrain ischemia over baseline values was found in all SHRSP rats, both immediately following ischemia (first hour) or during near-death stage (last hour), for all tested frequencies. Additional increase at the late stage of ischemia (last hour) over the early stage of ischemia (first hour) was observed for delta (feedback), theta (both feedback and feedforward), alpha (both feedback and feedforward), and beta (feedforward) frequencies. Directional asymmetry was also detected for theta and beta frequencies at the early stage of ischemia, with feedback connectivity dominated over feedforward connectivity. CCCon between each of the 6 cortical channels and the heart during baseline, first hour, and last hour at all frequencies was shown in Supplement Figure 7 in Appendix.

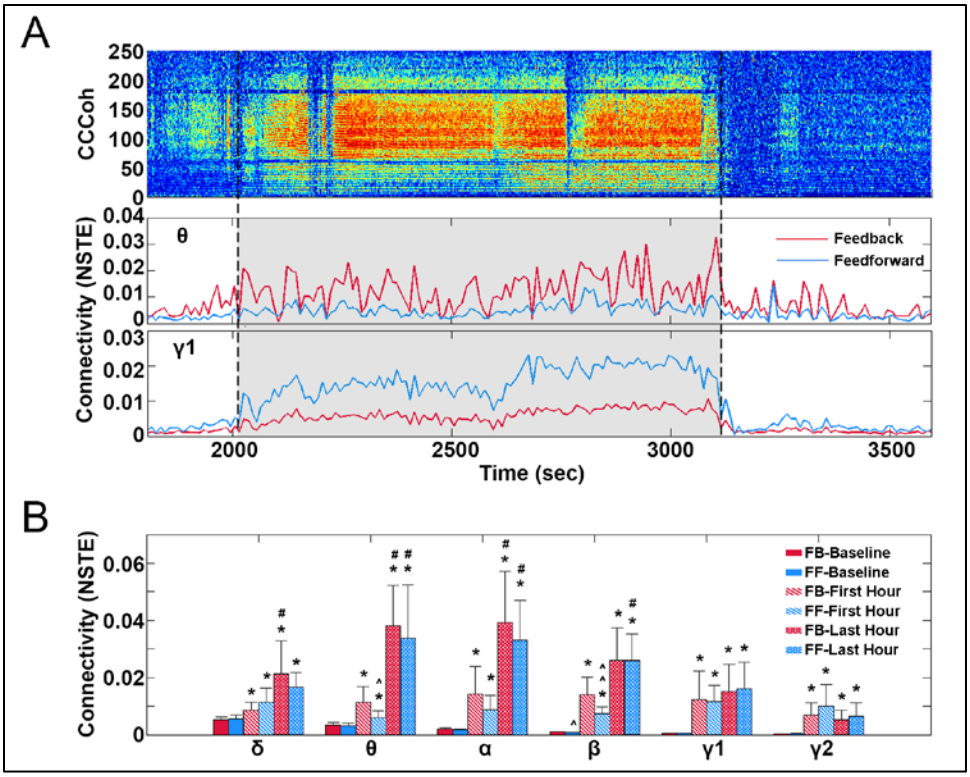

Figure 4.5 BCCAL results in increase of CCCon in SHRSP rats. **(A)** CCCon at theta and gamma 1 frequencies for one representative epoch that shows high CCCoh. **(B)** CCCon for selected epochs during baseline (-1-0 hour), first hour (0-1 hour or first few hours after BCCAL), and last hour (0-1 hour before sudden death). Data expressed as mean±SD. *Significant differences over baseline, #significant differences between first and last hour, ^significant differences between feedforward and feedback CCCon (*/#/^$p < 0.05$, **/##/^^$p < 0.01$, ***/###/^^^$p < 0.001$).

4.3.7 SHRSP rats displayed a marked reduction of HRV following forebrain ischemia

To understand the impact of forebrain ischemia on autonomic regulation of cardiac function during ischemic stroke-induced sudden cardiac arrest, HRV analysis was conducted for all the rats. The HRV before and after BCCAL in representative SHRSP and WKY rats was shown in Figure 4.6A. In SHRSP rat, HRV exhibited reduction at both frequency domain and time domain, showing precipitous decline especially at its last hour (upper panel in Figure 4.6A). In contrast, WKY rat showed an early reduction of HRV in first and second hour following BCCAL procedure, which was then recovered to normal levels in the following hours (lower panel in Figure 4.6A). These changes of HRV are conserved in all SHRSP and WKY rats. As shown in

Figure 4.6B, in SHRSP rats, both low frequency (LF, 0.25-0.8 Hz) and high frequency (HF, 0.8-3 Hz) components as well as the ratio of low and high frequency (LF/HF) displayed a reduction in first hour after BCCAL and last hour (0.5-1.5 hour before sudden death) than baseline condition (left panel in Figure 4.6B). Remarkably, the LF, HF, and LF/HF at last hour are significant lower compared to both baseline and first hour. In contrast, WKY rats showed an initial decline of LF and LF/HF in first hour after BCCAL, which was followed by a recovery of LF, HF, and LF/HF in last hour before sudden death. Different from SHRSP rats, these changes of HRV in WKY rats are not significant (right panel in Figure 4.6B).

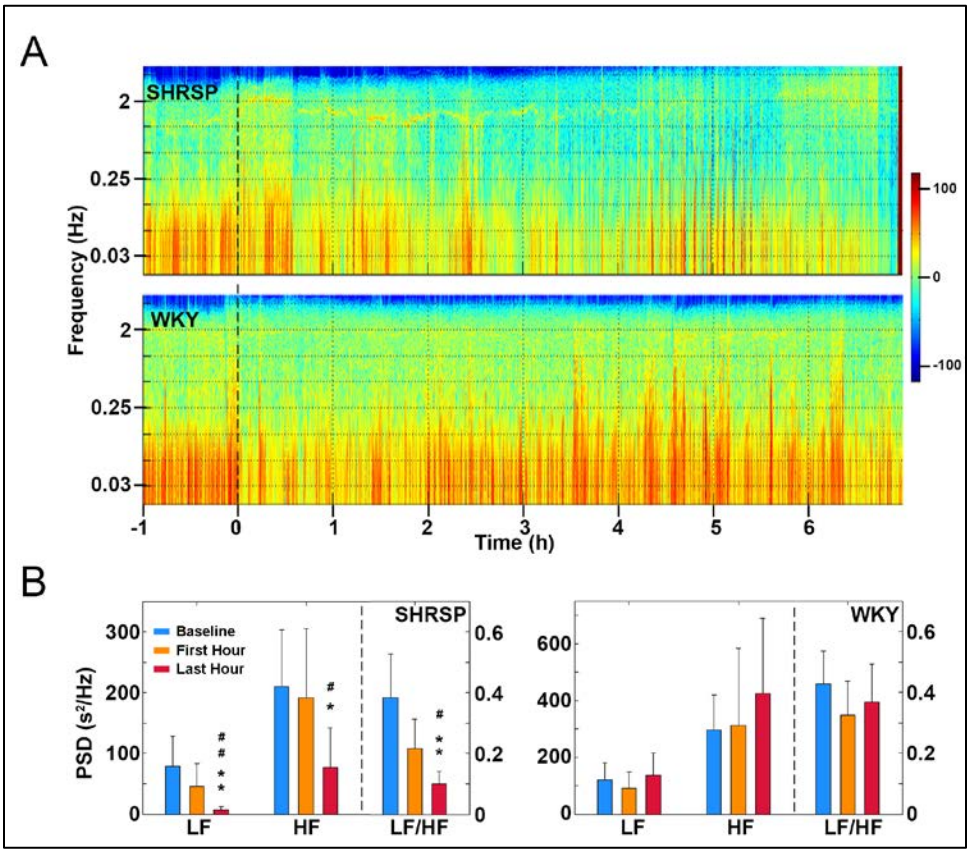

Figure 4.6 BCCAL results in marked reduction of HRV for SHRSP rats. **(A)** HRV before and after BCCAL (at time 0) for representative SHRSP and WKY rats. z axis represents power spectral density (PSD). Warmer color represents stronger PSD. **(B)** PSD of low frequency (LF), high frequency (HF), and LF/HF during baseline (-1-0 hour), first hour (0-1 hour), and last hour (0.5-1.5 hour before death) for all SHRSP (n=9) and WKY (n=8) rats. Data expressed as mean±SD. *Significant differences over baseline, #significant differences between first and last hour (*$p < 0.05$, **$p < 0.01$, ***$p < 0.001$).

4.4 Discussion

This is the first study to examine the dynamic changes of the brain, the heart, and the functional interactions between the brain and the heart in forebrain ischemic stroke-induced sudden cardiac arrest rat models. Our data demonstrated that there is a dramatic decline of cardiac functionality (increase of RRI and cardiac arrhythmias), disruption of the autonomic nervous system (decrease of HRV), and reduction of cortical electrical activity (EEG power) during forebrain ischemic cardiac arrest. Importantly, we identified a global increase of functional synchronization within the brain (CCoh), as well as a marked and intermittent surge of brain-heart coupling, indicated by high level of CCCoh and CCCon, from the onset of ischemia until death in rats that suffered from sudden cardiac arrest. These results suggest that abnormal brain-heart connection may be the mechanism for forebrain ischemic stroke-induced sudden cardiac arrest and the surge of CCCoh may be used as a biomarker to predict the risk of sudden death.

4.4.1 Animal model for sudden cardiac arrest

Unlike our previous studies [Borjigin et al., 2013; Li et al., 2015a; Tian et al., 2018] where rats experienced global ischemia (asphyxia) that affects the brain and the heart simultaneously, in the current model, we investigated brain-heart connection in sudden cardiac arrest induced by forebrain ischemic stroke. Comparatively speaking, forebrain ischemia model is scientifically more impactful than asphyxia model because it tests the direct influence of cortical ischemia on the function of the brain and the heart. In contrast, in asphyxia models, the cortex, brainstem, spinal cord, and the heart are globally affected by the experimental insult, making it difficult to test the role of the brain during the dying process. BCCAL in SHRSP rats is a well-established model for forebrain ischemia [Katayama et al., 1984; Lobanava et al., 2008]. One previous study showed that occlusion of the bilateral carotid artery caused the death of SHRSP rats within 6

hours, whereas the control WKY rats died within 8 hours after the occlusion [Kakihana and Nagaoka, 1983]. In our experiment, BCCAL successfully induced 100% death for SHRSP rats within 14 hours. However, no mortality was observed in WKY rats. The high mortality in previous study compared to our study may due to the genetic variations for outbred animals, as well as the high salt Japanese diet (4% sodium chloride in Japanese diet vs. 0.4% sodium chloride in standard chow), which accelerates the development of hypertension in SHRSP rats [Matsuo and Nagaoka, 1981; Stier et al., 1988; Schmidlin et al., 2005]. Nevertheless, large similarities in mitochondria abnormalities and cerebral blood vessel deficits during the development of stroke have been identified between SHRSP rats and humans, making BCCAL in SHRSP rats one of the most relevant model for studying sudden cardiac arrest induced by forebrain cerebral ischemia [Lobanava et al., 2008].

4.4.2 Deterioration of cardiac function and autonomic nervous system functionality during forebrain ischemic stroke-induced sudden cardiac arrest

Cardiac arrhythmias and ECG abnormalities are commonly observed after acute cerebrovascular events, such as ischemic stroke, intracerebral hemorrhage, and subarachnoid hemorrhage [Goldstein, 1979; Daniele et al., 2002]. In stroke patients, cardiac arrhythmias, especially the malignant ventricular arrhythmias triggered by the impairment of the central autonomic nervous system structures and catecholamine storm, are highly prevalent [Myers et al., 1982; Mäkikallio et al., 2004]. It is also known that ventricular tachycardia (VT), ventricular fibrillation (VF), and asystole, are often the fatal cardiac arrhythmias right before sudden death [Bayes de Luna et al., 1989]. However, none of previous studies have characterized the number and types of cardiac arrhythmias with the progression of cardiac arrest in forebrain ischemic stroke-induced sudden cardiac arrest rat model, except for one earlier study which reported the disturbance of cardiac

rhythm and increase in the number of PVC in SHRSP rats after BCCAL [Kakihana et al., 1983]. In our study, we showed that common arrhythmias including PVC, PAC, SP, JR and 2HB significantly increased after the surgery in both SHRSP and WKY rats, although on average more arrhythmias were found in SHRSP rats than WKY rats. The occurrences of those arrhythmias are sporadic and irregular in both strains. In contrast, in last 30 minutes before death, there is a sudden increase of cardiac arrhythmias only in SHRSP rats, suggesting that the disruption of cardiac function is essentially very sudden, which further proves the validity of current model for investigating the mechanism of sudden cardiac death. Interestingly, different from asphyxic cardiac arrest model, in which 3HB, JEB, VEB, VT, and VF are the last cardiac arrhythmias before sudden death [Tian et al., 2018], in forebrain ischemic cardiac arrest model, VT and VF are not identified. Instead a significant increase of MSB was observed in SHRPS rats right before sudden death.

HRV has been widely used for studying the autonomous nervous system control of cardiovascular function [Task force et al., 1996]. Reduced HRV has been associated with the risk of myocardial infarction [Lombardi et al., 1987; Buchanan et al., 1993], congestive heart failure [Saul et al., 1988], and sudden cardiac death [Politano et al., 2008; Wu et al., 2014]. Parallel with previous findings, our study demonstrated a significant reduction of LF, HF, and the ratio of LF/HF in SHRSP rats that suffered from sudden cardiac death, whereas the HRV in control WKY rats did not display significant changes during the entire process. These results indicate that forebrain ischemia leads to reduced level of activity for both the sympathetic and parasympathetic nervous system, with more severe suppression to the parasympathetic nervous system at near-death. The reduction of the autonomic nervous system functionality may be the cause for the dramatic increase of MSB during the ending phase of forebrain ischemic sudden

death. In contrast, in asphyxic cardiac arrest, the sympathetic nervous system is over-activated since the blockade of sympathetic nervous system via either spinal cord transection or adrenergic blockers prolongs the electrical activities of both the brain and the heart [Li et al., 2015a; Tian et al., 2018]. The cardiac arrhythmias observed in the ending phase are therefore VT and VF. The differences of cardiac arrhythmias and autonomic nervous system functionality indicate that global ischemia (asphyxia) and forebrain ischemia induced very different autonomic responses and cardiac pathological consequences.

4.4.3 Decrease of cortical power and increase of cortical coherence during forebrain ischemic stroke-induced sudden cardiac arrest

Consistent with previous studies in mice and rats that suffered from cardiac arrest induced by injection of potassium chloride [Borjigin et al., 2013; Weitzel et al., 2016], severe and sustained reduction in EEG power was identified in SHRSP rats after forebrain ischemic stroke. As expected, an initial decline and a subsequent recovery of EEG power was found in WKY rats that survived. Another study investigating the EEG power changes in spontaneously hypertensive rats (SHR has elevated blood pressure but rarely shows signs of stroke [Okamoto and Aoki, 1963]) and WKY rats after forebrain ischemia demonstrated that 20-minute BCCAL plus hypotension produces dramatic increase in delta power and decrease in theta, beta, and alpha activities [Mariucci et al., 2003], which is comparable to what we found in SHRSP and WKY rats that EEG power for all frequencies significantly decreased after permanent BCCAL. In addition, similar to what we found for SHRSP and WKY rats, EEG activity also recovered to normal values more quickly in WKY rats than in SHR rats, in which alpha and beta power did not recover even at 6 days of reperfusion [Mariucci et al., 2003]. The irreversible influence of forebrain ischemic stroke on brain electrical activity in SHRSP and SHR rats but not WKY rats

may due to the abnormal cerebral vascular structure, hypertension, and altered hemodynamics of spontaneous hypertensive rats, which makes SHRSP and SHR rats more susceptible to ischemic insult than normotensive rats [Ogata et al., 1976; Fujishima et al., 1980; Kakihana et al., 1983; Coyle, 1986; Brint et al., 1988; Duverger and MacKenzie, 1988; Lobanova et al., 2008].

Immediately after BCCAL, the functional synchronization (CCoh) between different cortical regions in SHRSP rats significantly decreased. This is possibly due to the dysfunction or death of a considerable number of cortical neurons that severely impairs the information transmission in cortical connection after forebrain ischemia. This result was consistent with findings from previous studies in Wistar rats undergoing BCCAL and in patients with acute thalamic ischemic stroke, both of which showed a decrease of cortical coherence or functional connectivity within the brain after ischemia [Kozhechkin et al., 2009; Liu et al., 2016]. Interestingly, within 1 hour after BCCAL, CCoh in SHRSP rats recovered to a level that was even greater than baseline, indicating that the brain is internally super-activated at near-death. The neurophysiological mechanisms underlying the marked surge of the functional coupling within the brain after ischemia is still unknown. Nevertheless, the large increase of brain functional synchronization after forebrain ischemic stroke until sudden death is consistent with our earlier findings in both potassium chloride injection- and asphyxia-induced cardiac arrest models, in which a dramatic increase of both functional and effective connectivity was identified within the brain before sudden death [Borjigin et al., 2013; Li et al., 2015a]. The identification of dramatic surge of CCoh exclusively in rats that suffered from sudden cardiac arrest provides further evidence to support our central hypothesis that the brain may play an active role in mediating the dying process.

4.4.4 Increase of brain-heart connection during forebrain ischemic stroke-induced sudden cardiac arrest

Despite growing evidence suggesting that abnormal interaction between the brain and the heart is the major cause of sudden death, the dynamical changes of brain-heart connection have not been characterized in any neurogenic sudden death models before due to the lack of effective study tools [Samuels, 2007; Dorrance and Fink, 2015; Gonzales-Portillo et al., 2016]. In previous study, we developed novel analysis methodologies, CCCoh and CCCon, to investigate the synchronization and bi-directional signal communication between the brain and the heart in asphyxic cardiac arrest models [Li et al., 2015a]. Consistent with our findings from that study [Li et al., 2015a], a surge of coherence (CCCoh) was identified between the brain and the heart in SHRSP rats that died after forebrain ischemia and the surge was absent in WKY rats as well as in SHRSP rats survived a milder form of stroke. In addition, strong bi-directional information transfer between the brain and the heart (CCCon) was also found in SHRSP rats whenever there was increased brain-heart coupling. However, there are two differences of CCCoh and CCCon between asphyxia- and forebrain ischemic stroke-induced sudden cardiac arrest models: 1) high level of CCCoh and CCCon was detected for all frequencies (0-250Hz) in forebrain ischemic cardiac arrest model, whereas in asphyxic cardiac arrest model, CCCoh was clustered at low frequency ranges (0-55 Hz); 2) The CCCoh in SHRSP rats after forebrain ischemic stroke is intermittent and unevenly distributed, however, in asphyxic cardiac arrest model, CCCoh displays homogeneous and continuous pattern. As the detailed biophysical mechanism underlying CCCoh and CCCon remain to be discovered, it still unknown what are the causes of the distinct frequency and temporal patterns in two different models. Results from this study and our previous study suggest that there are strong functional and directional connectivity between

the brain and the heart in the dying process, and the brain and the heart displays different modes of interaction during global (asphyxia) and forebrain ischemic sudden cardiac arrest.

4.4.5 Conclusion

In conclusion, this study demonstrated that during forebrain ischemic stroke-induced sudden cardiac arrest, elevated brain-heart electrical signal coupling and communication are highly associated with the increase of cardiac arrhythmias, disruption of the autonomic nervous system, and the risk of sudden death, and may be used a potential biomarker to predict sudden death. This study could improve our understanding on the mechanism of how the brain and the heart interact during forebrain ischemic sudden cardiac arrest. Based on results from this study and previous studies, we hypothesis that under normal condition, the brain and the heart communicate indirectly via the autonomic nervous system to ensure the homeostasis of fundamental physiological systems. However, when this homeostasis is disrupted by the external perturbations, either asphyxia [Li et al., 2015a; Tian et al., 2018], neurological diseases (current study), or cardiac abnormalities (Chapter 3), the regulation from the autonomic nervous system fails. The brain starts intense interaction with the heart via other unknown mechanisms, which are detected and quantified by the dramatic surge of CCCoh and CCCon. Till now, it is unknown what mediates the strong brain-heart interaction during sudden death. We hypothesize that it may be mediated by the vascular system as CCCoh is still detectable after spinal transection, but this needs to be tested in further studies. Our results may also provide important information for predicting and preventing sudden death after ischemic stroke. Since the bi-directional electrical signal coupling (CCCoh) and communication (CCCon) between the brain and the heart are only identified in dying animals, they could be used as potential biomarkers to predict the risk of sudden death. The diminishment of CCCoh and CCCon may also be used as parameters to

evaluate the effectiveness of drugs in preventing sudden death. In addition, this study further corroborates the possibility of functional investigation on brain and heart connection using advance signal processing techniques. Areas of future interests would include testing whether CCCoh is also detectable in other types of neurological injury-induced sudden death animal model or human patients.

4.5 Acknowledgements

This work was supported by the Department of Molecular and Integrative Physiology at the University of Michigan and American Heart Association Predoctoral Fellowship (to FT). We thank Drs. Richard Keep, Daniel Beard, Anuska Andjelkovic-Zochowska, and UnCheol Lee for their helpful discussions and comments.

4.6 References

Heart rate variability: standards of measurement, physiological interpretation and clinical use. Task Force of the European Society of Cardiology and the North American Society of Pacing and Electrophysiology. (1996). Circulation, 93(5), 1043-1065.

Barbosa Neto, O., Abate, D. T., Marocolo Junior, M., Mota, G. R., Orsatti, F. L., Rossi e Silva, R. C., . . . da Silva, V. J. (2013). Exercise training improves cardiovascular autonomic activity and attenuates renal damage in spontaneously hypertensive rats. J Sports Sci Med, 12(1), 52-59.

Bayes de Luna, A., Coumel, P., & Leclercq, J. F. (1989). Ambulatory sudden cardiac death: mechanisms of production of fatal arrhythmia on the basis of data from 157 cases. Am Heart J, 117(1), 151-159.

Borjigin, J., Lee, U., Liu, T., Pal, D., Huff, S., Klarr, D., . . . Mashour, G. A. (2013). Surge of neurophysiological coherence and connectivity in the dying brain. Proc Natl Acad Sci U S A, 110(35), 14432-14437. doi:10.1073/pnas.1308285110

Brint, S., Jacewicz, M., Kiessling, M., Tanabe, J., & Pulsinelli, W. (1988). Focal brain ischemia in the rat: methods for reproducible neocortical infarction using tandem occlusion of the distal middle cerebral and ipsilateral common carotid arteries. J Cereb Blood Flow Metab, 8(4), 474-485. doi:10.1038/jcbfm.1988.88

Buchanan, L. M., Cowan, M., Burr, R., Waldron, C., & Kogan, H. (1993). Measurement of recovery from myocardial infarction using heart rate variability and psychological outcomes. Nurs Res, 42(2), 74-78.

Coyle, P. (1986). Different susceptibilities to cerebral infarction in spontaneously hypertensive (SHR) and normotensive Sprague-Dawley rats. Stroke, 17(3), 520-525.

Daniele, O., Caravaglios, G., Fierro, B., & Natale, E. (2002). Stroke and cardiac arrhythmias. J Stroke Cerebrovasc Dis, 11(1), 28-33. doi:10.1053/jscd.2002.123972

Dorrance, A. M., & Fink, G. (2015). Effects of Stroke on the Autonomic Nervous System. Compr Physiol, 5(3), 1241-1263. doi:10.1002/cphy.c140016

Duverger, D., & MacKenzie, E. T. (1988). The quantification of cerebral infarction following focal ischemia in the rat: influence of strain, arterial pressure, blood glucose concentration, and age. J Cereb Blood Flow Metab, 8(4), 449-461. doi:10.1038/jcbfm.1988.86

Fauchier, L., Melin, A., Eder, V., Antier, D., & Bonnet, P. (2006). Heart rate variability in rats with chronic hypoxic pulmonary hypertension. Ann Cardiol Angeiol (Paris), 55(5), 249-254. doi:10.1016/j.ancard.2006.01.005

Frangiskakis, J. M., Hravnak, M., Crago, E. A., Tanabe, M., Kip, K. E., Gorcsan, J., 3rd, . . . London, B. (2009). Ventricular arrhythmia risk after subarachnoid hemorrhage. Neurocrit Care, 10(3), 287-294. doi:10.1007/s12028-009-9188-x

Fujishima, M., Tamaki, K., Nakatomi, Y., Ishitsuka, T., Nakagawara, K., & Omae, T. (1980). Experimental cerebral ischemia in spontaneously hypertensive rats (SHR): Importance of degree of hypertension. Stroke, 11(6), 612-616.

Goldstein, D. S. (1979). The electrocardiogram in stroke: relationship to pathophysiological type and comparison with prior tracings. Stroke, 10(3), 253-259.

Gonzales-Portillo, C., Ishikawa, H., Shinozuka, K., Tajiri, N., Kaneko, Y., & Borlongan, C. V. (2016). Stroke and cardiac cell death: Two peas in a pod. Clin Neurol Neurosurg, 142, 145-147. doi:10.1016/j.clineuro.2016.01.001

Kakihana, M., Shino, A., & Nagaoka, A. (1983). Cardiovascular responses to cerebral ischemia following bilateral carotid artery occlusion in SHRSP, SHRSR and WKY rats. Jpn J Pharmacol, 33(1), 17-26.

Katayama, Y., Terashi, A., Sugimoto, S., Inamura, K., Suzuki, S., Sekiguchi, F., & Akashi, A. (1984). Experimental cerebral ischemia after bilateral common carotid artery ligation in SHRSP, SHRSR and Wistar rats: correlation between blood pressure and degree of ischemia. No To Shinkei, 36(11), 1069-1075.

Kew, H. P., & Jeong, D. U. (2011). Variable threshold method for ECG R-peak detection. J Med Syst, 35(5), 1085-1094. doi:10.1007/s10916-011-9745-7

Kozhechkin, S. N., Koshtoyants, O., & Seredenin, S. B. (2009). Multiparameter analysis of EEG in old wistar rats after bilateral carotid artery ligation. Bull Exp Biol Med, 147(5), 573-577.

Kuwahara, M., Yayou, K., Ishii, K., Hashimoto, S., Tsubone, H., & Sugano, S. (1994). Power spectral analysis of heart rate variability as a new method for assessing autonomic activity in the rat. J Electrocardiol, 27(4), 333-337.

Lee, U., Kim, S., Noh, G. J., Choi, B. M., Hwang, E., & Mashour, G. A. (2009). The directionality and functional organization of frontoparietal connectivity during consciousness and anesthesia in humans. Conscious Cogn, 18(4), 1069-1078. doi:10.1016/j.concog.2009.04.004

Li, D., Mabrouk, O. S., Liu, T., Tian, F., Xu, G., Rengifo, S., . . . Borjigin, J. (2015a). Asphyxia-activated corticocardiac signaling accelerates onset of cardiac arrest. Proc Natl Acad Sci U S A, 112(16), E2073-2082. doi:10.1073/pnas.1423936112

Li, D., Tian, F., Rengifo, S., Xu, G., M Wang, M., & Borjigin, J. (2015b). Electrocardiomatrix: A new method for beat-by-beat visualization and inspection of cardiac signals. Journal of Integrative Cardiology, 1(5). doi:10.15761/JIC.1000133

Liu, S., Guo, J., Meng, J., Wang, Z., Yao, Y., Yang, J., . . . Ming, D. (2016). Abnormal EEG Complexity and Functional Connectivity of Brain in Patients with Acute Thalamic Ischemic Stroke. Comput Math Methods Med, 2016, 2582478. doi:10.1155/2016/2582478

Lobanova, N. N., Medvedev, N. I., Popov, V. I., & Murashev, A. N. (2008). Bilateral occlusion of carotid artery in awake hypertensive rats (SHR-SP) as a model of global cerebral ischemia. Bull Exp Biol Med, 146(6), 691-694.

Lombardi, F., Sandrone, G., Pernpruner, S., Sala, R., Garimoldi, M., Cerutti, S., . . . Malliani, A. (1987). Heart rate variability as an index of sympathovagal interaction after acute myocardial infarction. Am J Cardiol, 60(16), 1239-1245.

Makikallio, A. M., Makikallio, T. H., Korpelainen, J. T., Sotaniemi, K. A., Huikuri, H. V., & Myllyla, V. V. (2004). Heart rate dynamics predict poststroke mortality. Neurology, 62(10), 1822-1826.

Mariucci, G., Stasi, M. A., Taurelli, R., Nardo, P., Tantucci, M., Pacifici, L., . . . Ambrosini, M. V. (2003). EEG power spectra changes and forebrain ischemia in rats. Can J Neurol Sci, 30(1), 54-60.

Matsuo, T., & Nagaoka, A. (1981). Postnatal undernutrition accelerates incidence of stroke in stroke-prone spontaneously hypertensive rats. Stroke, 12(4), 509-512.

Myers, M. G., Norris, J. W., Hachinski, V. C., Weingert, M. E., & Sole, M. J. (1982). Cardiac sequelae of acute stroke. Stroke, 13(6), 838-842.

Ogata, J., Fujishima, M., Morotomi, Y., & Omae, T. (1976). Cerebral infarction following bilateral carotid artery ligation in normotensive and spontaneously hypertensive rats: a pathological study. Stroke, 7(1), 54-60.

Okamoto, K., & Aoki, K. (1963). Development of a strain of spontaneously hypertensive rats. Jpn Circ J, 27, 282-293.

Politano, L., Palladino, A., Nigro, G., Scutifero, M., & Cozza, V. (2008). Usefulness of heart rate variability as a predictor of sudden cardiac death in muscular dystrophies. Acta Myol, 27, 114-122.

Prosser, J., MacGregor, L., Lees, K. R., Diener, H. C., Hacke, W., Davis, S., & Investigators, V. (2007). Predictors of early cardiac morbidity and mortality after ischemic stroke. Stroke, 38(8), 2295-2302. doi:10.1161/STROKEAHA.106.471813

Samuels, M. A. (2007). The brain-heart connection. Circulation, 116(1), 77-84. doi:10.1161/CIRCULATIONAHA.106.678995

Saul, J. P., Arai, Y., Berger, R. D., Lilly, L. S., Colucci, W. S., & Cohen, R. J. (1988). Assessment of autonomic regulation in chronic congestive heart failure by heart rate spectral analysis. Am J Cardiol, 61(15), 1292-1299.

Schmidlin, O., Tanaka, M., Bollen, A. W., Yi, S. L., & Morris, R. C., Jr. (2005). Chloride-dominant salt sensitivity in the stroke-prone spontaneously hypertensive rat. Hypertension, 45(5), 867-873. doi:10.1161/01.HYP.0000164628.46415.66

Soros, P., & Hachinski, V. (2012). Cardiovascular and neurological causes of sudden death after ischaemic stroke. Lancet Neurol, 11(2), 179-188. doi:10.1016/S1474-4422(11)70291-5

Stier, C. T., Jr., Benter, I. F., & Levine, S. (1988). Thromboxane A2 in severe hypertension and stroke in stroke-prone spontaneously hypertensive rats. Stroke, 19(9), 1145-1150.

Tian, F., Liu, T., Xu, G., Li, D., Ghazi, T., Shick, T., . . . Borjigin, J. (2018). Adrenergic blockade bi-directionally and asymmetrically alters functional brain-heart communication and prolongs electrical activities of the brain and heart during asphyxic cardiac arrest. Frontiers in Physiology, 9, 99.

Weitzel, L. R., Sampath, D., Shimizu, K., White, A. M., Herson, P. S., & Raol, Y. H. (2016). EEG power as a biomarker to predict the outcome after cardiac arrest and cardiopulmonary resuscitation induced global ischemia. Life Sci, 165, 21-25. doi:10.1016/j.lfs.2016.09.007

Wu, L., Jiang, Z., Li, C., & Shu, M. (2014). Prediction of heart rate variability on cardiac sudden death in heart failure patients: a systematic review. Int J Cardiol, 174(3), 857-860. doi:10.1016/j.ijcard.2014.04.176

Yamori, Y., Horie, R., Handa, H., Sato, M., & Fukase, M. (1976). Pathogenetic similarity of strokes in stroke-prone spontaneously hypertensive rats and humans. Stroke, 7(1), 46-53.

Chapter 5 Conclusions

5.1 Significance of thesis project

Through this thesis project, we established a novel mechanism for sudden cardiac arrest. Different from the conventional view that the brain is hypoactive during sudden cardiac arrest, our data strongly suggest that the brain plays an active role in mediating the deterioration of cardiac function at near-death, and that corticocardiac coupling may be a common mechanism underlying sudden cardiac death induced by different causes, which include asphyxia that affects both the heart and the brain, cardiac abnormalities, and neurological diseases.

This thesis project is **significant** scientifically, clinically, and technically because: 1) It provides new insights into the neurophysiological mechanisms underlying sudden cardiac arrest. The bidirectional corticocardiac coupling has never been described in any sudden cardiac arrest animal models or human patients before. This is the first study demonstrating the existence of significant level of functional coupling and directional communication between the brain and the heart at near-death stage in different models. Interestingly, the functional and directional connectivity displays hemispheric asymmetry, frequency specificities, and different temporal dynamics in different models, suggesting the existence of diverse modes of communication between the brain and the heart in sudden death triggered by different factors or in different species. 2) Investigating the mechanism of how the brain and the heart interact during sudden cardiac arrest could contribute to the development of novel therapeutic approaches to predict and prevent sudden death. This project established that corticocardiac coupling may be used as a new non-invasive method to assess the risk for sudden death since corticocardiac coupling is

exclusively identified in rats or human undergoing sudden death. This study also validated the effectiveness of pharmacological interventions for prolonging the survival after cardiac arrest in experimental animal models. 3) This study successfully applied advanced signal processing technique to study the dynamic changes of brain-heart connection in rats and human patients suffering from sudden cardiac arrest. Although signal processing techniques have been widely used to explore the features associated with brain signals, no published studies have applied it to the investigation of the functional coupling and directional communication between cortical and cardiac signals in any human or animal models. Our study is among the first to use advanced analytical techniques to functionally characterize the dynamic interactions of the brain and the heart, and is expected to provide a new framework for functional investigation of both neurogenic as well as cardiogenic sudden death and many other diseases caused by abnormal brain-heart connection. Successful validation of this powerful new technology in probing the dynamics of corticocardiac network could also contribute to the understanding of the neurophysiological connections between the brain and other peripheral organs in normal and disease conditions.

5.2 Future directions

The understanding of the functional connection between the cerebral cortex and the heart is still in its early stage. Based on current finding, we think there are two future directions worth pursuing: 1) Further investigation on the biophysical nature of corticocardiac coupling. Although we identified consistent surge of corticocardiac coupling in different sudden cardiac arrest models, the neurophysiological pathways by which the heart and the brain communicate or the biophysical nature of corticocardiac coupling is still unknown. Understanding the biophysical nature of corticocardiac coupling and the way that the brain communicates with the heart will

provide important information for the development of novel strategies for predicting and preventing sudden death. We hypothesize that the corticocardiac coupling may be mediated by the vascular system though gap-junctions because corticocardiac coupling was still detectable in rats with spinal nerve transection, but this hypothesis needs to be tested in future studies. 2) Test the brain-heart connection in focal ischemic stroke model. Focal ischemic stroke is one of the major causes of mortality and morbidity around the world and is responsible for the leading health care costs of all diseases. Focal stroke can trigger cardiac autonomic imbalance, which may put susceptible patients at increased risk of cardiac arrhythmias and sudden death. In the current thesis project, we established the role of the brain in sudden cardiac death. To further test specific cortical regions that are important for cortical control of cardiac function, we plan to investigate the brain-heart connection in focal ischemic stroke model with 10 EEG electrodes implanted on the cerebral cortex. Questions of interest include how the injured cortical region interacts with the healthy region of the brain, and how different cortical region communicate with the heart during the development of focal ischemic stroke. This study is expected to contribute to our understanding on the temporal dynamics of cortical activity and key brain regions that may be involved in the regulation of cardiac function during focal ischemic stroke.

Appendix

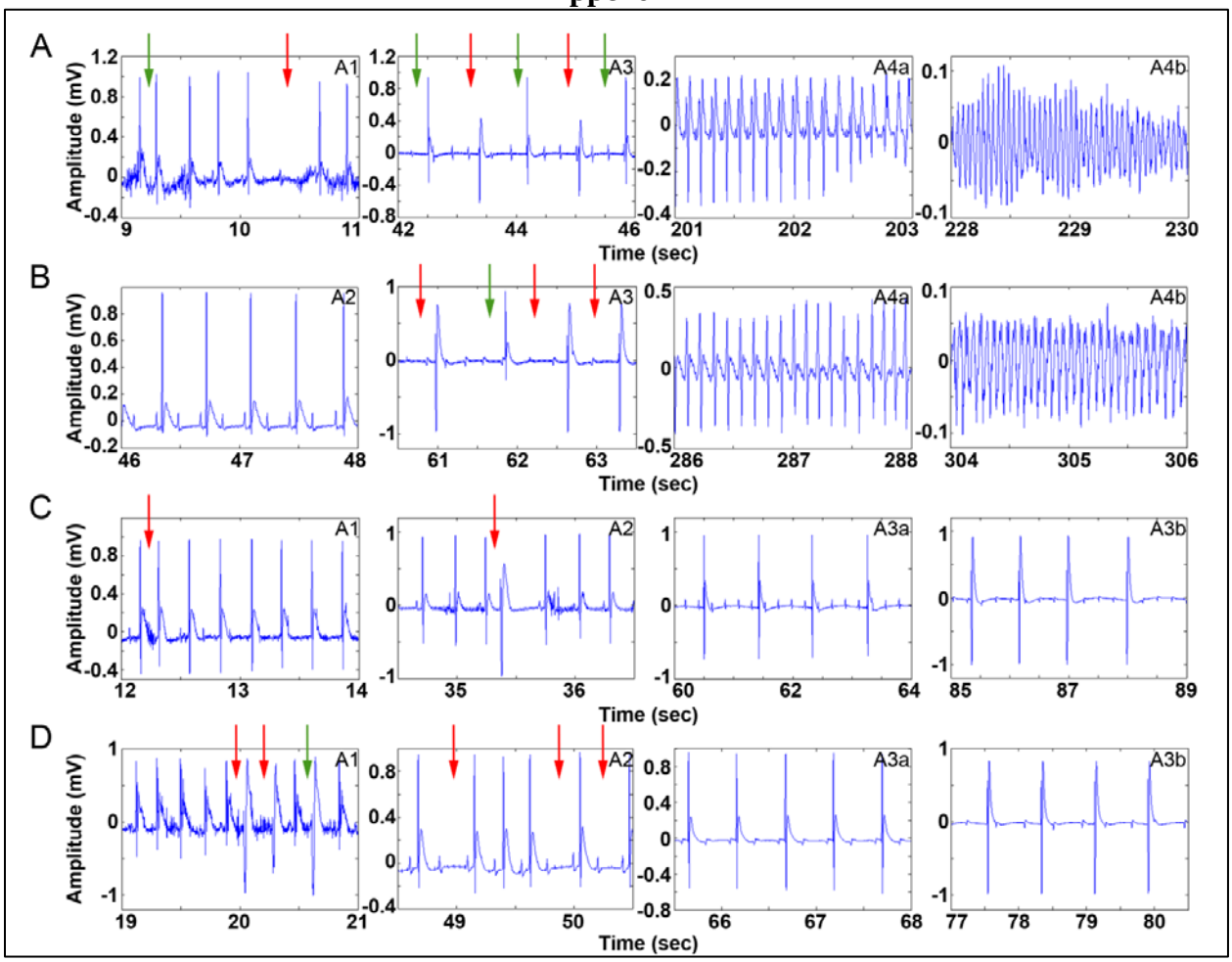

Supplement Figure 1 ECG signals with representative cardiac arrhythmias in each stage of asphyxic cardiac arrest for 4 groups of rats. **(A)** Saline group. A1: 1 premature atria contraction (green arrow) and 1 first-degree heart block (red arrow); A3: 3 junctional escape beat (green arrow) and 2 ventricular escape beat (red arrow) in a background of third-degree heart block; A4a: ventricular tachycardia; A4b: ventricular fibrillation. **(B)** Phentolamine group. A2: second-degree heart block type II; A3: 1 junctional escape beat (green arrow) and 3 ventricular escape beat (red arrow) in a background of third-degree heart block; A4a: ventricular tachycardia; A4b: ventricular fibrillation. **(C)** Atenolol group. A1: 1 premature junctional contraction (red arrow) in a background of junctional rhythm; A2: 1 premature ventricular contraction (red arrow); A3a: junctional escape beat in a background of third-degree heart block; A3b: ventricular escape beat in a background of third-degree heart block. **(D)** Phentolamine plus atenolol group. A1: 1 premature ventricular contraction (green arrow) and 1 ventricular couplet (red arrow) in a background of peaked T waves; A2: 3 second-degree heart block type II (red arrow); A3a: junctional escape beat in a background of third-degree heart block; A3b: ventricular escape beat in a background of third-degree heart block.

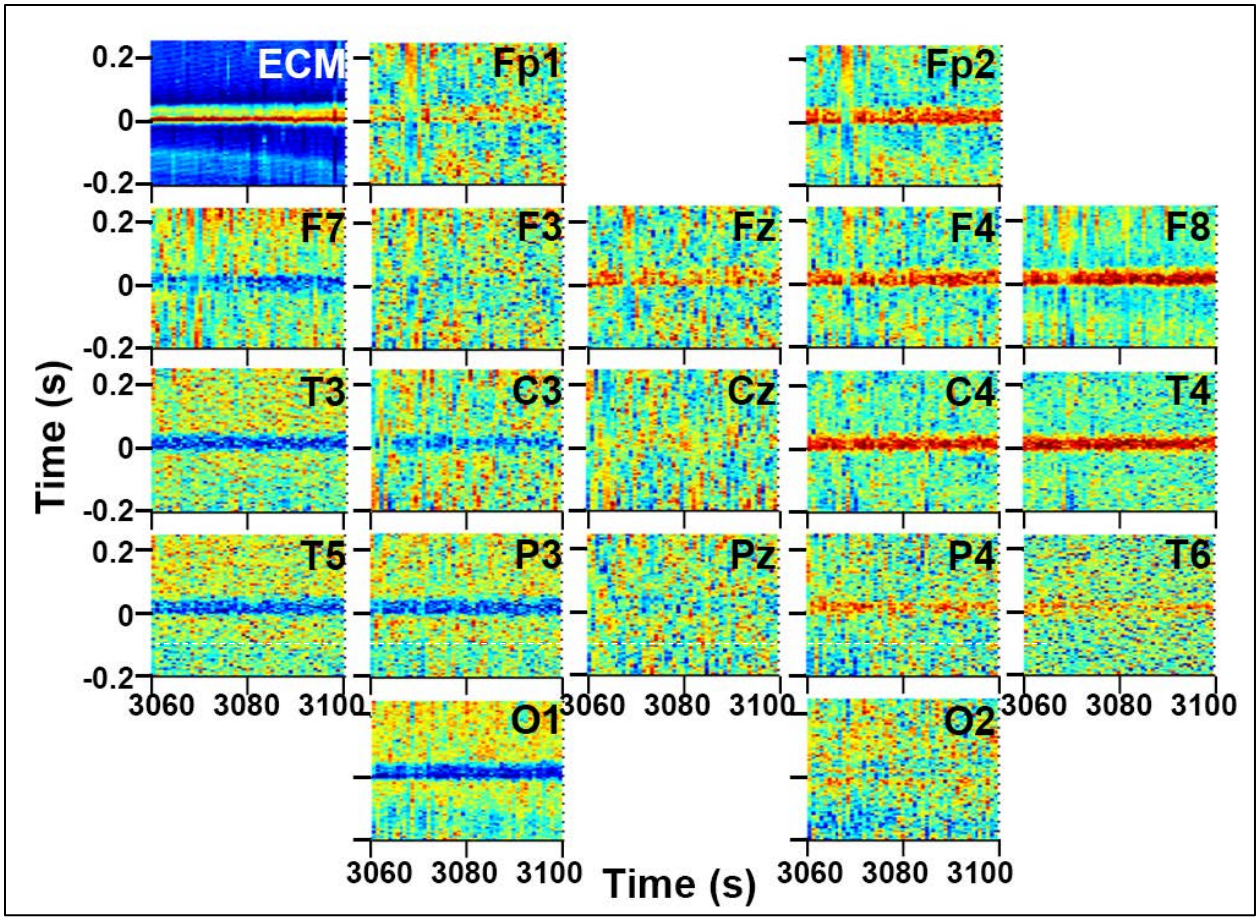

Supplement Figure 2 ECM and EEM for 19 EEG channels (arranged according to their locations on the skull) for a 40-second long epoch during S4.

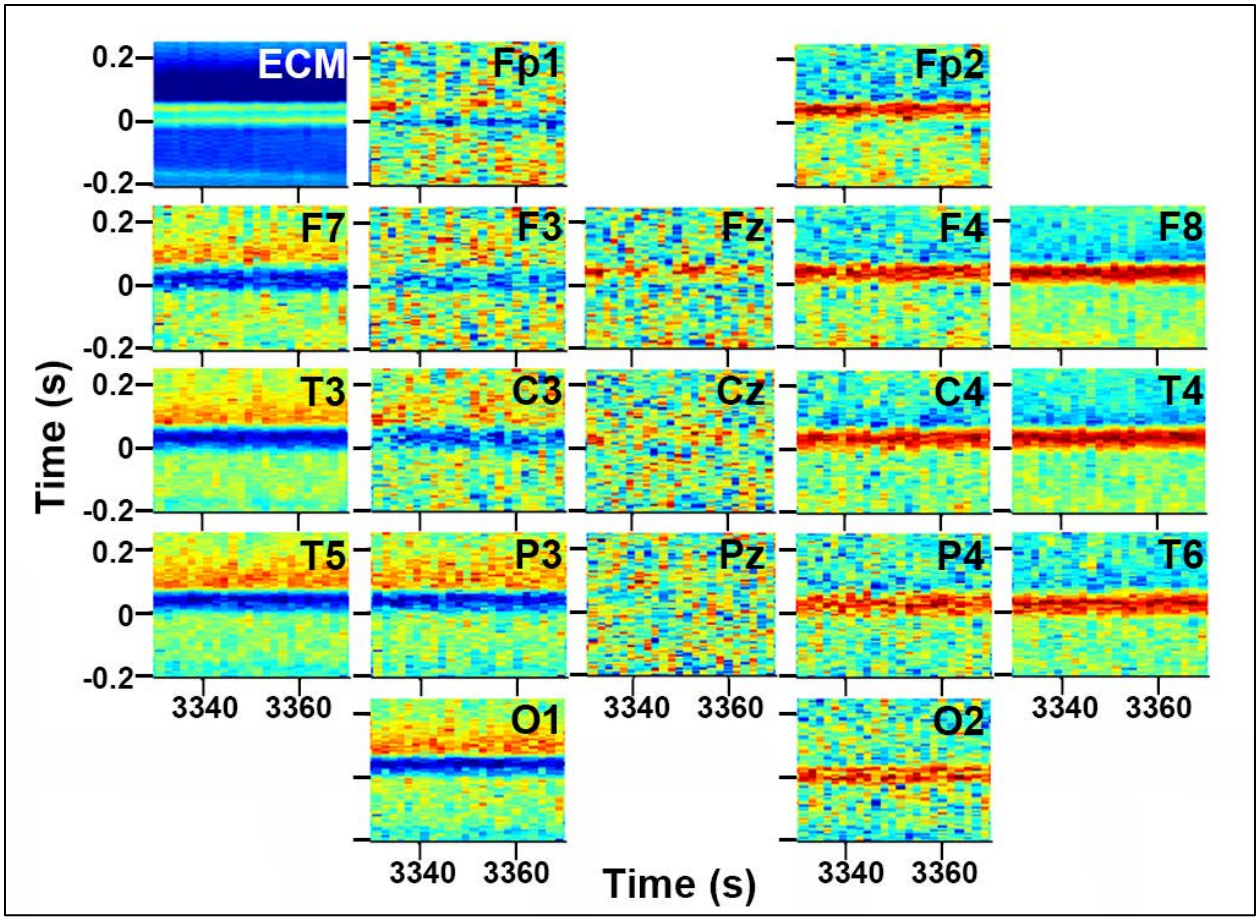

Supplement Figure 3 ECM and EEM for 19 EEG channels (arranged according to their locations on the skull) for a 40-second long epoch during S6.

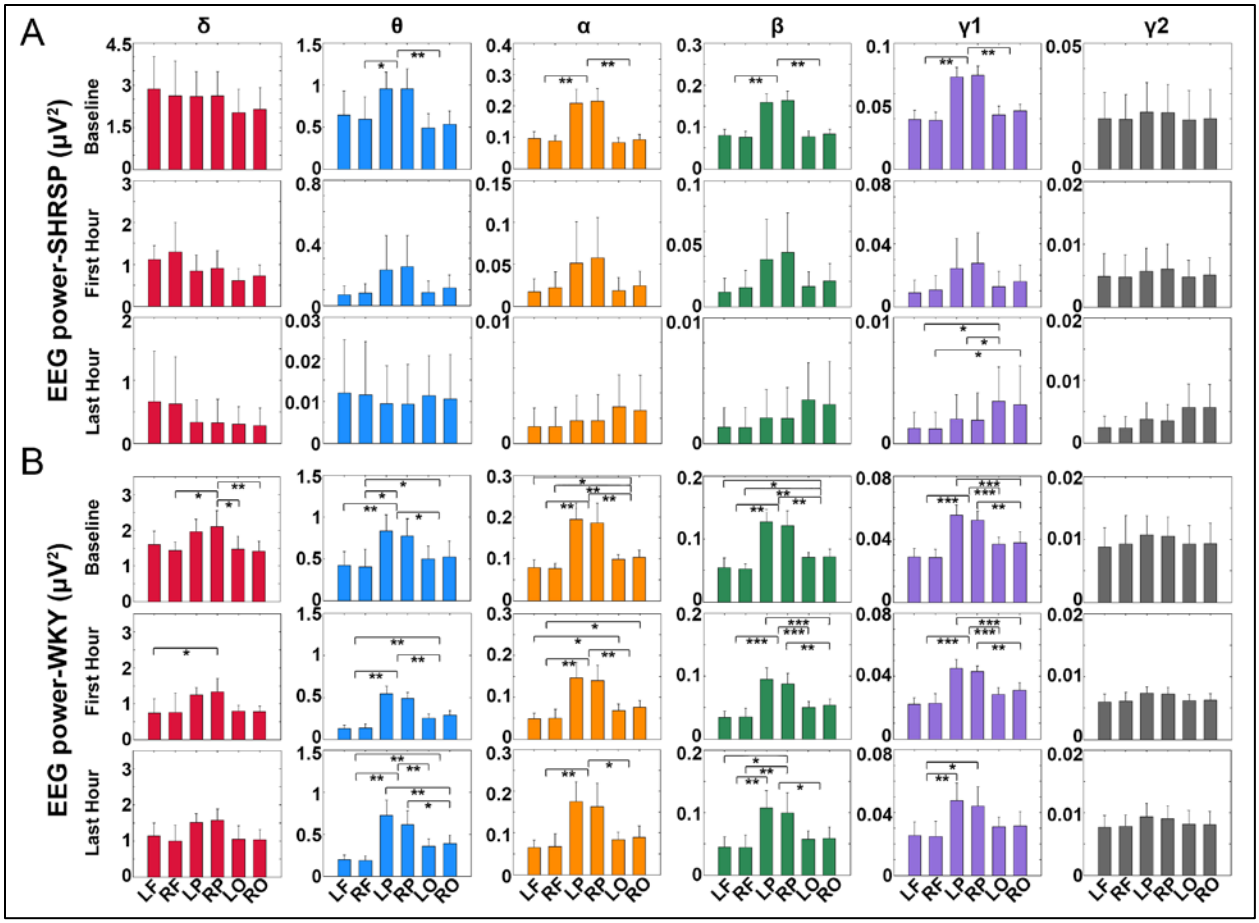

Supplement Figure 4 EEG power for each of the 6 cortical channels during baseline, first hour, and last hour in all SHRSP (n=9). **(A)** and WKY (n=8) **(B)** rats for 6 frequencies. LF: left frontal, RF: right frontal, LP: left parietal, RP: right parietal, LO: left occipital, RO: right occipital. Data expressed as mean±SD. *Significant differences between two channels (*$p < 0.05$, **$p < 0.01$, ***$p < 0.001$).

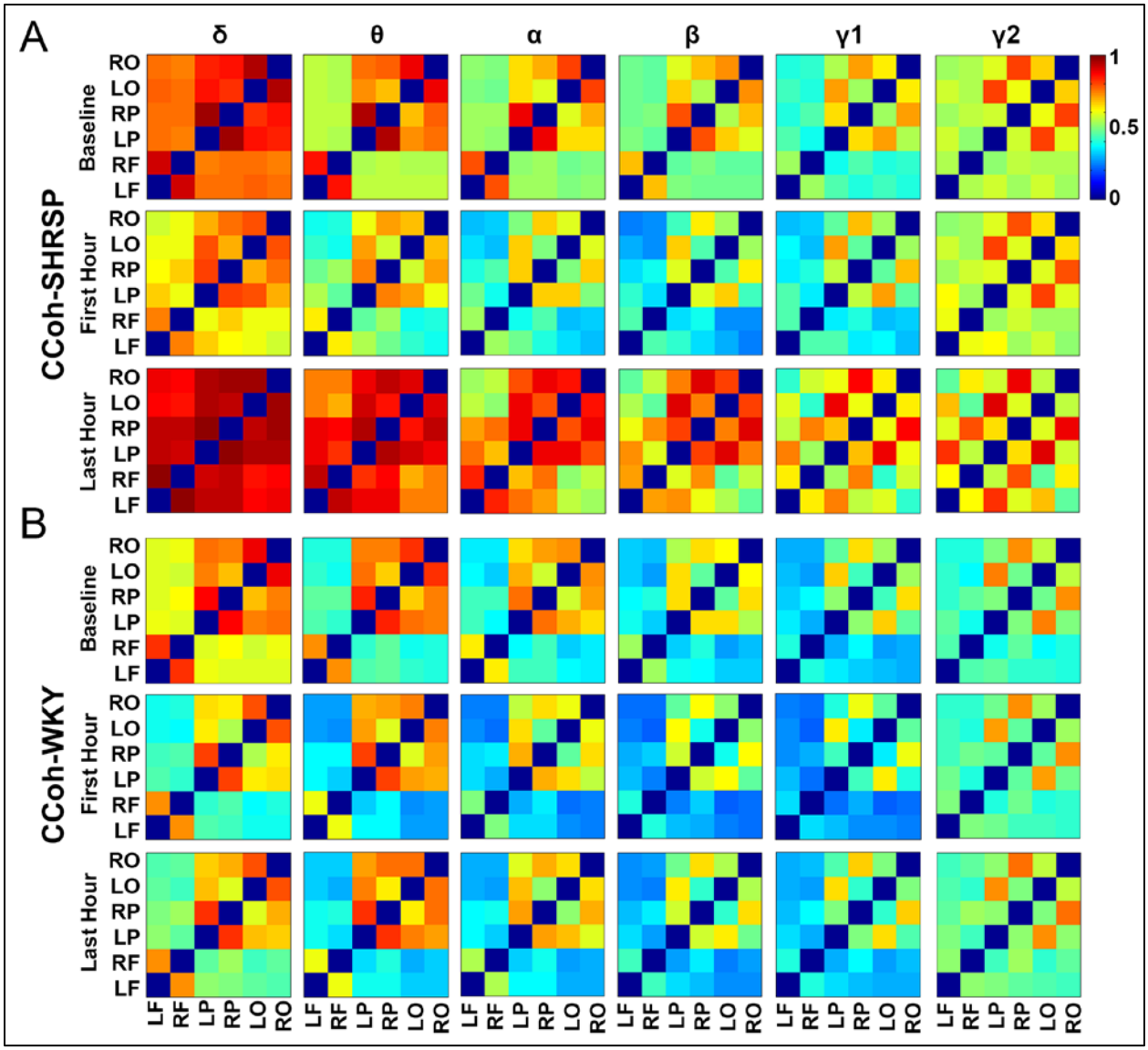

Supplement Figure 5 Cortical coherence (CCoh) between every 2 of the 6 cortical channels during baseline, first hour, and last hour in all SHRSP (n=9). **(A)** and WKY (n=8) **(B)** rats for 6 frequencies. LF: left frontal, RF: right frontal, LP: left parietal, RP: right parietal, LO: left occipital, RO: right occipital.

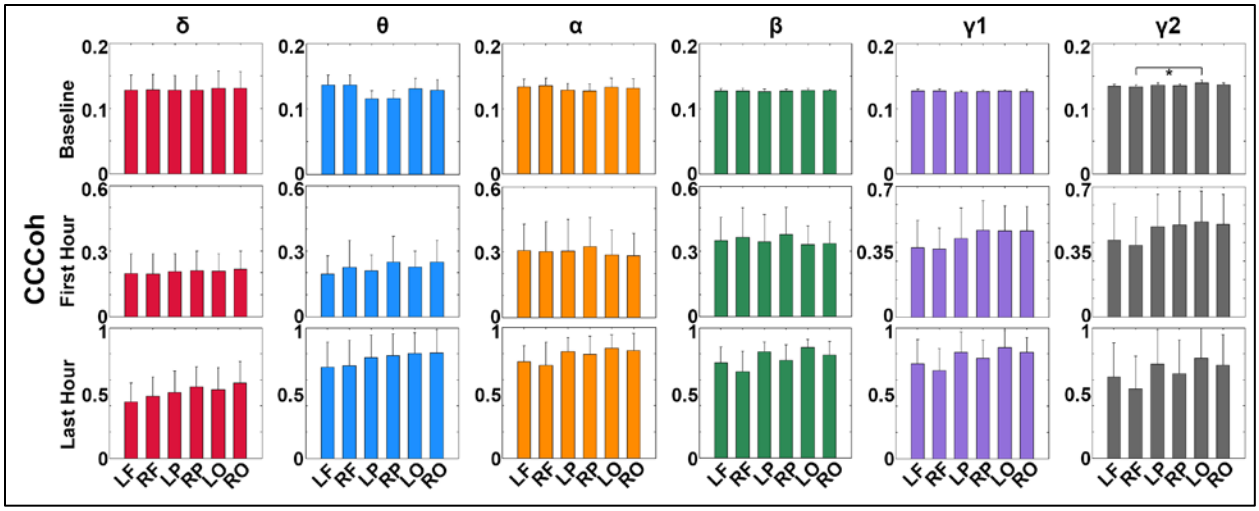

Supplement Figure 6 CCCoh for each of the 6 cortical channels during baseline, first hour, and last hour for in all SHRSP rats (n=9) at 6 frequencies. LF: left frontal, RF: right frontal, LP: left parietal, RP: right parietal, LO: left occipital, RO: right occipital. Data expressed as mean±SD. *Significant differences between two channels (*$p < 0.05$, **$p < 0.01$, ***$p < 0.001$).

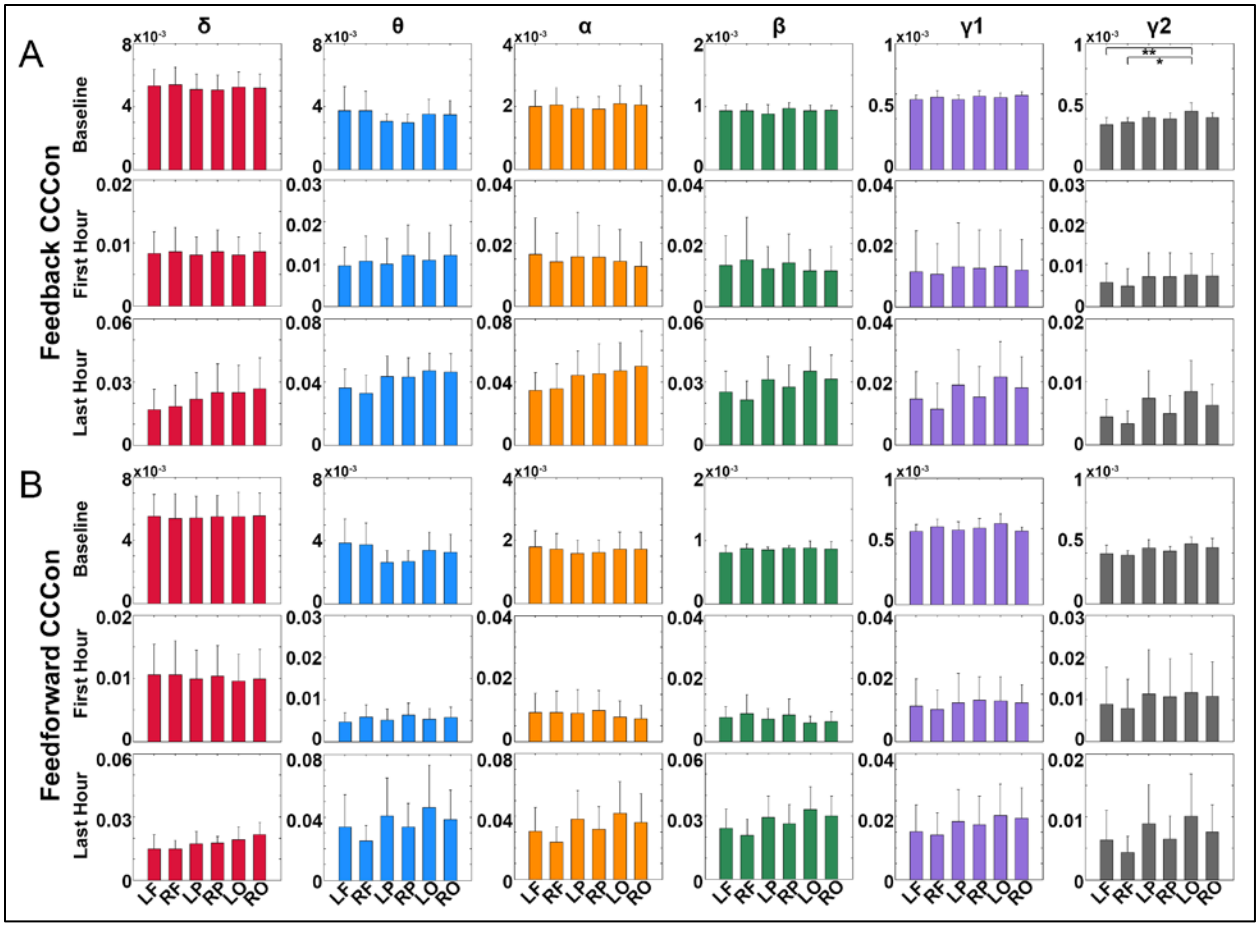

Supplement Figure 7 Feedback **(A)** and feedforward **(B)** CCCon for each of the cortical channels during baseline, first hour, and last hour in all SHRSP rats (n=9) for 6 frequencies. LF: left frontal, RF: right frontal, LP: left parietal, RP: right parietal, LO: left occipital, RO: right occipital. Data expressed as mean±SD. *Significant differences between two channels (*$p < 0.05$, **$p < 0.01$, ***$p < 0.001$).